Titanium Oxide and Bone Anchorage

Role of the Complement System, and Delivery of Osteoporosis Drugs from Mesoporous TiO_2

Necati Harmankaya

Department of Biomaterials

Institute of Clinical Sciences

Sahlgrenska Academy at University of Gothenburg

UNIVERSITY OF GOTHENBURG

Gothenburg 2013

Titanium Oxide and Bone Anchorage

Correspondence:
Necati Harmankaya
Box 412, SE 405 30 Gothenburg, Sweden
E-mail: neco@biomaterials.gu.se | necati.harmankaya@gmail.com

ISBN: 978-91-628-8883-1
Available online: http://hdl.handle.net/2077/34402

Printed in Gothenburg
Ineko AB

Printed in 150 copies

To my sisters and angels Neslihan, Dilan and Şehriban.

"Education is the most powerful weapon which you can use to change the world."
Nelson Mandela

CONTENTS

1 ABSTRACT

The clinical success of bone implants of titanium (Ti) is largely ascribed to the biological performance and the physicochemical properties of the outermost titanium(IV)dioxide (TiO_2) layer. Several advancements have been done on TiO_2 in order to optimize its healing and anchorage to bone, and there is a need for further understanding and control of the molecular reactions preceding long-term osseointegration. Next generation of implants advances with their ability to target specific molecular mechanisms.

In this thesis we performed mild surface treatments of TiO_2 with improved oxide properties and bone-implant anchorage in mind. First, we exposed titanium to (UV) illumination or mild heat treatment to control the complement activation ability of the surfaces. Secondly, we evaluated *in vivo* a mild heat treated mesoporous TiO_2 drug-delivery system on Ti implants.

Ti surfaces were heated or exposed for up to 96 hours to UV-light in combination with ozone (UVO) and tested for inflammatory activity *in situ* and *in vivo*. Surfaces were immersed in blood plasma for up to 60 minutes and the deposition of complement factor 3 was evaluated by ellipsometry. The *in vivo* bone response to UVO-treated Ti relative to complement activating control surface was evaluated by histology, histomorphometry, biomechanics and SEM.

The mesoporous coating was prepared on Ti screws (L=2.3 mm, Ø=2.0 mm) using the Evaporation Induced Self-Assembly (EISA) method. The coating was highly-ordered mesoporous TiO_2 with a thickness of 200 nm and possessed a narrow pore-size distribution. Two osteoporosis drugs, alendronate or raloxifene, were absorbed into the pores and the implants were evaluated *in vivo* in male and ovariectomized rat models.

The present results show that adsorption of complement factor C3 *in situ* can be strongly suppressed by mild heat treatment at 300°C or UVO-treatment for 12 hours or longer. A significantly lower gene expression of inflammatory markers was noted *ex vivo* on UVO-treated implants compared to complement-activating controls. Although UVO-treatment did attenuate the early inflammatory response on Ti, the bone-anchorage did not significantly benefit from this effect.

Mesoporous Ti implants loaded with a bisphosphonate, alendronate, or an oestrogen receptor antagonist, raloxifene were successfully retrieved after up to 28 days post-surgery. Raloxifene promoted a significantly higher bone-anchorage in comparison to control and ALN-loaded implants, and was supported by an increased gene expression of osteoblast and osteoclast markers. The distribution of alendronate in implant-close bone was followed for up to 8 weeks and the results show that alendronate has a long residence time in the close vicinity of the implants. Also, we have shown significant differences between local vs. systemic delivery of bisphosphonates; the local delivery promoted a significantly higher bone-implant anchorage.

In summary, the osteoimmunologic properties of TiO_2 result partly from stoichiometry of the oxide, which we have showed can be altered by means of mild heat-treatment or UVO-illumination. Mesoporous coatings may provide a unique reservoir on implant surfaces into which drugs can be loaded. This may serve to a better bone-implant healing, especially for patients suffering from osteoporotic bone-deficiency, where current pharmaceutical treatments come to short or are bound with systemic side effects when given at high doses.

2 SAMMANFATTNING PÅ SVENSKA

Framgången hos titan-baserade implantat beror i hög grad de fysikaliskt-kemiska egenskaperna hos dess tunna oxidskikt, titan(IV)dioxid (TiO_2). Trots dess utmärkta inre egenskaper i t.ex. ben utvecklas och optimeras ytorna fortfarande, och det finns ett stort behov av att förstå och kontrollera de molekylära och cellulära reaktioner som leder till god benförankring. Bland annat vet man att TiO_2 aktiverar den alternativa aktiveringsvägen hos det humorala immunförsvaret, det som kallas komplementsystemet, och det kontaktaktiverar blodkoagulationen. Nästa generation av implantat kan förhoppningsvis kontrollera dessa på ett mer optimalt sätt.

I denna avhandling har vi försökt att förbättra benförankringen vid korttidsimplantation efter behandling av titanytor med milda modifieringsmetoder. Först utvärderades betydelsen av ytaktivering av komplementsystemet genom att UV-ozon- eller milt värmebehandla titaytor. Dessa utvärderades såväl *in vitro* som *in vivo* i råtta. I ett andra utvecklingssteg belades implantaten med ett tunt milt värmebehandlat mesoporöst TiO_2-skikt. Porerna fylldes sedan med osteoporos-läkemedel och implanterades i råttans skenben (tibia).

Resultaten *in vitro* visar att titanoxidens komplementaktivering undertryckts kraftigt efter värmebehandling vid 300°C eller UVO-behandling mer än 24 timmar. Resultaten ex vivo visar då, efter qPCR analys, signifikant lägre gen-uttryck för inflammatoriska markörer. Minskad komplementaktivering resulterade i en något bättre benförankring, men skillnaden var inte signifikant jämfört med obehandlad titan.

De mesoporösa titanimplantaten visade att en mycket liten lokal dos osteoporosläkemedel med olika verkansmekanismer, i detta fall alendronat och raloxifen, båda förbättrade bentätheten eller den mekaniska förankringen kring ett implantat. Resultaten visar också att det föreligger signifikanta skillnader i inläkningsförloppet mellan systemisk och lokal läkemedelstillförsel.

Sammanfattningsvis, titanoxidens pro-inflammatoriska svar kan modifieras via UV-ozon behandling eller via en modest värmebehandling. Slika behandlingar ändrar oxidens tjocklek, stökiometri, kristallinitet och hydroxylering, och kan vara värdefulla då man önskar minimera immunrespons och oxidens löslighet, t.ex. då man önskar använda sig av titanoxid som bärare av läkemedel för lokal avgivning. Lokalt avgivet läkemedel förväntas dels ge en kring implantatet lokaliserad effekt, dels minska oönskade systemiska sidoeffekter.

3 LIST OF ORIGINAL ARTICLES AND MANUSCRIPTS

This thesis is based on the following original articles and manuscripts, referred to in the text by their Roman numerals.

I. Paula Linderback, Necati Harmankaya, Agneta Askendal, Sami Areva, Jukka Lausmaa, Pentti Tengvall, *The effect of heat- or ultra violet ozone-treatment of titanium on complement deposition from human blood plasma,* Biomaterials **2010**; 31 (18):4795-801.

II. Necati Harmankaya, Kazuyo Igawa, Patrik Stenlund, Anders Palmquist, Pentti Tengvall**,** *Complement activating Ti implants heal similar to non-activating Ti in rat tibia,* Acta Biomaterialia **2012**; 8 (9):3532-3540.

III. Necati Harmankaya[‡], Johan Karlsson[‡], Anders Palmquist, Mats Halvarsson, Kazuyo Igawa, Martin Andersson, Pentti Tengvall, *Osteoporosis drugs in mesoporous titanium oxide thin films improve implant fixation to bone*, Acta Biomaterialia **2013**; 9 (6): 7064-7073.

IV. Johan Karlsson[‡], Necati Harmankaya[‡], Stefan Allard, Anders Palmquist, Mats Halvarsson, Pentti Tengvall, Martin Andersson, *In vivo Drug Localization at the Implant/Bone Interface – Alendronate delivered from Mesoporous Titania,* Submitted.

V. Necati Harmankaya[‡], Johan Karlsson[‡], Anders Palmquist, Mats Halvarsson, Martin Andersson, Pentti Tengvall, *Bone remodelling following systemic or local delivery of BPs in OVX rats*, In manuscript.

[‡]*First and second author have contributed equally to this manuscript.*

4 CONTRIBUTIONS TO STUDIES I-V

Study I: I participated in formulating the research question around the mild surface treatments (heating and UV-illumination), and prepared and performed the experimental setup in this question. I prepared and characterized the optically smooth Ti surfaces by FTIR, XPS, and XRD, and wrote parts of the manuscript.

Study II: I formulated the research question in collaboration with the main supervisor and was responsible for the entire study plan. Implants were purchased as machined and were prepared specifically by me: cleaning, illumination, coating, etc. I did all characterization myself. The animal model as a whole I planned and executed myself. While histological sections were prepared by the lab personal, all analysis was done by me. QPCR was performed elsewhere. I did the analysis and prepared the manuscript draft.

Studies III-V: These studies were a part of a twinning PhD project with Chalmers University of Technology. In all studies, the research hypotheses were formulated in the twinning group. I was responsible for planning of the studies, the animal model, the methods in relation to it and execution of the plans. Implants were purchases, while the mesoporous TiO_2 coatings were developed, prepared and characterized by the PhD-student at Chalmers, Johan Karlsson. I also participated partly during the coating and drug loading processes. All histology, histomorphometry, qPCR and statistics were coordinated and analysed by me. The twin PhD-students prepared the first drafts of the manuscripts.

5 ABBREVIATIONS

AFM	Atomic Force Microscopy
ALN	Alendronate
ALP	Alkaline Phosphotase
AP	Alternative Pathway
BA	Bone Area
BIC	Bone Implant Contact
BMD	Bone Mineral Density
BMP-2	Bone Morphogenetic Protein
BMU	Basic Multicellular Unit
BP	Bisphosphonate
CATK	Cathepsin K
CP	Classical Pathway
EISA	Evaporation Induced Self-Assembly
FTIR	Fourier Transform Infrared Spectroscopy
HA	Hydroxyapatite
HMWK	High Molecular Weight Kininogen
IL-1(-6)	Interleukin-1(-6, etc.)
OC	Osteocalcin
ONJ	Osteonecrosis of the Jaw
OPG	Osteoprotegerin
OVX	Ovariectomy
PDGF	Platelet-derived Growth Factor
PVD	Physical Vapour Deposition
PZC	Point of Zero Charge
QCM-D	Quartz Crystal Microbalance with Dissipation
qPCR	Quantitative Polymerase Chain Reaction
RANK(L)	Receptor Activator for Nuclear Factor κB (Ligand)
RLX	Raloxifene
ROS	Reactive Oxygen Species
RTQ	Removal Torque
Runx2	Runt-related transcription factor 2
SAXS	Small Angle X-ray Scattering
SDF-1	Stromal Cell-derived Factor-1
SEM	Scanning Electron Microscopy
SERM	Selectrive Estrogen Receptor Modulators
TEM	Transmission Electron Microscopy
TNF-α	Tumor Necrosis Factor-α
TRAP	Tartrate-Resistant Acid Phosphatase
TSH	Thyroid Stimulating hormone
UVO	Ultra Violet Ozone
XPS	X-ray Spectroscopy
XRD	X-ray Diffraction

6 INTRODUCTION

6.1 Rationale

Titanium (Ti) is a widely used a metal in dentistry and orthopaedic practice, such as in dental root replacements and bone screws for temporary or permanent bone bonding and enforcement. They all contact blood directly upon insertion to tissues, as well as in cardiovascular applications such as prosthetic heart valve suture rings, leaflets and surfaces in circulatory assist devices. They all integrate well to bone and soft tissues but show often fibrous tissue formation and occasionally infection. However, spontaneously oxidised metals activate the intrinsic pathway of coagulation and to bind complement factor 3b (C3b) from blood plasma and body fluids. The *in vitro* and *in vivo* properties depend largely on the nature of the 3-5 nm thick dense oxide layer that is quickly formed upon contact to oxygen and water. The spontaneously formed amorphous Ti-oxides possess a point of zero charge, pzc~5-6, and the water solubility is at the order of 1-2 micromolar. Spontaneously oxidised metal surfaces are often subjected to chemical- and high temperature bakings for purposes such as: cleaning; surface roughening; and change of crystallinity. Crystallised oxides are normally much less soluble than amorphous ones. Some of the most well-known treatments are pickling/etching in acids such as hydrofluoric acid/nitric acid and hydrochloric acid/sulphuric acids. Topographic alterations and improved corrosion resistance can be obtained by anodic oxidation in sulphuric acid, phosphoric acid and acetic acid. Alkaline etching in NaOH/HCl followed by heat treatment of Ti increases its surface roughness and crystallinity. Recently Ti surfaces with anatase crystallinity were prepared superhydrophilic by means of extended UV-illumination (not UVOzone), and the surfaces indicated histomorphometrically improved osseointegration after 2 weeks in rat tibia. A similar treatment in another study showed, however, no improvement at 4 weeks of implantation. To further increase the biocompatibility of Ti implants, also other types of TiO_2-coatings have been developed. Coatings also could serve the purpose of targeting specific mediator mechanisms in bone osteoimmunology and histogenesis by delivering drugs locally to the site of bone-healing around implants. Evaporation Induced Self-Assembly (EISA) has shown to be a useful method to prepare anatase, mesoporous TiO_2 coatings with a highly ordered porous structure and narrow pore size distribution. Such coatings could potentially serve as nanoreservoirs for different agents, which under appropriate conditions can be loaded into the pores and remain there till in contact with a fluidic environment such as the circulation around bone-implants. For soon a decade, bisphosphonates (BPs) have been shown to promote enhanced bone-healing around implants when immobilized on Ti implants thru cross-linked

fibrinogen. BPs are clinically administered osteoporosis drugs which in line with other drugs, such as Selective Estrogen Receptor Modulators (SERMs), eg. Raloxifene (RLX), antagonizes the unbalanced bone remodelling characteristic of osteoporosis. As such, controlled local delivery of osteoporosis drugs from mesoporous coatings offers an alternative approach in research on bone-anchored Ti implants.

6.2 Aims

The main aim of this thesis was to employ mild surface treatment modalities in understanding and improving the osteoconductive properties of TiO_2 in relation to bone implants. More specifically we aimed to:

- Explore the effects of mild heating or UV-illumination of TiO_2 on the innate complement activation property *in situ*.
- Evaluate the inflammatory and osteogenic response to Ti implants after the mild treatments above *in vivo*.
- Develop and evaluate mild heat treated mesoporous Ti coatings as carriers for local delivery of osteoporosis drugs in terms of bone-implant anchorage *in vivo*.
- Study the distribution of alendronate that was released from mesoporous Ti implants *ex vivo.*
- Compare osteogenic response to mesoporous Ti-implants after local vs. systemic delivery of alendronate in an osteoporotic rat model.

7 TITANIUM AS A BIOMATERIAL

7.1 Advancements in Titanium Implants

The idea of using metals to replace structural components of the human body has been there and with us for decades. Titanium (Ti) as a medical implant material was first introduced into the medical field in early 1940s with a publication by Bothe, Beaton and Davenport on the reaction of bone to multiple different metallic implants[1]. They implanted a number of metals including Ti, stainless steel and cobalt-chromium alloy in the femur of a rat, and noted no adverse reactions. Further studies during the 1950s confirmed the lack of adverse reaction towards Ti[2, 3]. Nevertheless, the use of Ti had a slow beginning since a number of other metals, notably stainless steel and cobalt-chromium, were already applied in orthopaedics and dentistry and with good success at that time due to their superior mechanical properties. Over the years cobalt-chromium gradually replaced stainless steel mainly due to its superior corrosion resistance in the biological environment. And as of today, the dominance of cobalt-chromium as the metal of choice is for the most part replaced by Ti. In some applications where a particularly high mechanical performance is required, cobalt-chromium alloys are still superior to Ti, as it is the case in bearing surfaces in joint replacement devices. On the other hand, in bone support or replacement, the significantly lower elasticity of Ti makes it the metal of choice. Additional features which make Ti attractive as an implant material are its excellent corrosion resistance, chemical stability and low toxicity in biological environments. This in combination with a superb biocompatibility is shared with only a handful of other materials[4].

The list of past and current medical and dental applications of Ti is long. Nevertheless, a relatively small number of generic applications can be identified, and in fact, these applications and expectations are consistent with the general principles upon which material selection for medical devices are founded. As such, the clinical need for a medical implant can be in the context of replacement of a tissue/organ suffering from pain, malfunction, structural degeneration or any combination of these (e.g. an arthritic hip), support of a tissue/organ that is malfunctioning (e.g. a pacemaker), control of regeneration processes, i.e. to either enhance or repress tissue growth or proliferation (e.g. vascular stent), and/or transient and directed support of traumatized or deformed tissue (e.g. screws for bone fracture). Other examples are interior patient blood contacting surfaces of life supporting machines such as oxygenators, heart-lung machines and dialysis equipment[5, 6].

It is self-evident from this general nature of implantation that there is a set of generic requirements to any material in order for it to perform healthy, functionally and safe as a medical biomaterial. The first is that the material must have the appropriate mechanical properties, taking in to account the stress levels and frequencies that will be encountered, and the expectations for stress transfer within the relevant part of the body. The second is that the implantation and the consequences of any corrosion process should it take place in that particular situation should be limited. The third is that the material should have adequate biological safety, which will be predicted upon the absence of *cytotoxicity* (toxic to cells), *mutagenicity* (causing mutations), *carcinogenicity* (causing cancer), *immunogenicity* (causing adverse immune reactions) and *thrombogenicity* (causing blood-clotting)[7].

When considering these requirements, it is not surprising that Ti is widely used, and indeed has, for most demanding applications become the metallic material of choice for implantation. Ti has, in fact, become the archetypal biomaterial, and its uses are based upon the classical foundations of chemical inertness, biological safety and adequate mechanical properties. Particularly in bone support and replacement of function of hard tissue, other biocompatible materials have failed either due to imperfect mechanical properties (e.g. ceramics) or lack of anti-corrosion properties (e.g. stainless steel vs. Co-Cr alloys).

For biomedical applications, Ti is alloyed with other elements to stabilize the crystal forms that result in optimal mechanical properties. Grade 5 Ti, the Ti6Al4V alloy (6% aluminium and 4% vanadium) is the workhorse in Ti-industry, where the additives determine grain size and thereby also the mechanical strength. The addition of Al stabilizes the α phase, which is stronger yet less ductile, whereas V stabilizes the β phase, which is more ductile (**Fig. 7.1**). The Ti 6-4 ratio by weight provides ideal balance between the main phases and is significantly stronger than commercially pure (c.p.) Ti while having the same stiffness and thermal properties. This grade is an excellent combination of strength, corrosion resistance, weld and fabricability[8].

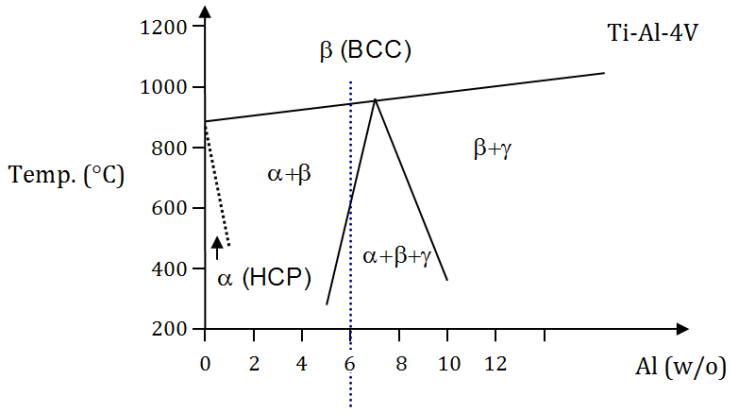

Fig. 7.1. Diagram showing changes in temperature for allotropic transformation of Ti-4V alloy with varying Al-content. At 6% Al the optimal compromise between the α and β phases is determined[9].

In combination with the abovementioned properties, the use of Ti developed remarkably as it was discovered and accepted as a metal with the capacity of *osseointegration*. It was evaluated in massive clinical multicentre trials led by Per-Ingvar Brånemark and colleagues from Gothenburg University from mid-sixties to 1970ies[10, 11].

This pioneering work introduced the concept of cementless implantation of Ti screws into *mandibular* and *maxillary* implantation sites, but also into *tibia*, *temporal* and *iliac* bones. From 1965 to early 1980ies, about 3000 dental Ti implants were inserted into humans. The persistent opinion back then predicted that *osseointegration*, meaning a direct contact between living bone and implant on microscopic level, could find place on ceramic implants or metallic implants. The trials performed by Brånemark and colleagues back then provided the largest clinical material[12]. Using refined methods for implant installation in edentulous jaws, based upon 15 years of clinical experience, the 5-year "survival rate" of functioning jaw bridges was in reported to be 100 % in the lower jaw and 95% in the upper jaw[13]. Remarkably, very recent investigations at Chalmers on atomic resolving of osseointegration point at the existence of an inorganic intermediate layer of calcium at the size of 1 nm (unpublished data).

7.2 Titanium(IV)dioxide as the Biocompatible Interface

The particular characteristic that makes Ti so useful is that it does not react adversely with the body due to its protective and chemically stable 3-20 nm thick oxide film layer, which forms spontaneously in the presence of oxygen and water. For most metals, when in contact with living tissue, a redox reaction takes place at the interface resulting in hydrolysis of oxide-hydrates as products of corrosion and formation of metal-organic complexes in the electrolyte. The consequence is denatured tissue. In contrast to many metals, Ti is inert toward this reaction[14].

Whether passivity toward biological environments is ideal, and whether tissue-material contact should involve a certain degree of a chemical interaction are ongoing questions, but this is currently out of the scope of this project. Instead, it is worthy to understand the so-called *bioinertness* of Ti in general terms.

Ti is almost universally said to be "biocompatible". The concept of biocompatibility has been formulated in this well-accepted definition:

> *"Biocompatibility is the ability of a material to perform with an appropriate host response in a specific application."*[15]

In the early days, 1960ies – 1990ies a material meant commonly a non-living material. Of course for the larger scale production and development, ISO standards and definitions of biocompatibility comes into play. However, despite the general acceptance of the above definition, we realize that the biocompatibility of Ti is in part a consequence of its chemical inertness toward its host.

Now, Ti belongs to the group of oxide-passivated metals (together with stainless steel, nickel, cobalt, and aluminium-based alloys) and show noble-metal-like properties resulting from the surface oxide layer that is formed instantaneously in oxygen, except under high vacuum and some equivalent conditions. This passivity toward any chemical reaction, including resistance to chemical corrosion, follows from the extreme reactivity of Ti metal with oxygen and water. This is due to its low position in the electrochemical series, with E_0= -2.6 V. However, this high reactivity also guarantees that in cases Ti implants are scratched or the oxide otherwise broken, it reacts immediately with the surroundings; the oxide heals within 30-40 milliseconds. Stainless steel, in comparison, needs seconds to heal a scratch. On Ti, the resulting oxide layer is dense, non-conducting, chemically inert and thermodynamically stable. In other words, it interacts relatively little with its surroundings during non-inflammatory conditions, During inflammatory conditions when reactive oxygen species (ROS) are released, TiO_2 acts as a catalyser to decompose H_2O_2 to O_2 and H_2O but may also sequester hydrogen peroxide to form the stable oxide bound radical TiO_3^-(Ti peroxide), that may alternatively be formed by TiO_2 plus O_2[16].

Ti is physiologically indifferent, meaning that it is tolerated by cells and tissues. without being an essential element and therefore without any positive or negative effects in contrast to iron and cupper, which are trace elements in homeostasis. Control of the properties of the oxide film is important because it is responsible for the chemical passivity of Ti and it contact with body fluids and tissues on site of implantation. For this reason, any modification of Ti and its

biological performance involves modification of the oxide film. There are varying reports on the thickness of the oxide film, as it depends on the surrounding media, temperature and surface finish, but in general a thickness between few nm to 20 nm is accepted[7, 17]. Commercially available implants can have much thicker oxides, such as that of TiUnite from Nobel Biocare®, which is reported to be up to 10 µm, synthesized using high-voltage anodic oxidation.

Total inertness is never achieved in metallic, polymeric, ceramic or composite biomaterials, and hence a measurable host response towards the presence of the biomaterial is to be expected and must be considered in selection of materials, the device design and implant application[8].

In short, the characteristics of pure Ti oxide films spontaneously formed at room temperature can be summarized in the following way:

- The oxide film is of amorphous or nanocrystalline nature and is typically 3-5 nm thick.
- It is mainly composed of the thermodynamically most stable oxide, with stoichiometry $Ti(IV)O_2$, especially in the outermost atomic layers.
- The Ti/TiO_2 interface, characterized by an O:Ti concentration ratio changing gradually from 2:1 within the TiO_2 film to the much lower, but non-zero value close to or inside the bulk metal.
- Ti-oxides are highly soluble in Ti metal.
- Hydroxide and *chemisorbed* water are strongly bound to Ti cations, especially in the outermost surface. Also weakly bound, *physisorbed* water can be observed on TiO_2 surfaces.
- An outermost oxide layer may consist – at least partly – of organic species adsorbed such as *hydrocarbons* (-CH-R[1]) or of metal-organic species such as *alkoxides* (-OR) or *carboxylates* ($-CO_2R$) of Ti. The oxide stoichiometry, purity and crystallinity depend on preparation and storage conditions. Composition and properties of TiO_2

The oxide film (TiO_2) that instantaneously coat the Ti surface forms quickly (order of 10ms) within the first exposure to ambient conditions and develops thereafter slowly with time (months to years). According to a least-square fit based approximation based on a logarithmic rate law for a TiO_2 thickness on polished c.p. Ti, which was confirmed by experiments[18], a thickness of ca. 3.17 nm is achieved after 1 day of exposure to air (calculated from the equation in the caption of **Fig. 7.2**).

[1] The "R" represents side chains with carbohydrates.

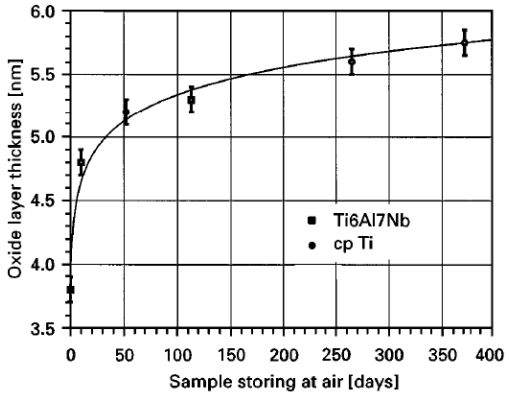

Fig. 7.2. The evolution of the oxide film thickness on polished c.p. Ti (●) and Ti-6Al-7Nb (■) dependent of storing time. The curve shown corresponds to a least-square fit based on a logarithmic rate law with $y=0.313 \cdot \ln(24\,900x+1)$[18].

Once a passivated thin oxide layer is formed on the metal atmospheric oxygen is prevented from reaching the metal. There is a generally accepted assumption that oxide growth at ambient conditions is controlled by diffusion of oxygen through the already formed oxide film. In effect, the oxide film has gradient properties as a result of variation of oxygen content within the oxide, with an interfacial gradient layer as reported in one study to be 39 ± 2 nm[19] while the outermost Ti(IV)O_2 stoichiometry itself was an order of magnitude thinner (4.5 nm in this case). Consequently, this provides reduced stress concentrations at the interface – and advantage toward mechanical (or thermal) stress.

The oxide TiO_2 exists in three different crystallographic forms: *rutile* and *anatase*, having tetragonal structure, and *brookite* having orthorhombic structure (see **Fig. 7.3**). The thermodynamically most stable forms are rutile and anatase, with the former as the most common. Anatase and brookite convert into rutile upon heating (500-800°C). Both in rutile and anatase Ti atoms are each coordinated to 6 oxygen anions, which is the preferred coordination number of Ti in many compounds. An amorphous structure in the oxide film is widely accepted[20], although it is generally recognized that crystallinity is preparation dependent with the preparation temperature as the most important factor. For Ti oxidized at room temperature, however, an amorphous structure is most common. But as we will see, this project deals with an oxide layer that naturally is crystalline along the (112) (A) plane and develops towards complete polycrystallinity with increasing annealing temperature.

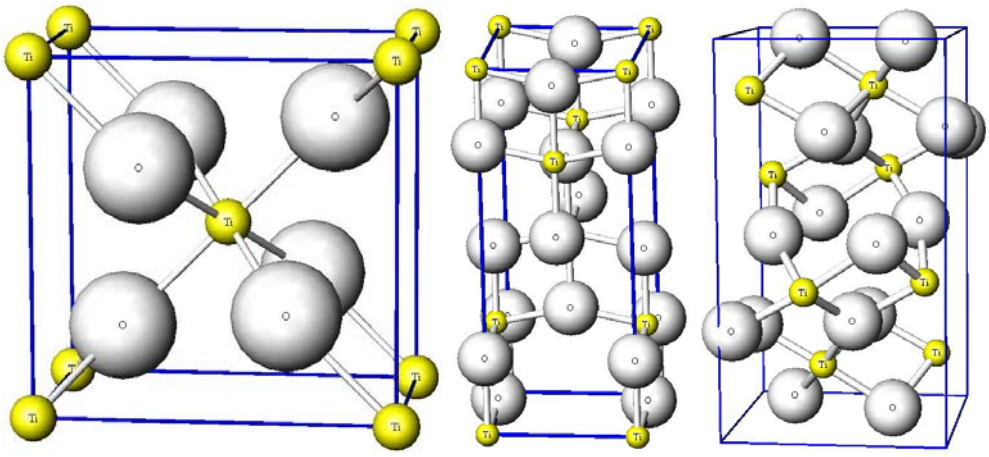

Fig. 7.3. Titanium(IV)dioxide exists in three crystal forms: rutile (left), anatase (middle), and brookite (right). The small yellow balls represent Ti cations and bigger white balls represent O anions[21].

A variety of different stoichiometries of Ti oxides are known, covering a wide range of oxygen to titanium ratios: from TiO_3 to Ti_2O, Ti_3O_2, TiO, Ti_2O_3, Ti_3O_5 and TiO_2[22]. This is a consequence of the fact that Ti exists in several more or less stable oxidation states, but also of the fact that oxygen shows relatively high solubility in Ti, leading to an almost gradual change (as discussed above) of the O/Ti ratio and thus variable physical properties. Corresponding to this gradient in oxidation state, Ti may exist in the oxidation state +IV for TiO_2, +III for Ti_2O_3, +II for TiO and 0 for Ti (metal). The most stable Ti oxide, however, is TiO_2, with Ti in oxidation state +IV.

Titanium oxides, especially TiO_2, are thermodynamically very stable and form immediately due to the fact that the energy for the formation of the oxide is highly negative (i.e. heat is evolved during the process) for a variety of oxidating media such as oxygen (ΔG_0=-888.8 kJ/mol oxide formed), water or oxygen containing organic molecules. Furthermore, the oxide layer adheres strongly onto the metal interface due to the high strength bonding strength of TiO_2 to Ti metal. The adhesion strength of such interface is mainly controlled by the process temperature during oxidation. The oxide TiO_2 is a non-stoichiometric n-type semiconductor with defects[23, 24]. The thermodynamic stability of TiO_2, is the foundation of biocompatibility of titanium. The stability over a wide pH-range, also in aqueous salt solutions can be studied in so called Pourbaix diagrams[25].

In an early study by Pouilleau and colleagues[19] it was found from comparison of different oxidisation techniques that oxidisation at room temperature followed by polishing showed XPS peaks stemming from TiO and Ti_2O_3:

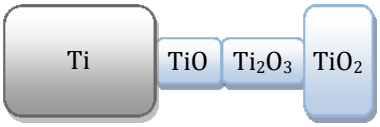

Fig. 7.4. XPS shows presence of Ti_2O_3 with Ti in oxidation state +III as an intermediate layer.

while thermal oxidation formed an intermediate oxide layer with a composition Ti_xO_y continuously varying quite linearly from pure TiO_2 to bulk Ti as Rutherford Back Scattering (RBS) revealed:

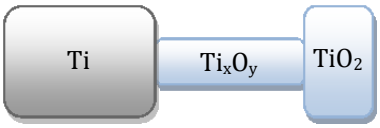

Fig. 7.5. Thermal oxidation formed progressively changing intermediate layers of Ti in various oxidation states.

This correlates with the interfacial gradient layer that we just described.

During physiological conditions, however, slow rate corrosion may occur under partially aerobic or peroxidic conditions with oxygen or peroxides as the oxidating agents. Normal tissue conditions are otherwise more reductive than oxidative during non-inflammatory conditions. The redox-reaction that occurs can be interpreted as an electrical circuit at the metal/media surface, and as with any other electrical currents, electrical (i.e. ohmic) resistance (in this case oxide film on the metal surface) determines the current of corrosion, and the less current in tissues the better.

X-ray diffraction (XRD) analysis can assist in to resolve the stoichiometry of Ti-O polymorphs, in particular to distinguish whether the outer TiO_2 film is configured in characteristic anatase or rutile forms. Now, this is a function of processing parameters. Non-stoichiometric compounds, however, where the composition varies continuously do not give rise to XRD diffraction peaks, so TiO_x cannot be observed for instance[19]. What we certainly can deduct from XRD literature is that an increasing thickness of the oxide layer is paralleled by an increase in crystallinity with a texture corresponding to the grain structure of the oxidized metal[20].

Apart from this, the nature of the oxygen species in the oxide film and particularly those at the outermost atomic layers are varied. The variability is also believed to be relevant to the behaviour of Ti when in contact with biological environments. In literature, a number of possibilities are reported:

- Oxide (O_2^{2-}): forms the bulk of the oxide film.

- Hydroxide (OH^-): reported to be present in the outermost part of the oxide film, i.e. not only at surface.
- Water (H_2O): reported to be chemisorbed, that is coordinately bound to surface Ti cations (Ti—OH), and physisorbed, that is water bound by very weak hydrogen-bonds, at the oxide/hydroxide surface (Ti—HO) and into the oxide. "Hydration" is the termed used for the combined effect of water adsorption, water splitting and hydroxide formation on and within the oxide films.
- Oxygen-containing organic compounds. Generally unintentionally adsorbed contaminants and reaction products of organic molecules at the Ti oxide surface: such compounds easily adsorb or are reactively formed at the Ti (oxide) surface as a consequence of the high adsorption power (many dangling bonds) at the clean Ti oxide film, e.g. (Ti—O—R) or carboxylates (Ti—OOC—R). In practice, a well cleaned Ti surface shows in XPS analyses 10-20% carbons at the surface.
- Oxygen-containing inorganic species such as nitrate (NO_3^-), phosphate (PO_4^{3-}), silica (SiO_4^{4-}) or sulphate (SO_4^{2-}) are often present in trace amounts.

In this discussion, the differently coordinated hydroxides and chemisorbed water in TiO_2 have gained lot of attention. Varying results have been reported with regard to alterations in composition, that is dissociation of water and desorption of chemisorbed water as a function of environmental factors, such as temperature and humidity. However, there is nowadays a fairly good overall agreement regarding the oxide composition and structure.

Firstly, strongly-bound OH-groups coordinated to Ti surface cations are formed as a consequence of dissociated water and chemisorptions at "empty" (5-coordinated) Ti sites. These groups desorb as recombined H_2O at temperatures around or above 250◦C[26]. Also, molecularly-adsorbed (i.e. undissociated) water binds to additional Ti cation sites at the surface. The desorption of strongly-chemisorbed water takes place at above 100°C. Finally, reversibly adsorbed water termed *physisorbed* water binds weakly to the oxide/hydroxide surface at mono- or multilayers. Such water layers form equilibrium and adjust to the atmospheric humidity and temperature. High resolution XPS provides detail information about the binding energies of different oxides, water and hydrocarbons at the Ti surface.

In conclusion, the biological performance of oxidized Ti is determined by the following physico-chemical properties[24]:

- Low overall solubility of Ti(IV) oxide, oxihydroxide and hydroxide, approximately 4 microM.
- Ti-peroxide has a solubility of approximately 40 milliM. Ti peroxide degrades to form hydrogen peroxide, oxygen and water.
- Low toxicity of oxidized surface and dissolved oxide/hydroxide species.
- Small proportion of charged species in soluble (oxide/hydroxide) hydrolysis products. Charged species lead to unfavourable strong interactions with biological molecules such as proteins. Neutral species interact less with surroundings.
- The isoelectric point (IEP = pH at which the oxide net surface charge is zero) of the oxide of 5-6. The passive-film-covered surface is therefore only slightly (negatively) charged at physiological pH.
- The dielectric constant of TiO_2 is comparable to that of water ($\varepsilon_r \approx 80$) with the consequence that the Coulomb interaction of charged species (e.g. proteins) is similar to that in water.

7.3 TiO_2 Hemocompatibility and Complement Activation

The almost immediate event that occurs upon implantation of biomaterials is adsorption of ions and proteins onto the material surface within milliseconds to seconds of contact. [27, 28]. These proteins first come from blood and tissue fluids at the wound site and later from cellular activity in the periprosthetic region. Once on the surface, proteins can desorb (native or denatured, intact or fragmented) or most noticeably remain to mediate tissue–implant interactions[29]. In fact, the nature of this 'conditioning film' deposited on biomaterials participates in the early host response, and influence the materials biocompatibility. This is realized when one follows the manner by which cells approach biomaterial surfaces, and considers that the "adsorbed state", which is the layer of immobilized proteins strongly bound onto the biomaterial. This is the first interfacial layer the cells meet[30].

Study of blood plasma protein interactions with Ti oxides is one possible way to understand blood interactions and the early tissue integration. The blood surface/protein interplay as well as attachment of blood cells is considered to affect wound healing around implants[31]. This is important in the context of Ti implants in contact with blood for a longer period of time, such as in vascular implants (e.g. leaflets of heart-valves), heart-lung machines and haemodialysis systems. In these applications hemocompatibility (biocompatibility in blood) is important. One aspect of hemocompatibility is contact activation of coagulation at negatively charged surfaces.

Ti, possessing a weakly negatively charged surface, is a contact activator, although not to the degree as the more negatively charged silica. Another important aspect of hemocompatibility is complement activation.

The complement system is the humoral part of the innate immune system and is comprised of about 20 blood plasma proteins (the complement factors). These serve to recognize foreign organisms, opsonize and lyse them, to participate in the general body's clearance system, and in regulation of inflammation and healing[32]. Also artificial and natural biomaterials are perceived as non-self-materials, and subsequently opsonized by complement proteins whenever the surface chemistry favours this.

Three different albeit interconnected pathways formulate the action of the complement factors: the classical pathway (CP), the lectin pathway, and the alternative pathway (AP). The lectin pathway is partly common with the CP and is initiated by certain *lectin* structures (i.e. sugar-binding proteins), many of which have been identified at bacterial surfaces. This pathway is not considered important for traditional biomaterials.

In both CP and AP, complement factors interact with each other, other tissue proteins, and cells through advanced molecular complexes and protein conformational changes. The adverse immune reaction is always initiated via factor C3, which is cleaved to C3a and C3b spontaneously or by a convertase. The CP and AP merge at the C3 activation step (**Fig. 7.6**).

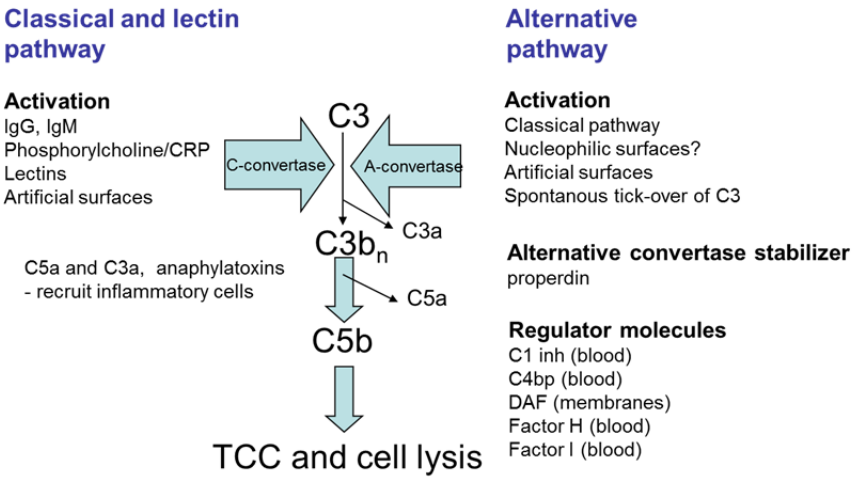

Fig. 7.6. Both pathways of the complement system, the classical and the alternative merge at the activation/conversion of factor C3. Titanium in particular activates C3. TCC: Terminal Complement Complex.

The CP may be activated by antigen-antibody complexes that form upon recognition of microorganism or molecular antigens, whereas the AP is more nonspecific and is often activated

by biomaterial surfaces. This pathway is also the effector pathway of the CP. The surface opsonization takes place as binding of C3b to partially denatured surface bound proteins that are simply recognized as "worn out" proteins, which need to be cleared out from the circulation[33]. Here, also the phenomenon "C3 tickover", i.e. the slow spontaneous cleavage of C3 to form C3a and C3b* (reactive C3b with half life time at the order of 60 milliseconds) is of crucial importance. When C3b* meet exposed –OH or $-NH_2$ groups of surface bound plasma proteins, surface bound C3 convertase forms and a complement activation amplification loop is formed. Complement activation at the C3 level is regulated by factors H, I and D that participate in the degradation of C3-convertases.

Upon complement activation, factor C3 undergoes nonselective conversions and form various complexes where it is fragmented to iC3b (inactivated C3b), C3c along with C3dg fragments via the cleavage of iC3b. Many inflammatory- and immune cells have receptors to these fragments. C3b marks most foreign surfaces via opsonization and is always present in plasma due to a continuous inactivation by hydrolysis, C3 tickover, and new formation by an *amplified* conversion of C3 to C3b. This is the amplification loop[34].

Factor C3 is of particular importance since many biomaterials bind C3, form surface bound C3 convertase and thereby amplify complement activation to C3-level. It seems actually that most materials become opsonized by C3b and its degradation products. C3b is in turn involved in the formation of a C5 convertase that cleaves C5 to C5a and C5b. C3a and especially C5a are inflammatory mediators that participate in the recruitment of leucocytes. C5b participates in the formation of new convertase, and so on[34,35].

Now, the ability of Ti implants to activate complement is crucial for the understanding of its hemocompatibility. As such, adsorption of complement factors and in particular factor C3b or its inactivated form iC3b to the Ti oxide film is regarded as a qualification of the materials complement interaction/activation.

A significant amount of research is done in this area, as reflected by a vast pool of results in the literature. Previously, the complement activation ability of TiO_2 was reported by researchers at Linköping University[36]. Commercially pure Ti powder was evaporated on flat silicon wafers and complement activation was quantified by *in situ* ellipsometry analysis of polyclonal antibody deposition on samples that were pre-immersed in human plasma at 37◦C.

It was also shown that Ti surfaces gave rise to an initial CP activation due to a transient affinity for C1q and IgG antibodies. The propagation occurred via the alternative pathway. as increasing

amounts of serum proteins and anti-C3c with time were deposited onto the Ti surface. In addition, it was reported that Ti has high affinity to coagulation factor XII (the Hageman factor) and high molecular weight kininogen (HMWK), both possessing a histidine rich and positively charged (at pH 7) domain that becomes exposed upon arrival of the protein to negatively charged surfaces. This shows that Ti is an intrinsic coagulation activator. In fact, it was reported that C3b and factor XII depositions take place simultaneously. Anti-C3c binding onto Si and Ti disappeared after incubation in factor XII deficient plasma or when a specific coagulation factor XII inhibitor, corn trypsin inhibitor, was added to normal plasma[37]. In this study, it was also indicated that the procoagulant property of Ti is transient as the binding of anti-HMWK decreased upon prolonged incubation times in heparinized plasma.

The complement activation ability of Ti has been attributed to various surface properties, among which surface charge is prevailing. The PZC (point of zero charge) value of Ti is ca. 5-6, which in turn means that Ti is weakly negatively charged at physiological conditions[38]. This explains its coagulation properties but not complement activation. On the contrary, the prevailing complement activation model at foreign interfaces, as proposed by Chenoweth, says that negatively charged surfaces are complement inhibitors (**Fig. 7.7**)[39].

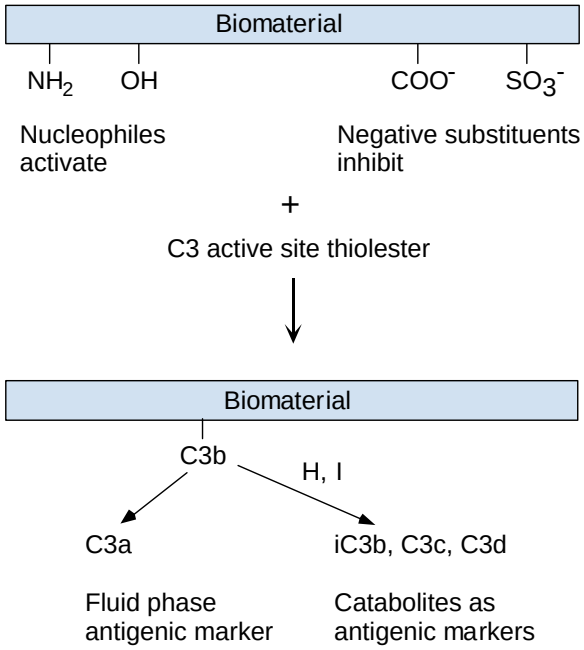

Fig. 7.7. Complement activation at foreign blood contacting surfaces, as suggested by Chenoweth[39].

So, what is then the mechanism? Most likely, the simple explanation is the inherent capability of especially C3 and its fragments (C3b, iC3b, C3dg, C3d) to recognize particles, viruses and denatured proteins and sequester them for further removal via the complement clearance

system[40]. Whether the nucleophilic –OH and $-NH_2$ groups then become exposed on adsorbed and partially denatured proteins and then participate in the complement activation process is today not well understood. Regarded this activation mechanism is valid, interfaces with low protein adsorption capacity or interfaces that do not denature adsorbed proteins should activate less. In fact, PEGylated surfaces are low protein binding surfaces and activate less. Also, nanostructured surfaces demonstrated in one study a lower C activation[41]. In this case the by us suggested C attenuation mechanism is that more serum proteins adsorbed onto the nanofeatures. A denser adsorbed protein layer is then less denatured, and hence less susceptible to opsonization by complement.

7.4 UV-illumination Alters Surface Physicochemistry of TiO_2

Titanium dioxide, particularly in the anatase form, is a photocatalyst under UV light. This property of TiO_2 was discovered by Akira Fujishima in 1965 and published in 1972 and was named the Honda-Fujishima effect[42]. In principal, it resembles the photosynthetic reaction in plants (see **Fig. 7.8**).

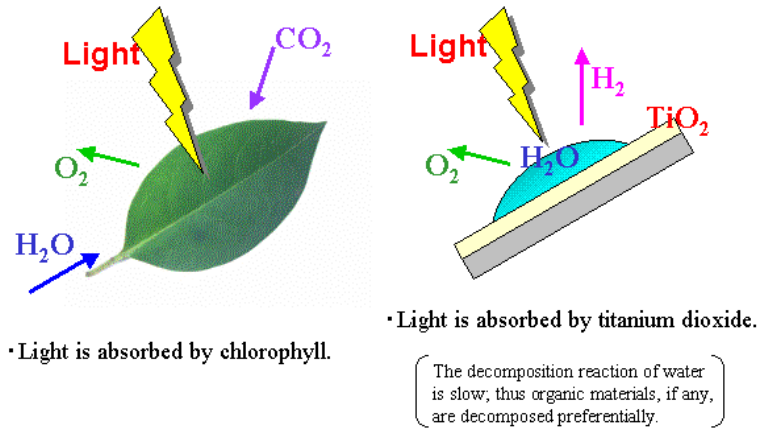

Fig. 7.8. The photosynthetic reaction in plants is basically similar to the photocatalytic reaction in TiO_2[43].

Moreover, in 1995 Fujishima and his group discovered the superhydrophilicity phenomenon for TiO_2 coated glass exposed to sun light[44]. They termed this *photoinduced superhydrophilicity*. When TiO_2 was exposed to UV-illumination the wettability of the surface increased remarkably with contact angles $< 1°$ compared to native contact angles above 20° that is usual for TiO_2 at room conditions. It was found by Atomic Force Microscopy (AFM) analysis that sun light had partly removed oxygen from the surface. These sites were hydrophilic whereas sites of no removal of oxygen remained hydrophobic. This *amphiphilic* characteristic follows from the following process: oxygen-titanium bonds in the Ti-O lattice aligned along the [001] direction of

the (110)(A) crystal face are weakened upon UV exposure upon which O atom is liberated and Ti is reduced:

(1) $$Ti^{4+} + hv \rightarrow Ti^{3+} + h^{+}$$

hv is energy, h Planck's constant and v the frequency of the light. h^{+} represents the positive hole that is formed.

The following O-vacancy is replaced by water in air that is chemisorbed to Ti as hydroxyls, OH^{-} (we can term this hydroxylation). Also, the strong oxidative potential of the positive holes oxidizes water to create hydroxyl radicals (OH^{*}). These also oxidize oxygen or organic materials directly. We explore eq. (1) further:

(2) $$TiO_2 + hv \rightarrow TiO_2 + h^{+} + e^{-}$$

(3) $$OH^{-} + h^{+} \rightarrow {}^{\bullet}OH$$

(4) $$2H_2O + h^{+} \rightarrow 2{}^{\bullet}OH + h^{+} + H_2$$

As such, when this surface is suspended in an aqueous environment e.g. in form a water droplet, this droplet will be remarkably bigger in dimension than domains with oxygen vacancies and those without vacancies, and a *2-dimensional capillary phenomenon* (surface pressure) reveals itself and a totally hydrophilic surface will be observed[17, 44-46]. Over a longer period of time the chemisorbed water is replaced by oxygen from air, hence the superhydrophilic effect is transient. Storage in dark can prolong the lifetime of the effect:

(5) $$\equiv Ti\text{-}O\text{-}Ti\equiv + H_2O \underset{dark,\Delta,\ k_{-2}}{\overset{hv \geq E_{bg},\ k_2}{\rightleftharpoons}} \equiv Ti\text{-}OH\ HO\text{-}Ti\equiv$$

In one study, TiO_2 films retained their original CA after 5 days in dark[17].

The photocatalysis on TiO_2 surfaces, in particular the hydrophilicity, has been explored for biomaterials in various contexts. Recently Ti surfaces were prepared superhydrophilic by means of extended UV-illumination (near UV, UVA, wavelength=352 nm), and such surfaces indicated improved osseointegration after 2 weeks in rat tibia[45]. The effect of high hydrophilicity on cell behaviour was also evaluated in terms of cell attachment, proliferation and morphology using pluripotent mesenchymal precursor C2C12 cells. Thereafter, bone formation around the hydrophilic implant inserted in the rabbit tibia was confirmed by histomorphometry[45]. These

surfaces indicated improved osseointegration after 2 weeks in rat tibia. The cell morphology on the hydrophilic disk was extremely flattened, with elongations of the lamellipodia, whereas a round/spherical morphology was observed on less hydrophilic control discs. The photo-induced hydrophilic implant enhanced the bone formation with a bone-to-metal contact of 28% after 2 weeks of healing in comparison with 18% for the less hydrophilic control.

A similar treatment in another study by the same group, however, showed no improvement at 4 weeks of implantation[46]. The plausible explanation was that the material in use did not possess enough low hydrophilicity due to smaller fraction of anatase crystals in the oxide. This was based on the findings by Wang et al., that PSH is in particular an attribute of anatase Ti[44].

Another *in vitro* study compared machined and acid-etched Ti surfaces after UV-illumination (both UVA and UVB, 360 nm and 250 nm). It was observed that UV increase the rate of cell attachment, spreading, proliferation and differentiation of rat bone marrow derived osteoblasts. UV-treated surfaces accomplished *in vivo* bone-Ti integration faster[47]. Furthermore, protein adsorption to hydrophilic Ti was investigated by others, and it was reported that adsorption is affected by hydrophilicity[48]. It was hypothesized that the increased surface charge and hydrophilic behaviour reduce hydrocarbon contamination on implants prior to surgery. However, the increased wettability was achieved through chemical modifications which inevitably brought along parallel modifications of the surface properties, such as topography. The use of UV for biomaterial surface modifications, sterilization and cleaning for different applications is still under investigation.

In our studies with UV/heat modifications of Ti-oxide we used a low-pressure mercury (Hg) discharge UV lamp in fused quartz envelopes with additional ozone (O_3) gas formed in the chamber, a treatment termed UVO. The lamp emits light at 184.9 nm and 253.7 nm (see **Fig. 7.9**)[49]. Our UVO system allowed infuse of air that is exposed to the UV light in the chamber. Upon UVO-illumination, atomic oxygen (O^-) is simultaneously generated when molecular oxygen (O_2) becomes dissociated by the 184.9 nm light and ozone (O_3) by the 253.7 nm light. However dissociation of O_2 by electric discharge at 184.9 nm in the presence of O^- results in additional O_3 formation via a 2-step process[50]:

(6) $$O_2 \rightarrow O + O \text{ and } O + O_2 \rightarrow O_3$$

The ozone formed in this process adsorbs UV light at 253.7 nm and is decomposed to O_2 and oxygen radicals (see also **Fig. 7.9**). If the gas phase contains molecules other than O_2, and these can be activated by the electric discharge to enter into reactions with atomic oxygen, the yield of

ozone is lower. A discharge in water vapour can produce excited water molecules or OH-radicals thereby consuming part of the atomic oxygen.

Since most hydrocarbons have a strong absorption band between 200 and 300 nm, the 253.7 nm wavelength emitted by the same lamp also is useful for the excitation or dissociation of organic contaminants.

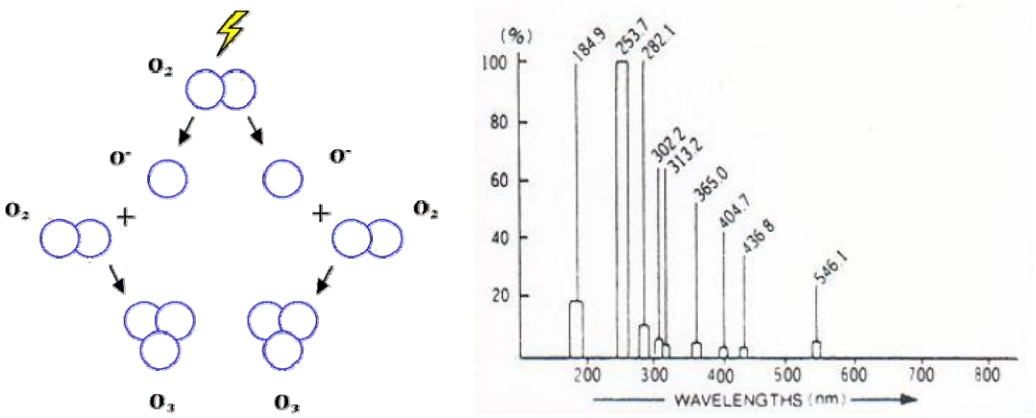

Fig. 7.9. (Left) formation of ozone (O_3) upon lightening of oxygen molecules (O_2), (right) Output profile of the mercury lamp. Most significantly, the 253.7 nm wavelength decomposes ozone[49].

The excited contaminants react with atomic oxygen, which is a very strong oxidizing agent to form simpler volatile molecules that desorb from the surface, i.e. CO_2, H_2O, N_2 etc. Therefore, when both UV wavelengths are present atomic oxygen is continuously generated, and ozone is continuously formed and destroyed[51]. Continuing from eq. (4) we can summarize the simplified process in the UVO-chamber:

(7) $$O_3 + e \rightarrow {}^{\bullet}O_3^-$$

(8) $$H^+ \; {}^{\bullet}O_3^- \rightarrow {}^{\bullet}O_3H$$

(9) $$ {}^{\bullet}O_3H \rightarrow {}^{\bullet}OH + O_2$$

(10) $$O_3 + hv_2 \rightarrow {}^{\bullet}O + O_2$$

(11) $$ {}^{\bullet}O + H_2O \rightarrow 2{}^{\bullet}OH$$

(12) $$O_2 + e^- \rightarrow {}^{\bullet}O_2^-$$

(13) $$ {}^{\bullet}O_2^- + O_3 \rightarrow {}^{\bullet}O_3^- + O_2$$

(14) $$2O_2 + hv_3 \rightarrow O_3 + O$$

Where $h\nu_2$ is energy UVC, long wavelength UV light, i.e. 253.7 nm, and $h\nu_3$ is the energy of the short wavelength at 184.9 nm[52]. Eq. (10) shows the generation of hydroxyl radicals. Effects of the wavelengths generated by our low pressure Hg discharge lamp (see also Chapter 12.1.3) are summarized in **Table 1**.

Table 1. Effects of the principal wavelengths generated by low-pressure Hg discharge lamps. Adapted from[53].

Wavelengths (nm)	Effects
184.9	Absorbed by O_2 and organic molecules. Creates O^- and O_3. Breaks contaminant molecule bonds.
253.7	Absorbed by organic molecules and O_3, not absorbed by O_2. Destroys O_3. Breaks contaminant molecule bonds.

The synergistic effect of O_3 and UV was described and explored for cleaning purposes already in 1985. Vig et al. found that while blacklight, i.e. UV light above 300 nm, did not show a particular effect, UV light at 184.9 nm and 253.7 nm produced atomically clean surfaces orders of magnitude faster[51].

Besides the impressive chemical cleaning, we were also interested in whether the volatile molecules formed on TiO_2 through the dissociation of molecular oxygen and ozone could induce chemical changes that in turn influence the biological behaviour of Ti.

In fact, it has been noted that extended exposure to short wavelength UV in combination with O_3 have effects other than surface cleaning. The most significant is *oxidation*. The oxidative power of ozone is second to that of fluorine and oxidizes most inorganic compounds to their final oxidative state. The oxidation effect of ozone was demonstrated for Gallium(III) arsenide (GaAs) where the oxide layer thickness increased from 30 Å to 300 Å. The oxide layer on aluminium surfaces behaved likewise, where 60 min of UVO-exposure increased the oxide layer thickness from 50 Å to 200[51]. Silicon substrates showed a similar pattern with oxide (SiO_2) thickness increase from 9 to 12 Å. In the same study, it was also observed that ozone produced by UV enhanced the growth rate of SiO_2 during thermal oxidation of Si at 800◦C[54]. In fact, the list of materials that have been investigated in this context grows steadily in literature.

Enhanced outgassing from material surface is another noticeable effect of UVO-treatment. The short-wavelength UV in presence of O_3 was shown to produce significant quantities of hydrogen, water, carbon dioxide, and carbon monoxide[53].

8 THE HUMAN SKELETON

The human skeletal system provides the scaffold around which support and movement of the body is coordinated and maintained. It performs the function of protection of vital organs, storage of minerals and fat and participation in endocrine regulation of the energy metabolism. In addition, when bone marrow forms at gestational age in the developing embryo, it becomes the anatomical site for the formation of most blood cells for the entire organism, i.e. the haematopoiesis. At birth, humans are born with over 270 bones, some of which at the time of adulthood fuse into a longitudinal axis leaving in total 206 distinct bones in the body; classified into long, short, flat, irregular and sesamoid bones, referring to their individual shape. The skeleton does also include teeth although these are not included in the number of different bones, due to differences in composition and appearance. **Fig. 8.1** shows the human skeleton with its individual bones. The skeleton contains the entire framework around bones and joints including bone-to-muscle connections, i.e. tendons, and bone-to-bone connections, i.e. ligaments. Both are fibrous connective tissues. For the rest of this section we shall discuss cells and mechanisms in the osseous tissue.

8.1 Gross Anatomy

Osseous tissue is a composite material advantageously combining inorganic ions and organic materials thereby forming compression resistant HA plates (65% by weight) embedded in a collagen-rich osteoid frame with tissue tensile-strength (35%). This yields bone with great strength. Thru the period of growth and development a process of bone formation, endochondral ossification continues with elongation of long bones. This occurs at a thin layer of cartilage, the epiphyseal plate, in the metaphysis at each respective ends of a long bone (e.g. tibia, femur, fibula)[32]. When full body length is achieved, this growth zone is replaced with bone thru ossification. As such, the anatomy of long bones finds definition as the epiphysis, metaphysis and diaphysis (**Fig. 8.1**).

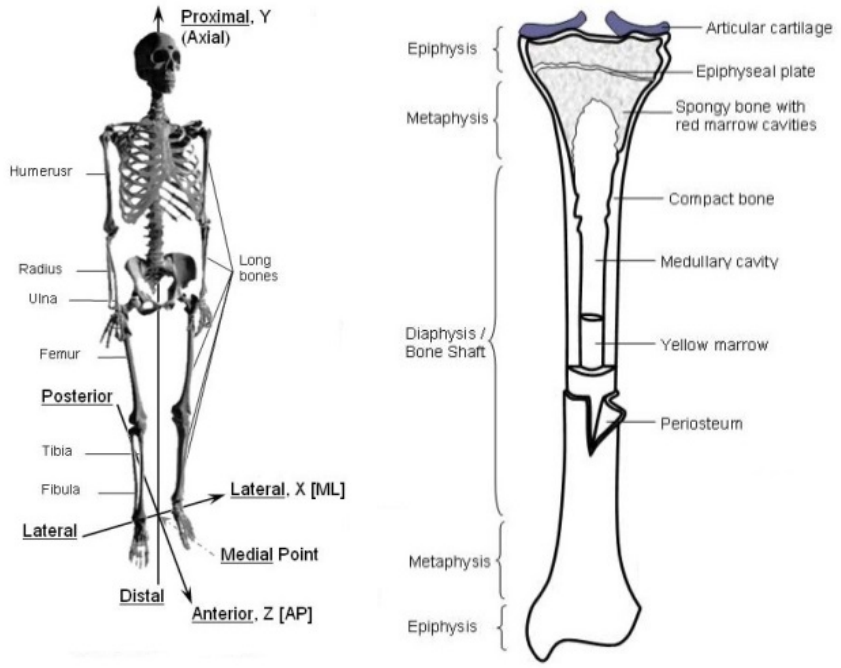

Fig. 8.1. The human skeleton with major bones and definitions of a long bone.

Although a reliable differentiation of bone morphology only can be achieved at microstructural level, bone is generally divided in terms of macroscopic structure in two forms: cancellous (spongy, trabecular) or cortical (compact) bone. Cancellous bone is a spongy, three-dimensional latticework of interconnecting bone processes called trabeculae arranged along lines of stress in the inner parts of the epi- and metaphysis, the shaft and at the end of the long bones, inside the spinal vertebrae and inside the flat bones of the pelvis. This network serves to transfer the load from the joints to the actual load-bearing part of the bone, the diaphysis, which is mainly made of cortical bone. Along this, cortical bone forms the outer shell, the cortex, of bone and is therefore much harder, stronger and stiffer than cancellous bone[55]. Thus, cancellous bone is mostly small cavities surrounded by bone matrix, whereas compact bone is mostly bone matrix with few small spaces. The diaphysis of a long bone, though, encapsulates the medullary cavity, which is filled with blood marrow. This is the actual site of haematopoiesis. The outer surface of bone is covered by periosteum, a connective tissue membrane of collagenous connective tissue with vessels, nerves and with bone cells; i.e. osteoblasts, osteoclasts and osteocytes (**Fig. 8.2**).

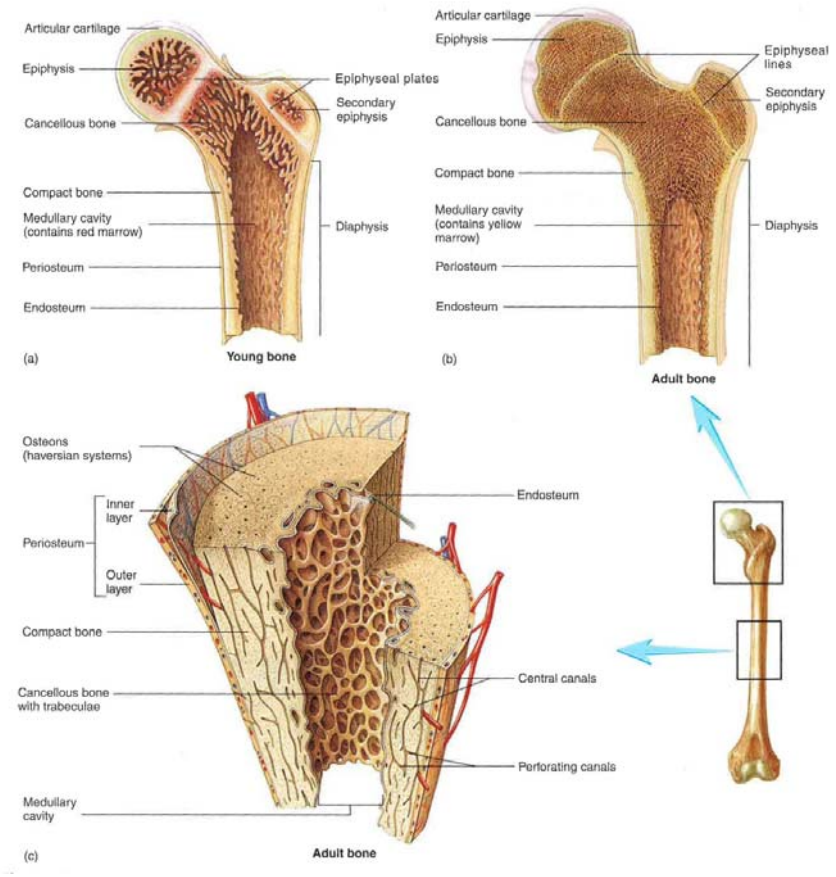

Fig. 8.2. Macroscopic structure of a long bone. (a) Young long bone (the femur) showing epiphysis, epiphyseal plates, and diaphysis. (b) Adult long bone with epiphyseal lines. (c) Internal features of a portion of the diaphysis in (a)[56].

8.2 Bone Histology

At first level of microscopic classification, bone is generally defined as *woven* or *lamellar*, termed primary or secondary bone, respectively. The difference herein is in the alignment of the collagen fibres during ossification of bone forming osteoids. During the fetal development and as a response to fractures (and in Paget's disease), bone is formed rapidly with the collagen fibres oriented in a haphazard fashion in all directions. This is called woven bone and is soon replaced by lamellar bone, which is highly organized in concentric sheets, lamellae of 3-7 μm thickness, and a much lower proportion of bone cells. In lamellar bone, the collagen fibres of a lamella lie parallel to one another giving the characteristic structure seen in the microscope. Its formation is slower in but is mechanically much stronger. Bone is constantly responding to changes in loading patterns, naturally occurring microstructures and growth, by degenerating and forming new bone[56, 57]. In the 19th century, the German anatomist and surgeon, Julius Wolff, formulated a theory, termed Wolff's law, that bone adapts to changes in loads[58]. Bone remodelling, as this is called, is orchestrated by three types of bone cells: *osteoblasts* that built new bone, *osteoclasts*

that degrade bone and *osteocytes* that locally orchestrate bone remodelling and changes to new needs.

De novo bone formation, osteogenesis, is performed by osteoblasts derived mesenchymal stem cells located in the inner layer of the periosteum. Osteoblasts produce collagen type I and proteoglycans, and accumulate calcium ions (Ca^{2+}), phosphate ions ($PO4^{2-}$) and enzymes including osteopontin and osteocalcin, which are involved in osteogenesis. Elongated cell processes from osteoblasts connect to cell processes of other osteoblasts through gap junctions. The interconnected network of osteoblasts releases their intracellular ingredients for bone matrix, which ends with surrounding the cells. Once bone matrix surrounds a cell, osteoblasts are differentiated to mature bone cells called osteocytes. Osteocytes are less active in de novo osteogenesis but maintain a status quo in the bone matrix, and are particularly sensitive to changes in mechanical load. The resorption of bone is performed by osteocytes and once activated they create tight contact to mineralized bone. Osteoclasts decalcify bone by creating an acidic environment through release of hydrogen ions (H+). In contrast to osteoblasts, osteoclats are derived from hematopoietic stem cells located in stem cell niches in the bone marrow[59]. Bone is thus constantly removed by osteoclats, and new bone is being formed by osteoblasts. The relative thickness of compact bone is maintained by the removal of bone of medullary surfaces by osteoclasts and addition of bone onto the dorsal surface by osteoblasts. Together, cells in any given region of the bone surface responsible for bone remodelling are known as the Basic Multicellular Unit (BMU).

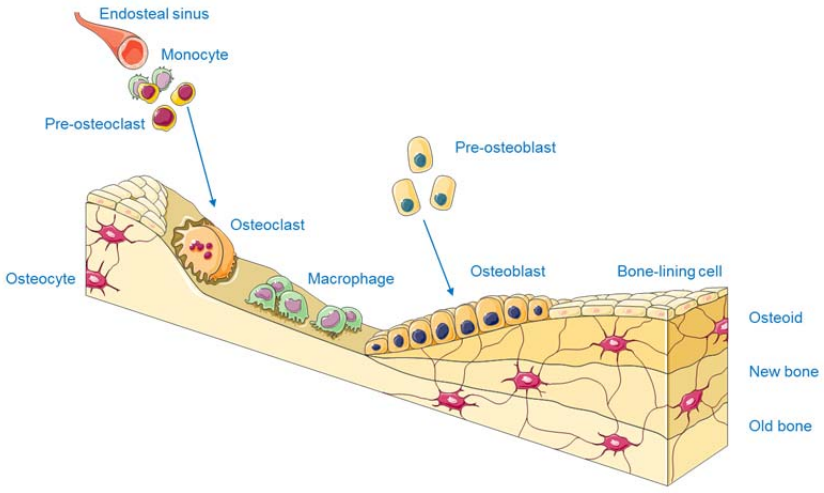

Fig. 8.3. Site of bone remodelling (Basic Multicellular Unit). Osteoclasts are from hematopoietic lineage and arrive at site of bone remodelling thru the circulation. Osteoblasts differentiate from pre-osteoblasts and are called osteocytes once they are surrounded by bone matrix. Source: Servier Medical Art.

In cortical bone, osteogenesis is concentrated around blood vessels which are contained within central, or Haversian, canals. The Haversian system, an osteon, consist of a single central canal, its contents and associated concentric lamellae and osteocytes, which in turn are interconnected through canaliculi. This model of bone forming is characteristic to larger vertebrates, as it is evident that the smaller the animal, the smaller is the size of the osteon and its canal[60, 61] (**Fig. 8.4**).

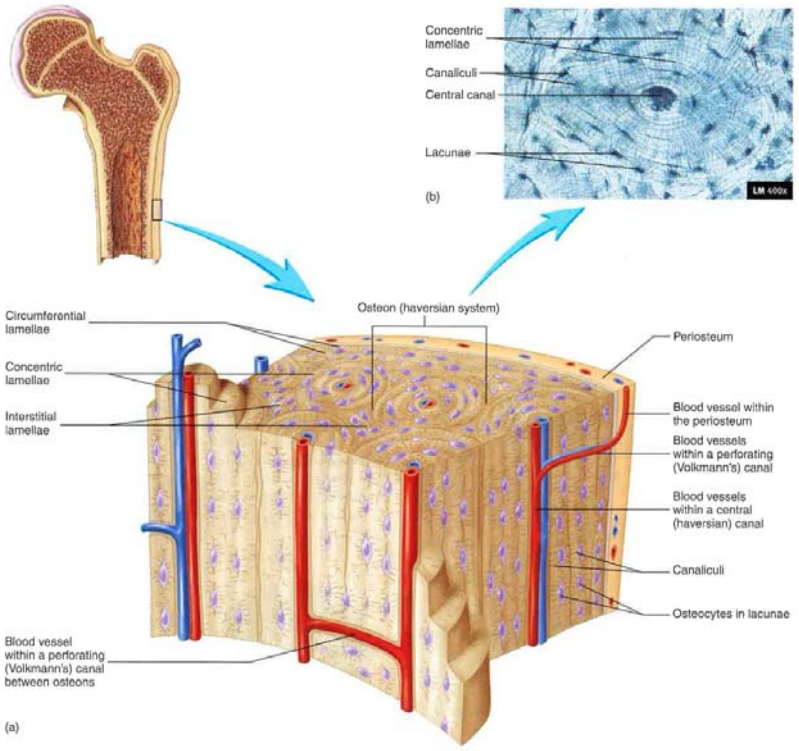

Fig. 8.4. Compact bone. (a) Compact bone consists mainly of osteons, which are concentric lamellae surrounding blood vessels within central canals (Haversian System). The outer surface of the bone is formed b circumferential lamellae, and bone between osteons consists of interstitial lamellae. (b) Microscopy image of an osteon[56].

8.3 Normal Bone Physiology

In life, bone formation occurs during fetal development following a process termed *intramembranous* ossification. As the foetus progresses, *endochondral* ossification takes over to form the adult skeleton which reaches its capacity at the end of the adolescence years (**Fig. 8.5**).

The embryonic mesenchyme condenses around the brain to form a membrane of connective tissue from which mesenchymal stem cells differentiate into osteochondral progenitor cells. These specialize into osteoblasts further to produce hard bone matrix, hydroxylapatite ($Ca_5(PO_4)_3OH$) around collagen fibres initially producing woven bone. The osteoblasts develop into osteocytes forming trabeculae (cancellous) bone, which becomes the site of red bone

marrow. At this time, an outer surface of compact bone is produced around the developing bone, and intramembranous ossification ends with bones with an outer compact bone surface and cancellous centres of ossification, completed at approximately 2 years of age[56, 62].

Bones of the base skull, part of the mandible, the epiphyses of the clavicles, and most of the remaining skeletal system develop through the process of endochondral ossification. This differs in the sense that mesenchymal cells differentiate into chondroblasts and in turn into chondrocytes. Chondrocytes produce a hyaline cartilage mesh named *callus* with the approximate shape of the bone that will later be formed[56]. On the surface of the callus, compact bone matrix is formed by osteoblasts. Surrounded by a calcified matrix, the chondrocytes undergo apoptosis due to limited diffusion of oxygen and nutrients, and bone development proceeds thru remodelling of the woven bone into lamellar bone. In fact, this pattern of bone remodelling, the ossification of a chondral, intermediate bone-mesh, underlies the fundamentals for natural healing of bone fractures, but it counts only for a minor part of bone healing around implants. The latter is primarily characterized by intramembranous bone healing, which proceeds without formation a cartilage model.[63]. We will become more familiar with the most recent findings within tissue healing in relation bone implants in the chapter 9.

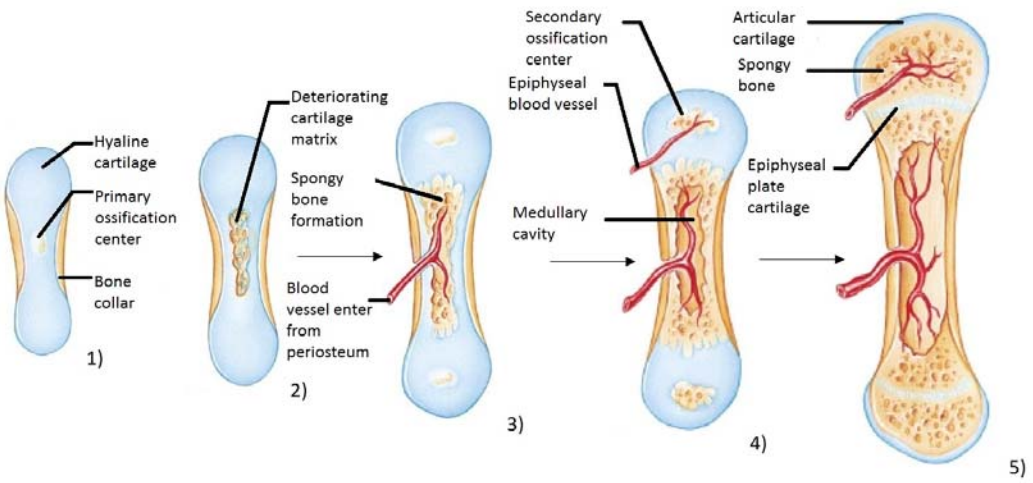

Fig. 8.5. Physiological bone growth and bone healing in fractures follow mostly an endochondral bone healing pattern, thru 1) a hyaline cartilage model and primary ossification (woven bone), 2) growth of collagen, 3) vascularization, 4) secondary ossification (lamellar bone), to finally 5) bone recontouring to gross shape. Adapted from[56].

8.4 Human vs. Animal Bone

There are generally three levels of identification that can be utilized to distinguish between bones of human and larger mammals; gross skeletal anatomy, bone macrostructure, and bone microstructure (histology). While gross anatomy differs dramatically, the differences in bone composition appear to be more of a kind of deviation rather than distinction and variances shrink still as smaller structures are considered. Animal bones have a greater density relative to size; they are less porous and are thicker in cross section than the bones of humans. Mean bone mineral density is in the range of 1.33 g/cm^3 and 0.47 g/cm^3 for primates and human (femur head), respectively.

Histologically, human share the Haversian system of bone microstructure with most animals, where differences appear in terms of ratio between primary and secondary bone. For instance, while adult human bone has a secondary osteonal structure (osteons greater than 100 μm containing blood vessels and with cement lines forming a boundary between adjacent lamellae), canine bone is found to have a mixed microstructure comprising predominantly secondary osteonal bone in the centre of cortical bone, but with, what is called plexiform bone in the areas adjacent to the periosteum and endosteum[64]. Likewise, sheep are described as having a predominantly primary bone structure with osteons less than 100 μm diameter.

In comparison, bone of smaller animals like rats and mice differ strongly in terms of mechanical strength with rats having mean BMD around 0.33 g/cm^3 for the femur. [65]. **Fig. 8.6** shows the skeletal system of rats.

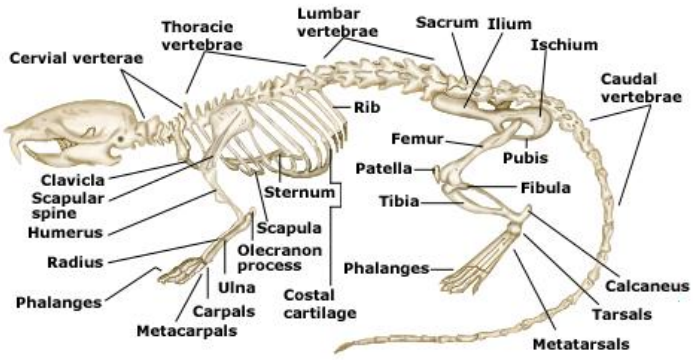

Fig. 8.6. The skeletal system of rats. Rats have 223 bones that are distributed into the axial skeleton and the appendicular skeleton.

Histologically, heavy debates characterize the discussions around similarity with human. Pearce et al. completely ignore rodents as an animal model for biomaterials research "due to significant dissimilarities between rat and human bone and the limitations of size"[66]. Others points to existence of a similar Haversian system in rats albeit much smaller in dimensions. Jowsey et al. reported in 1966 that rats have Haversian canals in the range of 36 μm, whereas rabbits, monkeys, and adult man had that of 54μm, 167 μm, and 173 μm, respectively. With this in mind we will in Chapter 1 return to important aspects in the selection of an appropriate animal model for implant research.

9 BONE HEALING AROUND IMPLANTS – A LITERATURE REVIEW

Insertion of an implant into human bone interferes with the intrinsic phases of bone remodelling presented in the previous chapter, and initiates successive bone healing processes in some way similar to when an injury or a long fracture is encountered[67]. Other models too have been proposed to examine the bone healing mechanism, including, distraction osteogenesis[68], large segmental bone defect[69], injured growth plate model[70], and marrow ablation model[71]. In all cases, a proper understanding of the recruitment of inflammatory and progenitor cells and the expression of different cytokines, matrix protein and growth factors at the implant interface – along with interaction with it – must come prior to an interpretation of the cascades of cellular and molecular signalling.

In late 1980ies, Frost consolidated the data hitherto and suggested that the sequential steps of bone healing are alike for majority of clinical problems, including fracture nonunions, osteoblastic metastases, osteotomies, arthrodesis etc.[72] The injury itself caused by the trauma initiates the release of growth factors and sensitizes the local pool of cells making them – mostly endothelial and smooth muscle cells, fibroblasts, osteoblasts, and osteoclast – more responsive to stimuli. Local mediator mechanisms facilitate the differentiation of precursors to new vessels, fibroblasts and supporting cells, which collectively form a soft granulation tissue for about two weeks. In this soft tissue, new chondroblasts and osteoblasts synthesize extracellular matrices of cartilage, and woven bone which begins to mineralize what is formed and called the *callus*. Subsequently, remodelling of the callus into new packets of lamellar bone occurs, and in this phase the marrow cavity is restored by the aforementioned remodelling BMU. Finally, the cortical-endosteal and periosteal surfaces begin to recontour their gross shape toward normal. That reshaping and sculpturing is called modelling (see also **Fig. 8.5**). This cascade lasts up to four years before complete replacement of callus with functionally competent lamellar bone has occurred.

However, in light of this we find that both intramembranous and endochondral ossification carry out healing around implants, although often one dominates the other[73]. In fact, during healing of a drill-hole, which precedes a Ti implantation, and marrow ablation injury, the intramembranous route is the principle mechanism of bone formation[74]. Following flow-diagram illustrates this route.

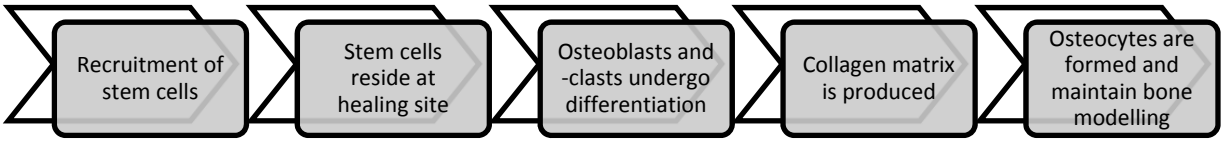

While endochondral ossification may take several weeks or years for complete replacement of cartilaginous tissue with bone, intramembranous healing occurs within few days after injury, depending on the species. Moreover, continuous movement in the tissue/implant interface will lead to a predominant formation of new local connective tissue instead of new bone, formulated as Wolff's Law[75], even if the exact mediator mechanisms are still being revealed. A certain level of mechanical loading is required for normal, healthy bone remodelling[76]. Misch observed that the change in bone strength from loading and mineralization after one year alters the stress-strain relationship and reduces the risk of microfracture during following years. Mechanical stress might induce a metabolic turnover of the bone based on the changes in osteocyte responses around the implant, resulting in bone remodelling[77].

In early 20th century, Georg Axhausen had published his classic article on free bone transplants in humans and carefully considered the morphological changes that followed[78]. He termed the special type of coupled osteoblast/osteoclast healing for creeping. However, following work of Frost and others, today the role of mediator mechanisms and autocrine-paracrine effects underlines this interplay rather than the single cell paradigm. One clinical meaning of this is that many different drugs may affect bone healing by acting in different ways on one or another healing stage or mediator mechanism.

9.1 Molecular and Mediator Mechanisms

All skeletal mediator and molecular mechanisms comprise the intermediary organisation, meaning everything that bridges isolated cells to intact organs[79]. Frost presented mediator mechanisms such as the BMU unit according to a stereo-typed sequence of "H→C→M", i.e. the histogenic, construction, and maintenance stages. We will present the sequence from histogenic stimuli, being intercellular, inflammatory, and osteogenic, toward differentiation of 'blasts to 'cytes, e.g. osteoblasts, osteocytes, etc.

First response to implant insertion is the inflammatory response mediated by hematopoietic immune cells, such as monocytes/macrophages, neutrophils and by cells from mesenchymal osteogenic lineage. Primary cytokines produced are TNF-α, IL-1β, and IL-6 which act proinflammatory with actual effecting depending on cell receptor reacted with[80]. The expression of these cytokines significantly increases during the initial inflammatory phase after bone injury

and show peak expression within the first 24 h following fracture[81]. This observation was confirmed by Omar et al., who investigated the gene expression of integrins and chemokine receptors in implant-adherent cells during early osseointegration around Ti implants. They reported a peak in expression of TNF-α and IL-1β after 24 hours of healing[82]. Others have reported that the level of expression declines rapidly to nearly undetectable values by day 3[83, 84].

In relation to bone injury, studies suggested that osteoblasts were removed from the injury site via a coordinately regulated apoptosis during bone healing[85] and evidence were found suggesting that IL-1β mediated the appearance and disappearance of osteoblasts, possibly by affecting the rates of differentiation and apoptosis[86]. TNF-α belongs to the TNF superfamily, which is recognized by more than 30 different receptors[87]. It stimulates osteoclastogenesis and bone resorption, however its function is coupled to TNF receptors on osteoblasts, which upon stimulation released an activity of increased osteoclast excavations[88]. In a growth plate injury model, TNF-α has been reported to activate p38 pathway, yet resulting in recruitment and proliferation of mesenchymal cells. And by suppressing the expression of cbfa1/Runx2, TNF-α signalling inhibited bone cell differentiation and bone formation[89].

The *in vivo* response of TNF-α has been much a matter of debate. In its effect, the function of RANK/RANKL/OPG axis has been bound with various interpretations. Osteoblasts express RANKL as a membrane-associated factor. Osteoclast precursors that express RANK, a receptor for RANKL, recognize RANKL through the cell–cell interaction and differentiate into osteoclasts[59]. OPG binding to RANKL on osteoblast/stromal cells blocks the RANKL-RANK ligand interaction between osteoblast/stromal cells and osteoclast precursors. This has the effect of inhibiting the differentiation of an osteoclast precursor into a mature osteoclast. Although some controversy exists about whether TNF-α can stimulate osteoclastogenesis by directly targeting osteoclast progenitors, it is well documented that TNF-α can stimulate osteoclastogenesis indirectly by enhancing RANKL in stromal cells and osteoblasts[90]. This effect is in fact mediated by IL-1[91]. **Fig. 9.1** illustrates the function of these and a variety of other cytokines in the maturation of and interplay between osteoblasts and osteoclasts.

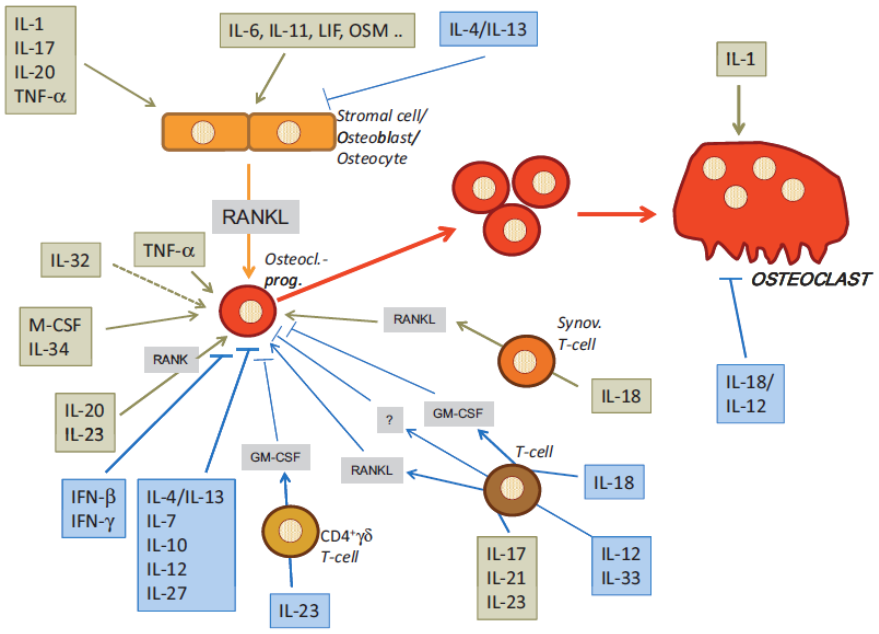

Fig. 9.1. Cytokines involved in osteoclastogenesis and the interplay between osteoblasts and osteoclasts. Reprint from[92].

The list of cytokines involved in the immediate response during the histogenic and construction stages is long and a thorough review of each is above the scope of this thesis. One subset important to address shortly is the specific category of chemokines, which further are divided into three families depending on the spacing of their first two cysteine residues: CC, CXC, and CX3C. Being recruited by leukocytes, chemokine activity leads to activation of host defence mechanisms and stimulates the early events of wound healing.

The best-characterized member of the CC chemokine family is the monocyte chemoattractant protein-1, MCP-1, also termed CCL2. In a tibial fracture site in normal mice, the expression of MCP-1 and its receptor was closely related to the recruitment and function of macrophages[93].

Within the CXC-family, IL-8 has gained attention for its involvement in neutrophil chemotaxis. More recently, stimulation of the mouse osteoblastic cell line MC3T3-E1 with IL-8 up-regulated RANKL expression at both mRNA and protein level[94], indicating the presence of functional IL-8 receptor, CXCR1, in osteoblasts and the possibility that IL-8 might enhance osteoclastogenesis indirectly. Also of interest in this family is IL-10, which is regarded as an anti-inflammatory cytokine[92]. IL-10 has been found to inhibit osteoclasts, although studies report that it does so by inhibiting maturation of osteoclasts precursors rather than effecting mature osteoblasts[95]. The interplay between inhibition of inflammation and reducing differentiation or maturation of osteoclasts, in other words inflammatory bone loss, is still not fully covered.

Another chemokine of interest for bone healing in general and around implant is CXCL12, also termed SDF-1. The coupling of SDF-1 and its receptor, the SDF-1/CXCR4 chemotaxis, is responsible for cytoskeleton rearrangements and integrin activation, which eventually leads to the directional migration of CXCR4-expressing cells towards high gradients of SDF-1. Moreover, SDF-1 stimulates chondrocyte hypertrophy, regulates BMP2-stimulated osteogenic differentiation, mediates differentiation of endothelial progenitor cells by enhancing cell adhesion and promotes early osteoclast differentiation. Also, CXCR4 regulates osteoblast development in post-natal bone[96]. The SDF-1/CXCR4 axis is also suggested to play a crucial role in homing of stem cells to site of tissue remodelling[97].

In the final discussion of mediator mechanisms, cytokines involved in the maintenance of osteogenic stimuli need attention. The markers which orchestrate differentiation along the osteogenic lineage are active at more than one cellular event. For one, ALP is involved increasing local concentrations of inorganic phosphate, destroying local inhibitors of mineral crystal growth, transporting phosphate, and in acting as a calcium binder. It is a hydrolase enzyme present in alkaline environments. Another protein involved in calcium binding in bone is OC, which however is only expressed by osteoblasts and osteocytes in bone. Whereas ALP represents an early marker during osteogenic differentiations for MSCs in vitro, and bone formation *in vivo*, OC is considered as a late differentiation marker of osteogenesis and bone formation. In the locations of intramembranous ossification during healing of femur diaphysis fracture, the expression of ALP peaked at d 5 and then declined, while OC levels were very low during the first 7 days[67]. Primary markers of relevance for understanding activity of osteoclasts are TRAP and CATK. TRAPs are a class of metalloenzymes that catalyse the hydrolysis of various phosphate esters under acidic conditions. It is primarily found in osteoclasts although a much lower level of expression has also been reported for osteoblasts and osteocytes[98]. CATK is among several cathepsins, which have been localized in vacuoles at the ruffled border membrane of osteoclasts. But unlike other cathepsins, CATK has the ability to cleave both helical and telopeptide regions of collagen I, which is major type of collagen in bone[99].

Activity of mediator mechanisms holds a complex and interdependent nature, which is known to have a temporal character. This character is very much of interest when we question the early tissue response during implant healing, such as inflammation, and when implant healing fails. In fact, a very recent review by Albrektsson et al. converge on the idea that the actual tissue response around a dental implant is merely a foreign body reaction which counts for the undisturbed osseointegration as a continued balance in form of foreign body equilibrium[100]. This

is true for a good clinical case, but as we will discuss in next secondary pathologies may compromise the healing.

9.2 Osteoporosis and Implant Healing

The mechanisms and molecular markers orchestrating bone remodelling in healthy bone or around implants that we discussed above are compromised in diseased patients. Instead, a dis-balance in the coupled bone healing between osteoblasts and osteoclast is observed. Although the balance may tilt in both directions, what patients most often suffer from is when bone quality is compromised due to excessive osteoclastogenesis, such as in osteoporosis. The impaired implant healing results in implant failure, which eventually necessitates follow-up surgeries of either oral or skeletal implants. Most importantly, the first clinical outcome of surgical procedures is the primary stability of the medical device, which consists in a rigid fixation of the implant within the host bone cavity together with a lack of micro-motion of the implant[101, 102].

Osteoporosis is a clinical condition that can compromise primary implant stability[103]. It is a skeletal disorder characterized by compromised bone strength that predisposes a person to increased risk of fractures (**Fig. 9.2**). The World Health Organisation defines osteoporosis based on bone mineral density (BMD), which must at score more than 2.5 standard deviations below the mean value of young adults (T-score). If the BMD score is between -2.5 and -1, then a diagnosis of osteopenia is made[104].

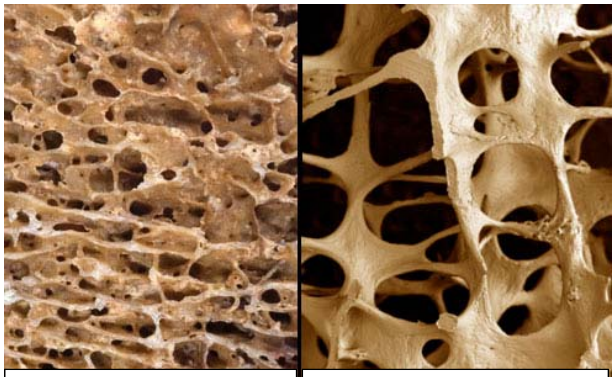

Fig. 9.2. Normal cancellous bone (left) and osteoporotic cancellous bone (right) which is much less dense, has lower BMD and hence prone to fractures.

Currently it is estimated that over 200 million people worldwide suffer from osteoporosis. Approximately 30% of all postmenopausal women have osteoporosis in the United States and in Europe. At least 40% of these women and 15-30% of men will sustain one or more fragility

fractures in their remaining lifetime. Ageing of populations worldwide will be responsible for a major increase of the incidence of osteoporosis in postmenopausal women following oestrogen deficiency[105-108].

In this discussion, it is important to discriminate failure in post-operative implant fixation (primary failure) and failure in long-term implant loosening (secondary failure). In contrast to biomechanical evidence that local osteoporosis affects anchorage of implants, this could not be reproduced in clinical studies[109]. In other words, patients with a diagnosis of osteoporosis or osteopenia were not significantly more likely to develop long-term implant failure compared to those without such a diagnosis. On the other hand, it is known that osseointegration is slower in osteoporotic subjects, with an increased rate of impaired primary implant stability both in dental and orthopaedics reconstructive surgery[110-114]. Of course, the actual preclinical model of evaluation, study characteristics of clinical trials, predispositions of patients are among many factors, which influence a generic conclusion.

10 LOCAL DRUG DELIVERY

10.1 Advancements in Local Drug Delivery

In order to obtain an improved implant healing, the hitherto development has to a large extent focused on modifications in macro and micro designs of prosthesis targeting surface topography, chemical composition and physical surface properties[28]. While this has formed the basis for perhaps first modern generation of biomaterials, the design of a new generation of biomaterials is expected to stimulate specific cell/gene responses at the molecular level. Construction of a desirable interfacial microenvironment to direct cell fate is an emerging field in biomaterials design. The convergence of technologies affords great convenience to construction of cellular microenvironment by the combining of drug/gene-delivery system matrices with biology[115]. Such delivery mechanisms were introduced to the field of bone implants in earlier 90ies with delivery of antibiotic agents (gentamicin, clindamycin) locally into bone tissue using bone-like carriers or degradable polymers[116, 117]. Peri-implant infections in particular have been much of debate[118]. Many carriers and agents have been developed. The rationale is two-fold: local consequences of systemic conditions can be addressed locally around implants with agents, or the local environment around implants can be induced more osteogenic with relevant drugs. In either ways, local delivery prolongs bioavailability and efficiency, lower systemic toxicity, and offer controlled release rate over longer periods of time and lower clinical costs.

BP treatments, which we will discuss down this chapter, were encapsulated in the local drug delivery paradigm in the beginning of this century. Simple delivery systems such as gelatin sponges with different concentrations of ALN induced reduced bone loss following elevation of a mucoperiosteal flap next to molars of the rat mandible[119]. Similar approaches were attempted but the actual bone-implant site was still not addressed in context of permanent metal implants; basically Ti implants since Ti dominated the implant field. Not until the work by Aspenberg et al. from Linköping University in 2004. Per Aspenberg together with Pentti Tengvall developed a novel routine of immobilizing pamidronate and ibandronate on stainless steel screws using cross-linked fibrinogen[120] and reported showed a 28% (p=0:0009) higher pullout force and 90% increased pullout energy for the BP coated screws, and introduced the idea that surface immobilized BPs can be used to improve biomaterials fixation in bone of male rats. Since, multiple studies confirmed success of this *patented* approach in healthy and osteoporotic animal models and in human upper jaw[121-124]. Very recently, researchers from the same group reported that local delivery of alendronate have an advantageous use when otherwise systemic treatment

bears the risk of promoting osteonecrosis of the jaw (ONJ)[125]. For discussion of ONJ see also Chapter 10.3.

10.2 Mesoporous Ti as a Drug Delivery Vehicle

Mesoporous coatings on biomaterials surfaces, as a nanoreservoir-type drug-delivery vehicle, have emerged recently and with great interest. A loading potential is gained from unique mesoporous structure (interconnected pores), large surface areas, tuneable pore size and excellent biocompatibility[126].

Mesoporous structures can be formulated in various ways, while the concept of forming it on top of biomaterials surfaces as coating gained momentum from the technology around ordered mesoporous *silica*, originally developed by researchers at Mobil Oil in 1992[127]. Different nanosized surface structures were formed: hexagonal (MCM-41), cubic (MCM-48), and lamellar (MCM-50). The technology was later extended to larger pore structures by use of nanosized *micelles* by self-assembly of amphiphilic block copolymers in aqueous solutions[128]. By linking two different polymers, one being hydrophilic the other being hydrophobic, as two unique chains, a new *block copolymer* is formed. This copolymer will have one side of its chain water soluble and the other lipophilic. The copolymer will in other words be *amphiphilic*. Following steric repulsions amphiphilic copolymers bear the property of functionalizing into cross-linked *micelles* when placed in an aqueous medium. Such micelles are spheres with hydrophobic cores and hydrophilic shells formed by either end of the block co-polymer. The hydrophilic blocks, which are often composed of poly(ethylene oxide) (PEO), can form hydrogen bonds with the aqueous surroundings and form a tight shell around the core of the micelle. In 2001, Vallet-Regi et al. revolutionized the area by proposing the mesoporous material MCM-41 as a drug-delivery system with the drug hidden in interior of the micelle and released after disruption of the shell (**Fig. 10.1**)[129]. Similar technology can now be used for the preparation of 2-dimensional mesoporous films on solid implant surfaces, often with a thickness at the order of a couple of hundred nanometres. Remarkably, this new approach is benefitting from the vacancies remained after removal of the micelles rather than the actual spherical volume.

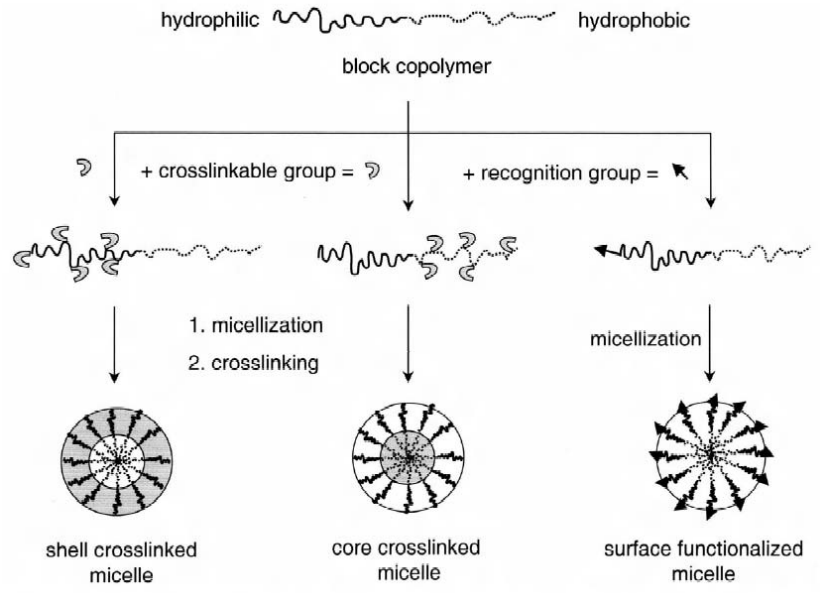

Fig. 10.1. Schematic representation of three different classes of functional amphiphilic block copolymers. Depending on the type of functionalization, either shell cross-linked micelles, core cross-linked micelles or surface functionalized micelles can be obtained[129].

In practice, mesoporous materials are often derived from supramolecular assemblies of surfactants (the amphiphilic copolymer), which template the inorganic component (commonly silica) during synthesis at surfaces. After the surfactant is removed, commonly by pyrolysis or dissolution with an appropriate solvent or by evaporation in air, the mesoporous matrices become potential drug carriers with the following features:

- An ordered pore network, which is very homogeneous in size and allows fine control of the drug load and release kinetics;
- A high pore volume to host the required amount of pharmaceuticals;
- A high surface area, which implies high potential for drug adsorption;
- A silanol-containing surface that can be functionalized to allow a better control of drug loading and release.

Large efforts have been made many research groups both in the preparation of materials with different pore sizes and in the synthesis of materials other than silica[130].

Instead of the original material silica, mesoporous *oxides* of transition-metals are of particular interest since these are easily combined with active, low molecular weight substances, hydrophobic as well as hydrophilic. While mesoporous TiO_2 was first synthesized by Antonelli et

al. in 1995[131], years passed before ordered structures were achieved since the control of crystallization of intact mesoporous structures posed a challenge. Today, highly ordered mesoporous TiO_2 thin films with relatively high anatase nanocrystal content have been synthesized[130]. Here, the photocatalytic property of anatase is of special interest.

As such, the possibility to prepare highly-ordered mesoporous TiO_2 as a drug-delivery system has gained new potentials. Whereas today the most common delivery routes are the oral and systemic administrations, the recent approach in implantology is to include drugs at the time of implantation[126]. There is though for several reasons a need to develop more efficient drug administration to sites of implantation. Then systemic side effects could be avoided, while lower and safer drug quantities would suffice with more localized efficacy and efficiency. A local administration of drugs from the specific implant-surface could provide a particularly interesting alternative to traditional medicine. Also, a systemic prophylaxis to minimize biomaterials related infections could possibly be cancelled.

Local delivery from mesoporous implants would meet the abovementioned challenges such as prolonged bioavailability and efficiency, lowered systemic toxicity, controlled release rate over longer periods of time and lower clinical costs[129, 132-134]. Mesoporous TiO_2 based matrices are in this context of particular interest due to their low toxicity, bio-stability, large specific surface area and a pore system with tuneable drug loading and release rate[135]. We refer to the latter in terms of temporal and distribution control. Because of the possibility to tailor the pore width, structure and surface chemistry they can be used for drugs with variable molecular weights, chemistry, hydrophobicity, etc., as we will see in present work.

10.3 Antiresorptive Drugs in Bone Remodelling

10.3.1 Bisphosphonate

The bisphosphonates (BPs), in the past erroneously called diphosphonates, have been known to chemists since the middle of the 19th century, the first synthesis dating back to 1865 in Germany[136]. Their use was industrial (mainly in the textile, fertilizer and oil industries) and, because of their property of inhibiting calcium carbonate precipitation, in preventing of scaling. Our knowledge of the biological characteristics of BPs dates back 30 years, the first report about them by Fleish et al., having been presented in 1968[137]. Now, for over 3 decades BPs have been used for the treatment of skeletal diseases with indications of excessive bone resorption, including postmenopausal osteoporosis, Paget's disease of bone, tumour-associated bone degradation, and hypercalcaemia of malignancy[138]. The therapeutical effect lies in their analogy

to the naturally-occurring phosphate bulbing block of hydroxyl apatite, pyrophosphate (PPi), which is an inorganic compound formed when adenosine triphosphates (ATP) are hydrolysed (**Fig. 10.2**). PPi is an important regulator of the Ca-balance in and calcification the body as it inhibits formation of hydroxyapatite in extracellular fluids. While PPi is unstable in aqueous solutions, BPs provide inhibition of formation of HA and prevent calcium precipitation without undergoing hydrolysis in body fluids. More interestingly, a long list of preclinical studies showed that BPs inhibit bone resorption *in vivo*[139-141]. It is now established that this beneficial effect of BPs can be obtained at significantly lower doses than those required for demineralization[142]. BPs reduce the number of bone remodelling sites where excessive osteoclastic destruction of bone takes place. Suppression of BP induced bone turnover by leads to overall improvement of bone strength and is reflected in reduction of fracture risk, which in turn can be attributed to improved bone mass, mineralization, and architecture[143].

Our knowledge into the mechanism of action of BPs is continuously adding up to the leading acceptance of their inhibitory effect on osteoclasts[144]. In fact, there is an emerging interest also into their effect on osteoblasts and the intriguing interrelation between bone cells[138]. And as of today, BPs can be distinguished based on their structure molecular (**Fig. 10.2**) and cellular mechanisms of action[145].

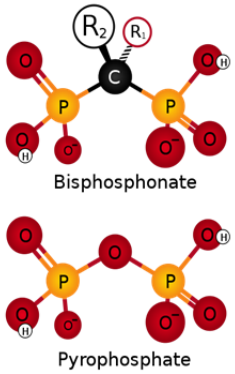

Agent	R_1 side chain	R_2 side chain
Etidronate	-OH	$-CH_3$
Clodronate	-Cl	-Cl
Tiludronate	-H	-S-  -Cl
Pamidronate	-OH	$-CH_2-CH_2-NH_2$
Neridronate	-OH	$-(CH_2)_5-NH_2$
Olpadronate	-OH	$-(CH_2)_2N(CH_3)_2$
Alendronate	-OH	$-(CH_2)_3-NH_2$
Ibandronate	-OH	$-CH_2-CH_2N$ (CH_3, $(CH_2)_4-CH_3$)
Risedronate	-OH	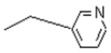
Zoledronate	-OH	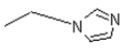

Fig. 10.2. Bisphosphonate is an analog to naturally occurring pyrophosphate, where the central oxygen is replaced by carbon with two possible side-chains attached. Depending on the side chain, R_2, Bisphosphonates are categorized into either nitrogen containing or non-nitrogen containing (notice the R_2 side chain). Source: Wikipedia.

The reported relative potency of BPs to inhibit bone resorption has been reported for etidronate, clodronate, pamidrante, olpadronate, ibandronate, alendronate, risedronate, zoledronate to 1:10:100:200-500:500-1000:1000-2000:2000:10000, respectively[146].

For ALN, for instance, a nitrogen-containing BP, the direct intracellular target is the enzyme farnesyl diphosphate synthase in the cholesterol biosynthetic pathway. This inhibition suppresses a process called protein geranylgeranylation, which is essential for the basic cellular processes required for osteoclastic bone resorption. ALN is currently proscribed clinically at an oral dose of 35-75 mg once weekly, and with a bioavailability of 0.7%. In other words, this represents an injected equivalent of less than 10 μg/kg. Research has revealed a dose-dependent manner for the biological effect of BPs. The *in vitro* effect of ALN was assessed in a study where the number of colony-forming units for fibroblasts and colony-forming units for osteoblasts were measured after administration of various concentrations of etidronate and alendronate. For the latter, a biphasic effect was observed, being stimulatory at concentrations below 10^{-7} M and inhibitory at higher doses[138]. In another study with osteoblastic sarcoma cells, MG-63, pretreatment for 4 hours with ALN at different doses (10^{-6} to 10^{-11} M) showed a dose-dependent manner for cytokine-induced IL-6 secretion with maximal effect at 10^{-7} and 10^{-8} M[147].

Adverse effects related to BP-treatment include osteopetrosis and more specifically, osteonecrosis of the jaw (ONJ). There have been reports of ONJ occurring in adult patients on intravenous pamidronate or zoledronate treatments[148]. ONJ has usually occurred in patients with malignancy type of cancer and other risk factors for osteonecrosis. However, no causal relation has been established[146]. A 2009 position paper by the American Association of Oral & Maxillofacial Surgeons, discussed that the risk of ONJ from low dose oral therapy (or slow release injectable) is between 0.01% - 0.06% for any procedure done on the jaws (implant, extraction, etc...). The risk is higher with intravenous therapy, procedures on the lower jaw, people with other medical issues, those on steroids, those on more potent BPs and people who have taken the drug for more than 3 years. The position paper recommends against placing implants in people who are taking high dose/high frequency intravenous therapy for cancer care. Otherwise, implants can generally be placed[149].

10.3.2 Raloxifene

Also other mechanisms than suppression of osteoclast metabolism can be used to treat osteoporosis. The development of SERMs, oestrogen-like agents that act both as oestrogen receptor agonist and antagonists, depending on the tissue, has shown promise in harnessing the beneficial effects of oestrogen on the skeleton without causing higher risks for breast and endometrial cancer, thromboembolic events, and myocardial infarction and stroke. This is a recognized side effect related to traditional oestrogen therapy. Raloxifene (RLX), a SERM, was developed as a bone therapeutic agent and is effective in the reduction of vertebral fractures but not in non-vertebral fractures[150]. An *in vitro* study suggested that raloxifene negatively

modulated osteoclasts while it positively affected osteoblasts[151]. Mechanism of action for raloxifene is thru the RANKL/OPG pathway in the osteoblastic lineage where inhibition of IL-6 release stays as the key step toward its antiresorptive effect *in vivo*. Receptor activator of nuclear factor (NF)-κB ligand (RANKL) is a membrane-bound protein of the tumour necrosis factor ligand family that is expressed on osteoblast cell surfaces and is along with macrophage colony stimulating factor major messenger molecules to induce differentiation of progenitor osteoclasts to mature osteoclasts. As a decoy receptor for RANKL, osteoprotegerin (OPG) can prevent its interaction with the cognate receptor RANK. Therefore, OPG is a key factor for maintaining the balance between bone resorption and bone formation. Raloxifene can stimulate the release of OPG in osteoblasts *in vitro*. Moreover, clinical data indicate that raloxifene can suppress osteoporosis through an increased OPG production by osteoblasts. However to further explore whether the anti-resorption effect of raloxifene is dependent of the OPG pathway *in vivo*, OPG knockout mouse model was used to illustrate the relationship between drug-regulated bone metabolism and the OPG pathway. And the results showed that bone mass and bone strength were increased in mice deficient in OPG after treatments with raloxifene, suggesting that raloxifene inhibits bone resorption via an OPG-independent pathway *in vivo*[152].

In another study from 2006, RLX was bonded to Ti implants thru silanisation and tested *in vitro* with MG-63 cells. By the use of DNA micro arrays containing 19200 genes, the authors identified differently expressed genes in the osteoblast-like cell line. Interestingly, expression of protein kinase C, which is involved in the mechanism of parathyroid hormone modulated IL-6 expression in osteoblasts, was increased. This leads to osteoclastogenesis and bone resorption[153].

10.4 Other Bone-inducing Drugs

What is or understanding the term “inducing” in this context? In bone-growth, osteoinduction occurs when primitive, undifferentiated and pluripotent cells become somehow stimulated to develop into a bone-forming cell lineage. One proposed definition is the process by which osteogenesis is induced[154].

For the purpose of the present thesis, we introduce three groups of substances with osteoinductive properties and of relevance for the treatment of osteoporosis: Ca-mineral and vitamin D, strontium ranelate and thyroid hormones.

10.4.1 Ca-minerals and Vitamin D

Calcium is the main osteoporosis vitamin / mineral. National Academy of Sciences recommends at least 1200 mg of calcium as a daily intake by people over the age of 50. Also, the human body requires vitamin D to be able to absorb calcium, the main constituent of bone mass. Active uptake of calcium from the diet occurs either as an active process mediated by vitamin D or passively thru diffusion.

While antiresorptive therapies for the prevention of bone fractures in osteoporotic individuals include BP and RLX, as previously described, there is today a consensus amongst osteoporosis experts that patients receiving antiresorptive and anabolic treatments need an adequate calcium intake and optimal vitamin D status to maximize the benefits. In a study by Koster et al., it was found that the etidronate was significantly more effective in patients with serum 25(OH)D ≥ 40 nmol L^{-1} than in those with levels < 40 nmol L^{-1}. The efficiency was assessed by bone mineral density (BMD) measurements at the lumbar spine and femoral neck[155].

10.4.2 Strontium Ranelate

Strontium (Sr) ranelate is a strontium(II) salt of ranelic acid medicated for treatment of osteoporosis, in particular in post-menopausal females. Although not approved by FDA, strontium ranelate is a prescription drug in more than 70 countries. The osteoinduction property of Sr is derived from the similarity between its atomic nucleus and that of Ca. Sr atoms are easily taken up by the human body and is incorporated into bone mineral and tooth enamel. In bone Sr stimulates the Ca sensing receptors, which lead to differentiation of preosteoblasts into mature osteoblasts. In fact, Sr ranelate is promoted as a “dual action bone agent” as it not only induces maturation of osteoblasts but also suppresses osteoclastogenesis thru OPG-release by osteoblasts. This in turn leads to an overall decrease of bone-resorption[156].

In a recent study, it was shown that preventive treatment with strontium ranelate (77, 154, and 308 mg/kg per day, 8 weeks) inhibited a trabecular bone loss induced by oestrogen deficiency, as shown by dual X-ray absorptiometry (DXA), bone ash, bone mineral content, and histomorphometric analysis of trabecular bone volume in the tibial metaphysis. Histomorphometric and biochemical analyses showed that strontium ranelate decreased bone resorption but not bone formation, which was maintained at a high level, indicating that strontium ranelate can exert a distinct action on bone formation and resorption[157].

10.4.3 Thyroid Hormones

The primary organ in regulation of the human metabolism is the thyroid gland, the largest endocrine gland in our body found in the neck below the thyroid cartilage. The thyroid

produces two hormones, triiodthyronine (T3) and thyroxine (T4), with the latter being the major form of thyroid hormone in blood. The production of thyroid hormones is regulated by TSH, thyroid stimulating hormone, which in turn is produced centrally by the pituitary gland, the hypophysis, placed inferior to the hypothalamus. In clinic this system is commonly referred to as the hypothalamic-pituitary-thyroid (HPT) axis. TSH is commonly subscribed to patients that suffer from hypometabolic disorders, that is when the thyroid gland is deficient in upholding normal plasma levels of thyroid hormones[145].

The role of the HTP axis in bone-remodelling has become a high profile and controversial area of research. Disruption of the HPT axis during growth strongly influence skeletal development and the effects may not be reversed fully by correction of thyroid status. Patients suffering from osteoporosis, and in particular post-menopausal women, have high risk of fractures following thyrotoxicosis[158]. The established view is that TSH is a negative regulator of bone turnover[159].

However, recent findings challenge this view. In a recent study in PNAS, the effects of intermittent TSH treatments on skeleton were addressed in oestrogen-deficient rodents[160]. Purified rat pituitary TSH was administered to ovariectomized rats at doses insufficient to affect circulating thyroid hormones. Rats were treated with TSH immediately following ovariectomy or after a delay of 7 months. TSH treatment resulted in increased BMD, the highest BMD being observed in animals treated with the lowest doses of TSH[158].

These studies suggested that TSH prevents bone loss and restores bone in ovariectomized rats, and that, in oestrogen deficiency, intermittent TSH treatment exercises both antiresorptive and anabolic actions.

11 ANIMAL MODELS IN IMPLANT RESEARCH

11.1 Rationale in Animal Models

"All animals are equal, but some animals are more equal than others."

George Orwell, Animal Farm

Development of new orthopaedic and dental implants requires intense elaboration on material stability and biocompatibility. All forms of implantations involve some degree of tissue injury which will initiate two principal reactions, *inflammation* and the complex, tissue-specific and orchestrated *wound healing*[161]. Any new candidate or optimization of an existing biomaterial must undergo rigorous preclinical testing of the biological response it elicits prior to human trials on its pathway to the clinics. Kirkpatrick *et al.* outlined three types of studies which yield data on factors influencing the biological response for materials intended for implantation in bone: studies on explanted biomaterials, relevant *in vitro* techniques and animal models[162]. As such, advocates of *in vitro* methods point at a few key requirements to be met when wanting to understand *in vivo* pathobiological reactions from cell studies: relevant cells of human origin, complexity of culture system (e.g. monolayers, co-cultures, etc.) and composition of external stimuli (growth factors, flow reactors, dynamic vs. static culturing etc.). All with the purpose to mimic the relevant site of the human body and with the clinical intervention in mind, e.g. a Ti implant in cortical bone. As an example, the common appearance of cells of the monocyte-macrophage lineage in the peri-implant tissue has led to the biological response elicited by these cells in presence of particles of prosthetic Ti. As such, *in vitro* studies have shown that particles of Grade 5 Ti (Ti6Al4V) induce the release of bone-resorbing mediators (IL-1 and IL-6) from rodent macrophages and human monocytes[163, 164]. It is now established knowledge that Ti implants possess an intrinsic pro-inflammatory property by activating the coagulation- and complement systems, as we discussed in Chapter 7.3.

However, *in vitro* characterization is not able to demonstrate the *tissue* response to materials. It is rather confined to the response of individual cell lines or primary cells taken from animals to a certain stimuli. When particular intercellular mechanisms or signalling pathways are in the pipeline of the research, co-culture models or tissue homegenates provide specific information. It is now established, for example, that the more potent nitrogen-BPs (N-BPs), such as pamidronate and zoledronic acid, and alendronate (ALN) used for treatment of osteoporosis inhibit osteoclast function by acting as potent inhibitors of the enzyme farnesyl diphosphate (FPP) synthase in the cholesterol (or mevalonate) biosynthetic pathway[165, 166] (see also Chapter

10.3.1). However – although cellular experiments will provide conformity as to cytotoxicity, genotoxicity, cell proliferation and differentiation adjacent to a material surface - *in vitro* assays may also overestimate the level of material toxicity. Also, due to the shorter lifespan of cultured cells (*in vitro* specialists converge around developing immortalized cell lines[162], *in vitro* methods are beneficial in acute studies of the effects of toxicity of material surface modification, drug delivery, or any implant modality. Finally, for the assessment of the biomechanical stability of implants, it is pivotal to produce a physical load that stimulates the *in vivo* situation. Other than few exceptional *ex vivo* systems approaching such physiological loadings[167], *in vitro* models generally comes to short in this question and leave animal studies as the preferred pre-clinical test model.

Although a proper cellular experiment with relevant cell source, cultivation conditions (2-D and 3-D) and extrinsic stimuli will certainly provide strong evidence for the cytocompatibilty of the material in choice, the cardinal rationale for favouring an *in vitro* assessment *before* animal studies is presumably to be understood from the philosophy of the 3R's: replacement, reduction and refinement[168]. In other words, animal trials should be *replaced* if possible, *reduced* to lowest reasonable number of animals and *refined* to avoid excessive sacrifice and inconclusive result acquisition.

The US Food and Drug Administration (FDA) recommends in its Guidelines for preclinical and clinical evaluation of agents used in the treatment or prevention of postmenopausal osteoporosis that:

> *"agents be evaluated in two different animal species, including ovariectomized rats and a second, non-rodent large animal model which possesses Haversian systems and remodelling patterns similar to the human situation"[169].*

Although this guidance counts drugs and chemical agents, the FDA regards a bone implant as a medical device, which is subjected to similar regulations[170].

11.2 Selection of an Animal Model

Animal models allow evaluation of biomaterials in a biological environment that largely resembles the healthy human body. By selecting of a proper animal model and loading vs. unloading conditions of a bone implants the local response in the vicinity of the implants can be evaluated with respect to implant safety and efficacy. A long list of cellular, molecular and biomechanical parameters is possible to evaluate, including temporal effects and bone response in the immediate vicinity of the implant, or in remote locations. Moreover, animal models can be

designed to stimulate the osteopenic pathophysiology secondary to implantation, such as osteoporosis. While animal models may closely represent the mechanical and physiological human clinical situation, it is only an approximation of the human patient, and each animal model has unique advantages and disadvantages.

When planning for an animal model some important considerations should be done: costs to acquire and care for animals, availability, acceptance by the society, species tolerance to captivity and ease of housing, which all are parameters governed by the a Federal Animal Protection Act. In Sweden, this is covered by regulations from Medical Products Agency (Läkemedelsverket). Other factors prioritized are: low maintenance care, ease of handling, resistance to infection and disease, interanimal uniformity, biological characteristics and analogy to humans, tolerance to surgery, adequate facilities and competence of support staff, and access to databases with biological information[66]. In studies where specifically the bone-implant interactions are addressed, an understanding of the species specific bone characteristics including bone microstructure, composition, modelling and remodelling properties is important for the evaluation of the phyletic generality of results and validity to humans. Also, the lifespan of the animal should be suitable for the duration of the study.

In international standards, species suitable for testing of bone implants primarily include dogs, sheep, goats, pigs, rabbits and – to an intemperate debate – rodents such as rats and mice. **Table 2** below summarizes the primary characteristics of animals used in bone research in comparison with human with respect to bone macro- and microstructure, -composition and –remodelling characteristics[171].

Table 2 Characteristics of the most common animals in implant research in comparison with humans. + least similar, ++ moderately similar, +++ most similar. (BMD=bone mineral density, IGF=insulin like growth factor). From[66]

Animal	Usage	Macrostructure	Microstructure	Bone composition	Bone remodelling	Conclusion
Dog	Often used in dental research. 9% of orthopaedic studies [Martini from [66]]	++ Commercially available implants. Quadrupedal gait loading. Most similar to human body.	++ Mix of secondary osteonal structure and laminar bone but generally similar to human.	+++ Weight, hydroxyproline, extractable proteins and IGF-1 content similar to humans.	++ Bone-turnover rate is much faster in dogs than in humans.	Resemblance to human anatomy, usage depends on study duration. Companion animal, ethical issues.
Sheep	Usage similar to that of dogs, 9-12% of orthopaedic research.	+++ Similar body weight and bone dimensions to that of humans.	+ Predominantly primary bone, but Haversian modelling at older age.	++ Shows higher density and greater strength. Location matters significantly.	++ Bone remodelling closest to humans, aged sheep is suitable for osteoporotic bone.	Bone turn-over similar to humans, and more often preferred over dog model due to ethics.
Goat	Use in cartilage, meniscal and ligamentous repair.	+++ Similar to sheep. Multiple, commercial implants possible.	+ Haversian system is not homogenous with lamellar bone in caudal sectors.	++ Similar to sheep and resembles human bone.	++ Suitable for implant studies and bone grafts.	Choice between sheep and goat matters availability, mobility, etc.
Pig	Small pigs overcomes problem with weight but difficult to handle.	++ Denser trabecular network but significant similarity in femoral cross-section.	++ Similar to humans. Haversian/lamellar bone network.	+++ Similar to human bone.	+++ Rate of bone regeneration more similar to humans than dogs.	Although the animal with most similarity with human, not often chosen for practical reasons. Suitable in blood compatibility testing.
Rabbit	35% of musculoskeletal research. Difficult with multiple implants.	+ Dissimilar to human bone.	+ Purely primary bone structure, osteons run parallel rather than centric.	++ Generally dissimilar to human but BMD similar in mid-diaphyseal bone/	+ Much faster bone turn-over but suitable for implant screening before larger animal testing.	Comes under purview of local ethical committee.
Rat	Preferred model for screening in osteopenia.	Dissimilar to human bone.	Haversian model exist to a low degree.	Much higher concentrations of IGF-1 and extractable proteins.	The fastest bone turn-over rate with similar mechanisms in early life.	Least similar bone characteristics, but available, ethically feasible and cost-effective.

The mineral composition of humans and animals is similar[172]. On the other hand there exist significant differences in bone anatomy and the remodelling characteristics between large animals and rodents in comparison to humans. In particular, the lack of Haversian modelling system in rodents (rats and mice) is a matter of debate since the 1960ies. Some investigators show species chauvinism and require that animal models must be isomorphic in all respect with the human condition, which is being modelled. However, we shall appreciate that there is no perfect animal model, and that 1) no single model is appropriate for all purposes, 2) no model can be dismissed as inappropriate, and that 3) the research field as a whole must exploit diverse models. One shall emphasize the need for multiple animal models, but at the same time show caution against a prior exclusion of any particular animal model.

Among possible animal models discussed above, the rationale for the selection of larger animals lies in the similarity to humans in bone architecture and dimensions– considering *implant stability*. Larger animals (dogs, sheep, goats, and pigs) provide the possibility to use commercially available implants (implants > 6 mm in length is not possible in rabbit lone bones) and even multiple implants in same bone location (max 6 implants per rabbit, International Standard ISO 10993-6, 1994). More importantly, although bone-turnover rate varies between species, the fashion of remodelling – namely secondary bone building in BMUs called osteons – in larger animals is similar to that in humans. For this reason, as mentioned above, rats are often considered non-suitable in implant research. On the other hand, although the rabbit model is often discussed as the preferred due to similarities in the bone modelling with humans[173], the rat model provides the benefits of accessibility, cost-effectiveness, ethical ease – yet not significantly compromising phyletic generality with larger animals and humans. Frost et al. concluded in 1990ies, that the rat model may provide a very useful model for human osteopenia and for some other currently important human skeletal problems, e.g. osteoporosis[174], hence the FDA recommendation. Today, since implants can be custom made in appropriate sizes, and benefits in cost-efficiency and ethical ease are considered, the rodent model is often preferred for the screening of bone anchored implants [73].

11.3 The Ovariectomized Rat Model

As we discussed in Chapter 9.2, osteoporosis possess a challenge in primary implant fixation. Fracture and implant research is often performed in an osteoporotic animal model in order to approach the clinical situation as much as possible. This is also recommended by FDA as mentioned above. In comparison with human bone specimens or *in vitro* models, an animal

model provides effects of central control of bone turnover and feedback mechanisms involved in physical activity[175].

Osteoporosis or osteopenia in animal bone can be induced in various ways, including change of diet[176], administration of drugs (in particular corticosteroids)[177], immobilisation[178], and breeding[179]. Loss of oestrogen seems to be the most important mechanism causing osteoporosis. The ovariectomized rat is the animal model studied most for osteoporosis[65]. This model mimics postmenopausal cancellous bone loss when examined over relatively short periods of time. Following ovariectomy, removal of the ovaries, this model shows a biphasic loss of bone, with an initial rapid phase of bone loss up to 100 days, followed by an intermediate period of relative stabilization of cancellous bone volume at an osteopenic level. After 270 days, a slow phase of bone loss occurs, during which cancellous bone volume declines[180]. However, the total loss of bone mineral density is less than the loss seen in humans. Also, observation periods of 12 months and more have revealed higher values of bone mineral content, bone area and body weight for ovariectomized rats than are seen in humans[181].

In conclusion, important requirement for an animal model to perform research in implants for osteoporotic patients include in addition those discussed in previous chapters implant dimensions, intracortical bone remodelling, and model reproducibility. Ovariectomized rats should provide a good model for human osteoporosis and osteopenia[174].

12 MATERIALS AND METHODS

12.1 Implant Preparations and Characterizations

In study I optically smooth Ti surfaces were prepared on clean silicon wafers in an evaporation chamber with final pressure below $1x10^{-8}$ Torr. Approximately 200 nm of medical grade titanium grade IV (ca. 0.18 % O_2) was then physical vapour deposited (PVD), and thereafter spontaneously oxidized at room conditions. Thru studies II-V machined and spontaneously oxidized Ti implants were used as the base implant material. In study II, machined c.p. Ti implants with a thin layer (7–10 nm) of amorphous oxide in the as-machined state were used as the control. The implants were cylindrical threaded screws, 3.2 mm long (Ø = 2.0 mm) and with an external quadrant head for screwing (produced at University). In studies 3-5, cylindrical, threaded screws with a length of 2.3 mm (Ø = 2.0 mm) were machined from medical grade Ti (grade IV) rods (Elos Pinol, Gørløse, Denmark) and fitted with an internal hexagonal hole at the top (**Fig. 12.1**). Implants were cleaned in a series of hexane–acetone–ethanol and distilled water in an ultrasonic bath and dried under nitrogen gas.

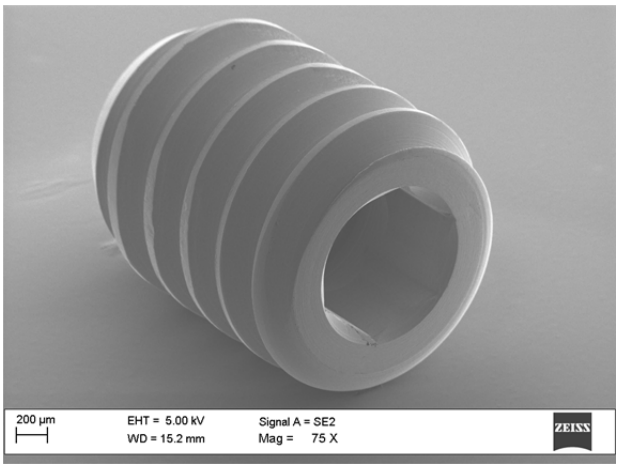

Fig. 12.1. SEM image of Ti implants used in studies 3-5. L=2.3 mm, Ø=2.00 mm, fit: internal hexagonal in top (Elos Pinol, Gørløse, Denmark).

12.1.1 *In situ* Coating of Implants

In studies I-II, immune-positive control surfaces were prepared by immobilizing a thin IgG coating of ~2 nm on the surface. The adsorption procedure was similar in both studies. The immobilisation was performed by silanisation of Ti screws/Ti coated wafers, followed by incubation in a dialdehyde solution. In brief, surfaces were first immersed in 0.05% v/v APTES ((3-aminopropyl) trimethoxysilane, 97%; Aldrich) in pure (dry) xylene for 30 min. After rinsing in xylene, 70% ethanol and drying, the samples were immersed in 0.1% v/v diglutaraldehyde

(Sigma Aldrich) in PBS for 10 min. After a repetitive rinsing procedure in PBS, the implants/wafers were immersed in a solution of 1 mg/ml IgG (rabbit anti-human IgG, DAKO A/S, Denmark) in PBS for 5 min, rinsed in PBS and distilled water and dried. The organic layer thickness after the silanisation and IgG immobilisation processes was measured by null ellipsometry (see following chapter). Both the machined and machined plus PVD-coated Ti implants were sterilized by immersions in 70% ethanol. The IgG-coated surfaces were sterilized prior to the coating procedure and kept in sterile glass tubes until surgery. The UVO-treated surfaces were sterilized in the UVO chamber.

12.1.2 Determination of Proteins on Thin Films

Adsorption of blood plasma proteins and complement factor antibodies in study I were quantified by *in situ* null ellipsometry (Rudolph Research ELL III, USA; k = 632.8 nm). In study II, quantification of the immobilized IgG-layer on similar surfaces was also determined by ellipsometry. Measurements were done on flat reference surfaces (silicon wafers PVD-coated with 200 nm Ti), owing to the complex geometry of screw shaped implants.

Ellipsometry is a common optical technique for measuring thin films and bulk materials. It relies on the polarization (behaviour of electromagnetic waves in space and time) changes caused by reflection or transmission from a material structure to deduce the material's properties. Whereas light has completely random orientation and phase, i.e. unpolarised waves, ellipsometry benefits from traceability and specificity of polarized light, which is elliptical in polarization, i.e. waves of arbitrary amplitude and phase (**Fig. 12.2**).

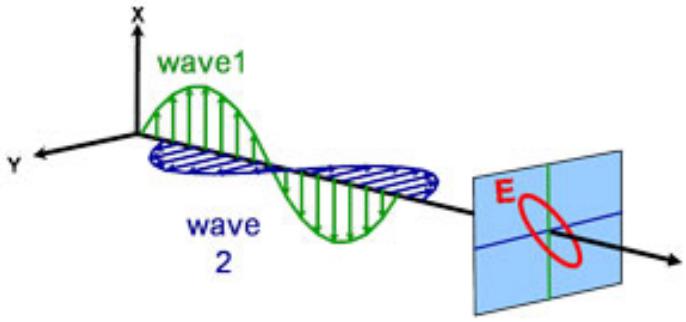

Fig. 12.2. Light waves of arbitrary amplitude and phase are elliptical in polarization.

When polarized light interacts with material, it is either reflected or refracted (transmitted) and a change in polarization follows. This change is represented as an amplitude ratio, Ψ (psi), and the phase difference, Δ (delta), which is function of material thickness and optical constants of all layers in the material, i.e. underlying base-material, adsorbed proteins, molecular

contamination, etc.[9] The primary tools for collecting ellipsometry data all include the following: light source, polarization generator, sample, polarization analyser, and detector. In our equipment, monochromatic light was emitted at λ=632.8 nm by a He-Ne laser. Ellipsometry is typically used for films whose thickness ranges from sub-nanometres to a few microns. As films become thicker than several tens of microns, interference oscillations become increasingly difficult to resolve, except with longer infrared wavelengths. Other characterization techniques are preferred in this case.

When optical properties (refractive index or dielectric constant) of the film and molecular layers on top are assumed constant/homogenous as we did in our case, i.e. proteins share refractive index with oxides around $\tilde{n}$ = 1.465[182], the ellipsometrical constants, Psi and Delta, can be converted to total thickness of protein film using the McCrackin equation[183]. In study I and II, we had software to perform this. In other, more advanced setups, the refractive index of the material is calculated thru a regression analysis over multiple angles of reflection.

12.1.3 UV-illumination

The effect of UVO treatment was investigated upon illumination for 96 h in a UVO preparation chamber (Jelight Company Inc., Irvine, USA) (immune negative test surfaces) (**Fig. 12.3**). The wavelengths of the emitted light were 253.7 nm (81% of irradiated light energy) and 184.9 nm (19%), respectively. PVD-coated samples were then placed within 2 cm of the lamp (Novakemi AB, Handen-Sweden), with maximum UVO-chamber temperature ~95°C (368 K). The illumination was programmed such that it ended shortly before surgery. As photocatalysis is a reversible process, this way the optimal effect of illumination could be preserved.

Fig. 12.3. The UVO-chamber emits light at 184.7nm and 253.7nm (Jelight Company Inc., Irvine, USA).

12.1.4 Synthesis of Mesoporous TiO_2 films on Ti

Cubic mesoporous TiO_2 films were prepared by EISA[184]. The cubic pore structure was chosen in order to ensure that the pores were directed out from the surface. In the inorganic precursor solution, 4.2 g titanium tetraethoxide (TEOT) was dissolved in 3.2 g HCl, and 1.0 g poly(ethylene oxide)–poly(propylene oxide)–poly(ethylene oxide) (EO20PO70-EO20), Pluronic P123, in 17 g ethanol. The solutions were vigorously stirred and mixed together[130, 185]. Spin-coating at 6500 rpm (60 s) was used for the prepare thin sol-gel films on glass slides, titanium discs, a quartz crystal microbalance with dissipation monitoring (QCM-D) sensors and screw shaped titanium implants (**Fig. 12.4**).

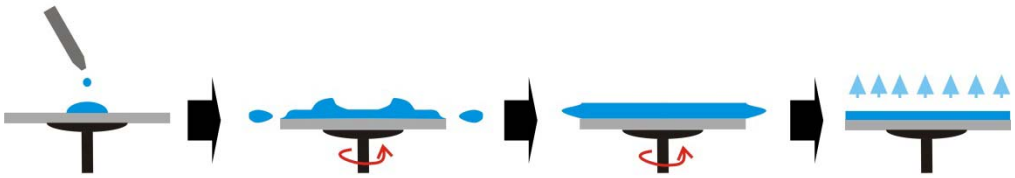

Fig. 12.4. The principle of Evaporation Induced Self Assembly (EISA). The *sol* with all the ingredients is deposited on sample of interest positioned on a spin-coating platform. During spinning the *sol* is spread and the alcohol is evaporated. This is when the self-assembly occurs.

Surfaces or implants were stored at room temperature overnight to achieve complete self-assembly of the template, pluronic polymer P123, and evaporation of ethanol and hydrochloric acid. Calcination was thereafter performed by heating to 350°C, with temperature ramping 1°C/min, followed by a constant temperature held for 4 h, and finally left for spontaneous cooling to room temperature. During the calcination, the template (P123) was removed, and the crosslinking density of the TiO_2 matrix was increased[135]. The procedure resulted finally in an Anatase type crystal structure. For comparison, nonporous TiO_2 films were formed using the above described procedure, but with the difference that no Pluronic was added to the reaction mixture.

12.1.5 Characterization of Implants

In all studies, implants were thoroughly characterized in terms of surface roughness, topography, wettability, ultrastructure, crystallinity, and chemistry. The methods in use were Light Optical Profilometry, Scanning Electron Microscopy (SEM), contact angle measurement, Focused Ion Beam (FIB), Transmission Electron Microscopy (TEM), X-ray Diffraction (XRD), and X-ray Photoelectron spectroscopy (XPS), respectively. Moreover, porosity was assessed by nitrogen adsorption and Small Angle X-ray Scattering (SAXS). While most of these methods are traditional analytical tools, we will describe how we analysed the bone-implant interface in

details with respect to topography in FIB-TEM, and how we performed elemental analysis by Energy-dispersive X-ray Spectroscopy (EDS) in Scanning TEM mode. It should be noted, that we along the way made use of model surfaces like flat Si wafers coated with Ti rather than actual screw-shaped Ti implants due to geometric limitations of some of the methods, such as contact angle measurement.

The physical principle of Focused Ion Beam (FIB) is similar to SEM, except from that it uses an ion beam rather than an electron beam. When operated at high beam currents, the ionic bombardment is used to sputter or mill a specimen, in this case the interface between bone and implant or between Ti and mesoporous coating, to subsequent imaging in SEM and TEM. At higher primary currents, a great deal of material can be removed by sputtering, allowing precision milling of the specimen down to a sub micrometre or even a nanoscale. The advancement used in our approach, which Anders Palmquist from Gothenburg, co-supervisor of this thesis, developed in his thesis in 2008, is the novelty around using FIB to prepare sections *in situ* which are imaged in same instrument rather than in a separate SEM instrument as previously described[186]. In brief, the region of interest is protected by platinum deposition, rough trenches are milled on either side using high ion beam current. A micro manipulator is attached to the lamella, which are subsequently cut free and transferred to a TEM grid. Final thinning is done using a decreased ion beam current, until a final thickness of roughly 100 nm is obtained. The FIB system used was a Strata DB235 FIB/SEM (FEI Company, The Netherlands), equipped with a FEG SEM and a Liquid Gallium source, operating at 5 kV and 30 kV, respectively. **Fig. 12.5** shows the principle in the sectioning and imaging of a mesoporous Ti coating interface.

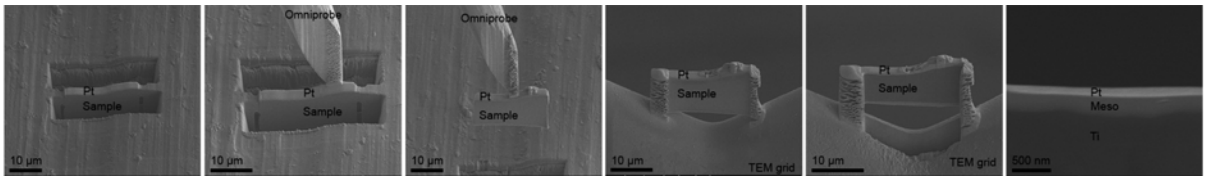

Fig. 12.5. Step-wise sectioning of sample (protected by a Pt coating) of Ti implant coated with a mesoporous coating, which is performed and analysed under SEM. Courtesy of Anders Palmquist.

The analysis in TEM was done in both bright field mode (BF-TEM) and high angle annular dark field scanning mode (HAADF-STEM), in order to obtain high resolution, increased contrast and minimizing the beam damage. In order to further understand the bone-implant interface at a submicron level, we combined elemental analysis with electron microscopy using EDS in STEM mode. The physical principle in EDS is to benefit from the characteristic pattern of excitation of electrons and the energy released in form of x-rays when that electron is replaced by energy

from a higher energy-state. This pattern is individual for all elements and specific electrons, which are excited during a high-energy beam from an electron or x-ray source. The radiation energy (KeV) released from an electron "relaxing" into a lower energy level is measured by an energy-dispersive spectrometer, which upon comparison with a computerized reference spectrum reports the amplitude and presence of an element, e.g. Ti, P, O, Ca. EDS can be combined with STEM, where the electron beam is narrowed to a spot, which is scanned over the sample in a raster. High-angle detectors make the imaging possible in conjunction with elemental analysis. The microscope used was a Tecnai G2 20 (FEI Company, The Netherlands), equipped with a LaB6 filament operating in 200 kV acceleration voltage. See also Fig. 8 in Study III (or **Fig. 14.8**).

12.2 Drug Loading and Release

In studies 3-5, Ti implants with mesoporous coatings were loaded with ALN or raloxifene (RLX). ALN and RLX were absorbed into hydrophilic and hydrophobic mesoporous TiO2 films, respectively. Their respective water solubilities were 10 mg/ml and 0.25 mg/ml. Since the polarity of RLX is lower than that of ALN, mesoporous films were methylated with dichlorodimethylsilane (DDMS, 1% methanol, 30 min). RLX (0.8 mg/ml) was then absorbed and dissolved in methanol (0.8 mg/ml) and loaded into the hydrophobic pores (RT, 1 h). ALN was dissolved in and absorbed from Milli-Q water (0.8 mg/ml, RT, 1 h).

The *in situ* absorption and release rates of ALN and RLX were measured by QCM-D[187]. The measurements were performed with a Q-Sense E4 instrument (Q-Sense, Stockholm, Sweden). Mesoporous and nonporous TiO_2 thin films were prepared on QCM-D sensors (QSX 310, Q-Sense, Sweden). In the ALN experiments, a flow of Milli-Q H_2O was first passed through a sample chamber into which both the test and control samples were inserted. Upon a stable baseline, ALN solution was added, and absorption followed by changes in frequency (Df, Hz) and energy dissipation (D). The frequency shift (Df) corresponds to the amount of absorbed/released substance and was converted to mass (ng/cm^2) by the Sauerbrey equation[188]. After 15 min of absorption, rinsing was applied with Milli-Q water, and ALN desorption monitored by following f(t) and D(t). In RLX experiments, DDMS hydrophobized mesoporous and non-porous sensors were inserted into the flow modules. A flow of methanol gave a stable baseline. The flow was then switched to a flow containing 0.8 mg/ml RLX, and monitored for 2.1 h, followed by rinsing in methanol. The flow rates were 50.0 ml/min.

12.3 Sterilization and Evaluation of Contamination

Implants were sterilized during the heat treatment process, which provided a clean environment at temperatures above the traditional autoclave sterilization (120°C). From retrieval at this point till surgery implants were kept in aseptic storage, which were sterilized prior to packaging. A sample batch was kept to test for presence of toxic residues of bacteria, endotoxins. Endotoxin is used synonymously with the term lipopolysaccharide (LPS), which is a major constituent of the outer cell membrane of Gram-negative bacteria. In 1970 Hausmann et al. reported that endotoxin from *Bacteroides melaninogenicus* stimulated bone resorption in fetal rat bones[189]. Since then, several studies have shown that LPS can activate bone resorption *in vitro* and *in vivo*. In our studies, the endotoxin contamination test was done according to routine FDA protocol (Sahlgrenska Hospital, Gothenburg, Sweden) with Limulus Amebocyte Lysate (LAL test), and showed values below the recommended maximal level of 1.25 EU per rat (250 g).

12.4 Animal Surgery

As discussed in Chapter 1, the benefits and challenges of the rat model were considered. In our laboratory, we believe that the advantages of availability, practical feasibility and ethical ease of the rat model provide an excellent model for screening of implants for bone research. As such, in all *in vivo* studies a model of male or ovariectomized rats was used. In studies II-IV, mature male rats 3 months of age and in study V ovariectomized rats of 3 months of age comprised the animal model. In all studies, the animals were of Sprague-Dawley strain. **Table 3** summarizes the scope of the animal studies.

Table 3 Summary of animal studies in studies II-V. In studies II-IV rats were delivered by Tacomic, Denmark, whereas in study V rats were from Harlan Laboratories B.V., Netherlands. All in strain Sprague Dawley. *In addition to materials characterization.

Study	Animal (rats)	Scope	Hypothesis/ Question	Analysis*
II	Male, 3 months old.	44 rats, 4 groups (n=8), 2 implants/tibia. Time points: 1d, 7d, and 28d.	Mild heat or UVO-illumination decreases complement system activation at surface. This is positive for Ti-implant healing in bone.	RTQ, qPCR, histology, histomorpho metry.
III	Male, 3 months old.	32 rats, 4 groups (n=8), 1 implant/tibia. Time points: 1d and 28d.	Local delivery of ALN and RLX from mesoporous Ti implant and healing in bone.	RTQ, qPCR, histomorpho metry.
IV	Male, 3 months old.	20 rats, 2 groups (n=4), 1 implant/tibia. Time points: 28d	The local distribution of ^{14}C-ALN ex vivo.	Autoradiograp hy (^{14}C is a β-emitter), liquid scintillation.
V	Ovariectomize d 1 month before surgery, 3 months old.	32 rats, 4 groups (n=4), 1 implant/tibia. Time points: 28d	Comparison of implant healing between local vs. single systemic delivery of ALN.	RTQ, μCT, histomorpho metry..

The following subsections will present each *in vivo* protocol in order of implementation from preparation to analysis.

12.4.1 Surgical Procedures

The animals were delivered to animal facility centre (Laboratoriet för Experimentell Biomedicin (EBM), University of Gothenburg) and kept for one week before surgery in order to habituate the animals to the surroundings. In study V animals were delivered one week after the ovariectomy (OVX) and kept for 4 more weeks prior to implantation in order to let the animals heal and arrive to osteoporotic bone level[190]. Animals were fed on a standard pellet diet and water and taken care by professional caretakers and the project personnel during the project periods.

In all studies, the animals were anaesthetized by isoflurane inhalation (Isoba Vet, Schering-Plugh Uxbridge, UK) using the Univentor 400 anesthesia unit (Univentor, Zejtun, Malta). Prior to implantation, rats were shaved and cleaned (5 mg/mL chlorhexidine in 70% ethanol) around implantation sites and then given one 0.1 mL subcutaneous injection of anaesthesia (Xylocain)

locally in lower leg in proximity to the tibia. Xylocain also served as a vasoconstrictor preferably to lower blood flow and bleeding in site of implantation.

The site of implantation and groups of implants were decided according to a predetermined schedule ensuring randomization and rotation. The anesthetized animal was placed in dorsal recumbency with tail towards the surgeon. The medial aspect of the proximal tibial metaphysis was exposed through an anteromedial skin incision followed by reflection of skin and periosteum as tissue was dissected. Screw installation site(s) were prepared with Ø 1.4 mm and 1.8 mm round burs under profuse irrigation with 0.9% NaCl. The two-stage drilling procedure was chosen in order to avoid excess heat formation and to lower the risk of unforeseen fractures or other means of compromising bone quality. Implants were screwed into holes drilled in the tibia in this sequential order using screwdriver with internal quadrant (study II) or external hexagonal (studies III-V) (**Fig. 12.1**). Site of implantation was either proximal and distal tibial metaphysis (study II) or solely single medial tibial metaphysis (studies III-V). Following insertion, the subcutaneous wound was closed with resorbable sutures made of polyglactin in simple interrupted square knots (5-0, vicryl, Ethicon, Johnson & Johnson, Brussels, Belgium) (**Fig. 12.6**) and the skin with non-resorbable nylon suture (4-0, Ethicon) holding the tissue tied in a subcutilar fashion thru the dermis and dermal/epidermal junction. The subcutilar suture was preferred in order to avoid risk of wound dehiscence from scratching by the animal.

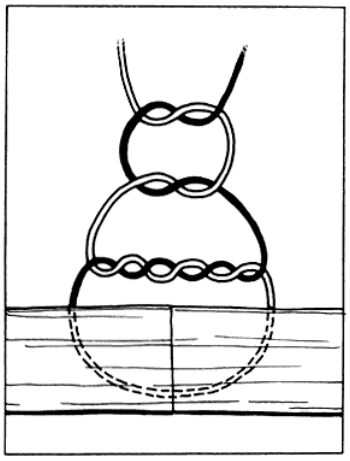

Fig. 12.6. Illustration of a square knot suturing connective ends of tissue

Finally, each rat were given one injection of 0.3 mL analgesic (Temgesic 10%, 1.0 ml/kg) subcutaneously thru the neck skin and return to original cage to be in thru implantation period allowed free postoperative movements with food and water *ad libitum*.

Animals at EBM were under surveillance of the PhD-student and staff during this period. In any matter of disturbance, e.g. wound dehiscence, swelling, etc., a veterinarian was consulted and appropriate action was undertaken, e.g. re-suturing in case of ethical and medical feasibility, or alternatively euthanization of the animal in concern.

Upon retrieval, each rat was anaesthetized with a 0.5 mL mixture of pentobarbital (60 mg/mL), sodium chloride, and diazepam (1:1:2) and then sacrificed giving an intraperitoneal overdose injection of 3 mL of sodium pentobarbital (60 mg/mL, ATL Apoteket Production & Laboratories, Kungens Kurva, Sweden) in 50 % saline. Following heart arrest, wound and bone were dissected and the implant retrieved by relevant methods for the concomitant analysis in intention. The next section explains this in short. Finally, if necessary, organs of interest were dissected and retrieved prior to finalization of the surgery.

12.4.2 Harvesting the Implant for Analyses

Implants were destined in two categories of analyses: first, the RTQ/qPCR/SEM group, where the implants were unscrewed and retrieved, and secondly the histomorphometry/ immunohistochemistry/µCT group, where the implants were kept in bone and retrieved *en bloc* for further fixation and processing. In other words, individual groups of implants were implanted for each group, which in fact also doubling the number of implants in the study.

We performed in all studies a biomechanical testing of implant anchorage by measurement of the removal torque (RTQ). With the implant area exposed, the animal was placed under the RTQ-tool and removal torque measured. Following this, implants were unscrewed with adherent cellular and tissue debris and either placed in RNA*later*® (Life Technologies Europe BV, Stockholm, Sweden) solution to immediately stabilize and protect cellular RNA for qPCR analysis or formaldehyde for analysis in SEM. When peri-implant tissue gene expression was of interest , a trephine with internal Ø 2.3 mm was used for the retrieval of biopsies from the implant site. Approximately 0.3 mm of implant surrounding bone was then transferred to RNA*later*®.

For histomorphometry and immunohistochemistry, implants were kept in position and cut out *en bloc* in ca. 5 mm sections and immediately placed in formaldehyde for fixation prior to further processing.

12.4.3 Hysterectomy of Rats

In study V, the uterus of a group of eight ovariectomized (OVX) rats were removed and collected (hysterectomy) 4 weeks after OVX and compared in terms of change of weight with healthy

females. In short, the euthanized animal was placed in dorsal recumbency with tail towards the surgeon. The abdominal area was shaved and swabbed with surgical scrub (iodine and alcohol). A 2-4 cm midline incision was made from the midpoint of the abdomen to a point anterior of the urethral opening through the skin and abdominal wall exposing the peritoneal cavity. The uterine horns are retracted to identify the wound from the OVX. The anterior end of each uterine horn was incised from the wound tissue of the oviducts. Using scissors, the cervix was cut anterior to the ligature and both uterine horns were removed. The isolated uterus was dried overnight in air and weighted.

12.4.4 Blood Collection, and Injection

In study V, it was originally intended to measure any outburst of acute phase response (APR) after local delivery from mesoporous implants or systemic delivery of ALN. Rat blood was therefore analysed with respect to a handful symptomatic markers. But due to unfortunate complications with ELISA, the actual blood values were not achieved, and APR was not assessed. Instead, we choose to present the method. Intravenous blood was collected from the tail veins at time of implantation and then daily for 3 days. Each time, the animal was kept conscious and held in position in a rat-restrainer (LE5054, AgnTho's AB, Lidingö, Sweden). A hole at the base of the door of the restrainer allows the whole tail be available for both injection and blood collection (**Fig. 12.7**).

Fig. 12.7. Restrainers for rats of different sizes. To the left model LE5024 for rats between 300-440 grams (AgnTho's AB, Lidingö, Sweden).

An infrared light was kept in safe distance above the animal to keep it warm and to ensure vasodilation for a better collection. Animal was covered to avoid irritation from the light as rats have very sensitive eyes. Furthermore, the tail was warmed in a warm water bath while rubbing down it and the base of tail was kept compressed using a home-made tourniquet. The tail vein

was accessed with a delicate venipuncture using a 23G needle from a blood collection kit (Safety-Multifly® 23G, Sarstedt, Nümbrect, Germany) with the tube of kit cut shorter. In puncturing the skin, needle was held as parallel as possible to the tail and lowered to minimize angle of puncturing. Blood was collected in microtubes for serum collection with a clotting activator inside (Serum Z/1.3, Sarstedt, Nümbrect, Germany) and left for clotting for two hours at room temperature. Then whole blood was centrifuged for 20 min. at 1000g and serum aliquotted into polypropylene microtubes and kept at -80°C prior to ELISA analysis. No more than 5% of total blood volume of the rat was collected on daily basis. For a rat weighing ca. 300 g, this amounts to ca. 1 mL of whole blood[191]. The setup also came into use when injecting ALN or saline intravenously. Here, we entered the circulation from the lateral tail vein and performed the injection over at least 1 min to allow adequate perfusion. Maximum 0.5 mL of solution (ALN or saline was injected).

12.4.5 Ethical Permissions

Animal experiments were performed with ethical approval by the Regional Ethics Committee for Laboratory Animals, University of Gothenburg, Sweden (Dnr. 236-2009, 227-2011 and 36-2012) and carried out in accordance with European Guidelines for Care and Use of Laboratory Animals (European Council Directives 86/609/EEC, updated and replaced by 63/2010/EU of 22.09.2010). Organ dissection and blood collection was performed under surveillance of a veterinarian. Also, in study 4, an additional risk assessment for using radioactive a substance, ^{14}C labelled ALN was performed in relation to the ethical application. The experiments with radioactive ALN were done following laboratory practice at Chalmers Technical University (CTH), Gothenburg, Sweden.

12.5 Post-surgical Analyses

Evaluation of biological, biomechanical and histological performance of Ti implants was performed by a battery of analytical tools established in our laboratory. During this thesis work both existing methods along with the development of new approaches came into use. The following sections describe the materials and methods of each of the post-surgical analyses performed during this thesis work (see also **Table 3**).

12.5.1 Bone Anchorage by Removal Torque

Removal Torque (RTQ) is a direct assessment of anchorage of the Ti implant in bone tissue in the drilled socket. The stronger an osseointegration in the interface of the implant and bone, the higher a torque is necessary to remove the implant by unscrewing it[192]. At the end of the implantation periods in studies II, III, and V, the rats were sacrificed and the implants exposed

by careful dissection of the overlying tissues, as described above. A special abutment was connected to the implant and the biomechanical testing equipment (**Fig. 12.8**). RTQ vs. angle measurements were performed using a constant rotation speed of 0.1 degree/s and real time monitoring, this is an optimized approach of a previous method[193]. During measurement, the RTQ value at both breakpoint, where the bone-material interface starts to disintegrate following the rotational friction, and max-point, where bone–implant integration is broken, typically with further rotation, were recorded. After measurement, the same implants were completely unscrewed and immediately immersed in an RNA preserving solution, RNA*later*®, for subsequent analysis by quantitative polymerase chain reaction (qPCR).

Fig. 12.8. Removal torque (RTQ) is measured using the specially designed abutment for unscrewing the implant during force monitoring.

12.5.2 Gene expression by qPCR

Evaluation of the biological response during implant healing and bone remodelling can be indirectly addressed using qPCR and quantification of *expression* of markers for bone remodelling, inflammatory, and other relevant mechanisms on the very implant surface and/or in *peri-implant* tissue. Collection of either or both the implant-adherent and peri-implant tissue were done immediately after RTQ-analysis, by preserving either solely the unscrewed implant or the trephined peri-implant tissue in RNA*later*®. The samples were stored at 4°C overnight, and then at -80°C till analysis. qPCR analysis was performed elsewhere (**Fig. 12.9**).

Fig. 12.9. The process of quantitative polymerase chain reaction (qPCR) of implant and peri-implant tissue material.

We will now describe this process in brief. Except from **sample homogenization,** where cells are disrupted and intercellular RNA material is made accessible for extraction, all steps are very similar for both implant and peri-implant tissue analyses. During this step, the implant was processed in RLT buffer and TissueLyser® whereas the peri-implant tissue, the bone, was processed in a phenol/guanidine-based Qiazol lysis reagent using 5 mm stainless steel bead and TissueLyser® (Qiagen AB, Sollentuna, Sweden). **RNA extraction** was done by centrifugation of the sample and collection of the aqueous phase using RNeasy® Mini kit® or Micro kit® for the bone and implant samples, respectively. Contamination from genomic DNA was eliminated by treatment of the sample in DNAse for **RNA purification.** The cDNA synthesis was performed by **Reverse transcription** carried out using iScript cDNA Synthesis Kit in a 10 µl reaction. Finally, **real time PCR** was run in duplicates using the Mastercycler ep realplex in 20 µl reactions following standard cycling conditions. **Quantification** of target genes was done either as total or normalized to either 18S ribosomal RNA or that of the most stable reference gene out of a panel of 12 plausible reference genes. The normalized relative quantities were calculated by the delta Ct method with 90% PCR efficiency ($k \times 1.9\Delta^{ct}$)[194].

The qPCR assays/primers, spanning and/or with one primer covering an intron/exon boundary, were designed for two genes. The criteria for good performance were: good linearity; high efficiency (>85%); high specificity (no amplification of gDNA or at least 7.5 cycles difference between the target and genomic Cq-value); and negative NTC (no template control).

The design of IL-1β, BMP-2, TNF-α, CATK, OC and 12 reference gene primers was performed with PrimerBLAST[195]. The qPCR assay was quality assured by a purified PCR product generated from cDNA of rat soft tissue.

12.5.3 Bone Growth by Histomorphometry

The quantitation of bone growth outside the threaded implant screws and bone-implant contact was assessed by *in situ* staining of ground sections and followed by examinations under light microscope[73]. The methodology to use undecalcified ground sections was implemented in 1983 at the University of Gothenburg in collaboration with Professor Karl Donath, oral pathologist at the Department of Pathology, University of Hamburg, Germany. This is the so called Sage-Schliff (sawing-grinding) technique[196].

The bone biopsy with the implant in place was collected *en bloc* upon euthanization of the animal and placed in a commercially available fixative containing zinc and formalin (4 % zinc formaldehyde, Mallinckrodt baker B.V., Holland). The initial fixation is crucial for section quality, and therefore it is important to clean the biopsy thoroughly in PBS prior to fixation. Otherwise

blood interferes significantly with fixation. A week after the immersion in the fixative under stirring and vacuum a series of immersions was performed. First, the sample was dehydrated by immersions in series of increasing concentration of ethanol. Then, the first step in resin embedding involved a dilution series of a pre-infiltration compound, Technovit 7200 (Heraeus Kulzer GmbH, Germany). This is based on a methyl metacrylate resin, and done under stirring and vacuum conditions. Finally, the sample was embedded in the ultimate acrylic resin system (LR White, London Resin Company, UK)(**Fig. 12.10**).

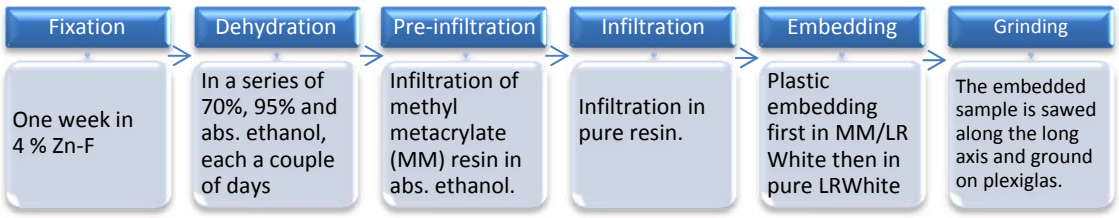

Fig. 12.10. Preparation of ground sections for histomorphometry.

The embedded sample was divided along the long axis and grinded using the EXAKT cutting and grinding system (EXAKT® Apparatebau GmbH & Co., Germany). First, a section of approximately 150-200 µm was sawed out. This was then ground using rough (800) to fine grains (1200) to a final sample thickness of 10-15 µm. The thicker the section is, the greater is the overestimation of the implant-bone-contact[197].

The in-house routine staining was 1% toluidine blue in 1% borax solution, mixed in a 4:1 proportion with 1% pyronin-G solution[196]. In this staining, bone is seen in light microscopy (Nikon Eclipse E600) in various blue and purple stains where the lighter colour reveals newer bone.

In light microscope, bone-area (BA), that is bone growth within and around the implant threads and actual bone-implant-contact (BIC), i.e. the percentage of bone contacting the implant surface in the section in question, was measured by manual evaluation of bone quality in the stain (**Fig. 12.11**). In this thesis, all threads of the implant within the bone environment and only the area within the threads were evaluated. In terms of BIC, tissue within a distance of 10 µm (order of cell size) from implant surface were regarded in contact with the exception of obvious contact as evaluated subjectively but detached from the implant under sample preparation.

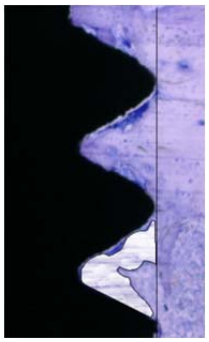

Fig. 12.11. Bone-area (BA) and bone-implant-contact (BIC) is outlined in the interface between the implant (black) and the surrounding bone tissue (purple).

12.5.4 Bone Remodelling by Immunohistochemistry

The histological evaluation of cellular activity in terms of release of proteins was done by immunostaining of decalcified sections, which in other words is an enzymatic reaction with antibodies of interest. In this routine, the initial fixation in formaldehyde was followed by post-fixation of the bone-implant *en bloc* specimen in modified Karnowsky media for 2 h, decalcification in 10% EDTA for 10 days where after implants were unscrewed and sample embedded in paraffin. Then implants were unscrewed from the blocks and sections of 10 µm thickness were produced and mounted on glass slides. Sections were stained in traditional hematoxylin and eosin illustrating cell nuclei blue and eosinophilic structures in various shades of red, pink and orange. Furthermore, the immunostaining was done on 4 µm sections mounted on poly-L-lysine slides (Menzel GmbH & Co. KG, Braunschweig, Germany), deparaffinized, hydrated and incubated with primary antibodies; CD163 (sc-58965, Santa Cruz Biotechnology, Inc., Texas, USA), and periostin (ab14041, Abcam, Cambridge, UK). CD163 is a marker for monocyte/macrophage cells and periostin a marker of mesenchymal stem cells and osteoprogenitor cells[198]. Negative control slides were prepared by omission of the primary antibody and incubation in 1% BSA in PBS. Immunosections were analysed in an optical microscope (Nikon Eclipse 600).

12.5.5 Bone-Implant-Contact in µCT

Evaluation of bone growth around implants and the specific bone-implant-contact (BIC) were performed in study V in µCT (Computed Tomography), which was used to generate a three-dimensional image of the inside of an object from a large series of two-dimensional radiographic images taken around a single axis of rotation. In brief, embedded implant bone blocks and embedded bones with defect, were mounted in the micro-CT (Skyscan 1172, Brücker microCT, Kontich, Belgium), placed so the implant were aligned along the long axis, while the bones with defect were aligned with the long axis of the bone in relation to the rotation axis.

Acquisition was done in settings 100 kV with CuAl filter and 70 kV with CuAl filter for implants and bones respectively. For the samples without implant, phantoms were scanned in order to evaluate the bone mineral density (BMD) in the defects. All samples were scanned with a fixed resolution of 9.76 µm voxel size.

The data sets were reconstructed, aligned and evaluated using different software provided by Skyscan (Recon, CTan). The region of interest was set to:

- For bone-implant contact, the bone tissue which was in contact with an implant enlarged by 10 voxels, measured in 2D along the entire threaded implant.
- For bone area, the amount of bone volume surrounding the implant of a volume consisting of 10-40 voxels from the implant surface.

12.5.6 Assessment of beta-Radiation from ^{14}C-ALN

In study IV, ^{14}C-labelled ALN was delivered locally *in vivo* from mesoporous implant surfaces and distribution in the implant close bone was monitored *ex vivo* by autoradiography and total amounts determined by liquid scintillation counting (LSC)[199]. ^{14}C decays via β-radiation.

All the ex vivo harvested samples were embedded in acrylic resin and prior to autoradiography analysis a central cross-sectional cut was made axial through each implant with surrounding bone. A duplicate of each sample was received and all samples were analysed. A schematic illustration of the sample preparation procedure is shown in **Fig. 12.12**.

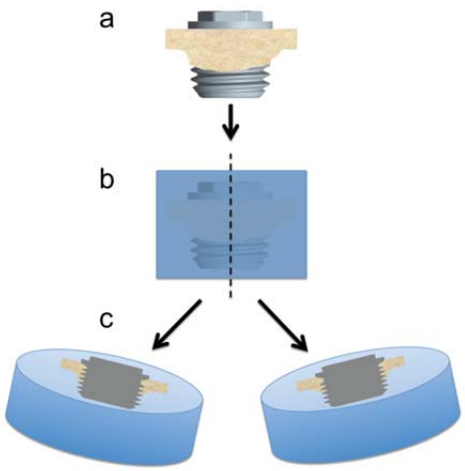

Fig. 12.12. Illustration of the sample preparation prior to autoradiography analysis.

An imaging plate (BAS SR-3X310055) was covered with a thin plastic film upon which the samples were placed with the cross-sectional implant-bone side facing the imaging plate. To

protect the imaging plate from light during exposure, the setup was covered by a light exempting box. The exposure time for the samples towards the imaging plate was 3 h, followed by insertion into the autoradiograph. Images were acquired with a FLA-7000 autoradiograph (Fujifilm), with the instrument sensitivity set to 10 000, latitude to L5, and the pixel size to 25 µm. The ionizing β- radiation induced excitation in the phosphorus layer of the imaging plate, which was de-excited by a 650 nm autoradiograph laser. The following 440nm photo-stimulated luminescence is directly proportional to the β-decay activity. Multi Gauge analysis software (version 3.2, Fujifilm) was used to visualize and relatively quantify the radioactivity of the ^{14}C-labeled ALN samples. All images displayed in the results section were recorded simultaneously.

The 14C-content was quantified using LSC. Prior to the LSC analysis, the polymer embedded implants were dissolved in concentrated nitric acid (HNO_3). Each sample consisting of cross-sectional duplicates were put in a vial containing 10 ml of concentrated HNO_3 for 72 h in order to dissolve the bone. The dissolution vial was connected via a thin tube, through which a minute N_2-gas flow was kept, to a trap vial filled with 15 ml of 5M NaOH in order to be able to quantify a possible loss of ^{14}C-labelled ALN through evaporation or volatilization in the form of CO_2. 0.5 ml samples from both dissolution and trap vials were collected. To each 0.5 ml sample, a 15 ml Hionic-Fluor liquid scintillation cocktail (Packard-Bioscience) was added and the mixture shaken to obtain a homogenous solution. The measurements were then performed using a Wallac Guardian 1414 Liquid Scintillation Counter (PerkinElmer). To properly assess quenching effects during quantification, a ^{14}C standard was added to samples prior to re-measurements.

12.5.7 Statistics

Comparison of means in most experiments (RTQ, BA, BIC, etc.) was performed by ANOVA, followed by the post-hoc Tukey test. The gene expression data were based on a comparison of the relative expression of each gene from implant residing cells compared with the most stable reference gene. Statistical differences were assessed by the non-parametrical Kruskal–Wallis test, followed by pair-wise comparison of respective surfaces by the Mann–Whitney U-test (SPSS Statistics v. 20, IBM Corp., USA). Number of blocks were often n=8, if not otherwise stated. The confidence level of either test was set to 95%, ($p < 0.05$). If not otherwise stated, data were given as mean ± standard error of mean.

13 SUMMARY OF RESULTS

13.1 Study I

In this study of the complement activation properties of spontaneously oxidized Ti and heat- or UVO-treated Ti was investigated in context of tissue healing when in contact with blood plasma. We have aimed to make use of mild treatments modalities to alter this property, questioning whether or not physicochemical changes to the topmost nanolayer of TiO_2 by means of prolonged UVO-treatment and mild heating will affect. Short term UV-illumination induced reversible superhydrophilicity, i.e. the Fujishima-effect which describes photocatalysis within the TiO_2 lattice upon radiation, resulting in contact angels <3°. However, upon prolonged exposure to UVO-illumination for up to 96h, the physiochemical change in topmost 5-7 nm TiO_2 manifested itself as an irreversible chemical shift in atomic % of oxygen and titanium. Presence of O1s-electrons increased in XPS analysis by nearly 44% while Ti2p3/2 metal electrons were reduced by half. Next to reorganisation of the Ti-O stoichiometry, as we anticipated, a change of hydroxylation was caused by the ozone/TiO_2/UV catalytic combination. The compelling finding was the remaining effect by prolonging the illumination time. In contrast to spontaneously formed TiO_2, which strongly adsorbed C3c-antibodies after incubation in blood plasma, surfaces treated under UVO for 24 h and more or heated at 300°C and above were absolutely free from anti-C3 binding. A more pure and Ti(IV)O_2 stoichiometry, improved crystallinity and altered surface hydroxylation are the plausible explanations to these findings.

The effect of healing was also observed for sol-gel derived Ti with no anti-C3c binding in comparison with PVD-coated Ti surfaces. Sol-gel prepared TiO_2 surfaces adsorbed the expected 20-30 Å of plasma proteins. The effect of heating Ti appeared to be most significant at high plasma concentrations, which underlies the necessity of IgG for complement activation. As such, a provocation experiment of pre-adsorbing IgG to annealed (sol-gel) or PVD-coated Ti was performed. The sol-gel derived Ti surface showed a significantly lower C3 antibody binding than PVD-prepared Ti, indicating a lowered IgG mediated complement activity on annealed Ti, i.e. the annealed surfaces presented the adsorbed and partially denatured IgG's differently compared to non-annealed titanium, with a lower susceptibility to complement proteins in the former case. And finally, the anti-HMWK binding profile, after incubations in diluted plasma indicates a more rapid HMWK deposition to non-annealed PVD-prepared Ti than to annealed ditto or sol-gel derived Ti, and also paralleled by a higher anti-Fib binding to non-annealed Ti.

The crucial effects on TiO_2 with attenuated complement activation compelled us to evaluate effects of mild heating and UVO-treatment *in vivo* in rat bone.

13.2 Study II

In this rat study, our hypothesis was in line with other contemporary groups questioning the effects of superhydrophilic Ti oxide on bone healing. While others reasoned to find the clue in increasing oxide crystallinity towards anatase, we pounded upon changes in Ti-O stoichiometry and hydroxylation, which gave rise to lowered complement deposition and could improve the healing of Ti implants in bone. The rationale of the present work became therefore to elucidate whether complement active IgG-coated Ti surfaces gave rise to a different healing kinetics and bone growth compared to UVO-treated Ti with low complement binding. Firstly, relative atomic concentration of O1s on UVO-treated Ti implants confirmed previous findings, in comparison with the three other groups: machined, PVD-treated, and the IgG-coated, complement activating control. The UVO treatment decreased the surface carbon concentration from 47% to 12% (simple cleaning) and increased oxygen concentration from 38 % to 54%. The effect on inflammation was most profound at the mRNA level. Data from day 1 revealed that surface cells from complement active IgG-coated Ti evoked significant upregulation of IL-1β and TNF-α than UVO-treated Ti, and the IgG surface expressed significantly more TNF-a compared with all other surfaces. The UVO-treatment apparently gave a hundredfold lower inflammatory activity on the implant surface. Interestingly, the opposite was the case in peri-implant tissue. All groups showed a significantly higher inflammatory activity (IL-1b and TNF-a) by surface-located cells as compared to peri-implant cells and, conversely, a significantly higher bone healing and remodelling activity was indicated by cells positioned at some distance from implant than by surface adherent cells (CATK and OC). Surprisingly, the CATK expression by implant-located cells was significantly lower at UVO-treated Ti and PVD-coated Ti.

The general tendency at day 7 was that inflammation in terms of upregulation IL-1β and TNF-α had passed their peaks and decreased thereafter, whereas bone growth in terms of CATK and OC expressions showed a constant but high level. After 4 weeks of healing, inflammatory activity at implant surfaces was down-regulated in implant surface and in peri-implant tissue. This was supported by higher degree of presence of macrophage-like cells (MLC) and multinucleated giant cells (MGC) in the threads of IgG-coated Ti and lesser in the threads of UVO-treated Ti. The UVO-treated surfaces showed after 1w and 4w a non-significantly higher BA compared to the other surfaces. While the same trend was observed for BIC of *de novo* bone, a significantly higher BIC-value was observed for UVO-treated surfaces after 7 days of implantation compared to

machined Ti. The total BA inside the threads was after 4 weeks of implantation nearly 60% for all implant types, lowest for IgG-coated surfaces (58%) and highest for UVO-treated surfaces (65%). The RTQ value at breakpoint was after 7 days significantly higher for UVO-treated surfaces compared to the machined control. And after 28 days, the machined and UVO-treated surfaces showed the highest RTQ. However, no statistically significant differences between the implants were observed.

The results suggest that, although a slightly lower bone formation was observed for complement activating surfaces, complement activation at non-passivated machined surfaces is not detrimental to integration in rat tibia.

13.3 Study III

Studies III-V present our research aimed at enhancing bone healing around Ti implants by local delivery of osteoporosis drugs from implant surfaces. Mesoporous TiO_2 coatings with a thickness of 200 nm were prepared on screw shaped Ti implants by EISA. The BJH method[200] revealed a narrow pore width distribution with average pore width of 6 nm. Synchrotron SAXS data demonstrated two visible peaks, indicating a long-range order within the mesoporous structure. The diffractogram corresponded well with the Im3m symmetry of cubic mesoporous materials. A 30 times higher ALN absorption was observed into porous TiO_2 films compared with non-porous films. Three times more RLX absorbed into methylated porous TiO_2 compared with the methylated non-porous TiO_2 control. The total loading of ALN and RLX was 157 ng/implant and 268 ng/implant, respectively.

Gene expression analysis of implant-adherent cells showed a significantly higher expression of CATK, OC, TNF-α around raloxifene releasing implants. This, in turn, may be translated into high osteoblastic and osteoclastic activities along with tissue remodelling at the implant surface. In fact, a significantly higher removal torque (RTQ) was observed for RLX in comparison with the other surfaces. The drug-loaded mesoporous implants displayed significantly stronger bone-to-implant attachments than their references, 4.1 Ncm and 5.0 Ncm, for ALN and RLX, respectively. Besides, unscrewing vs. torque monitoring revealed a distinctive pattern of bone-implant detachment for RLX.

After 28 days, the surfaces showed 44–67% bone area (BA) inside the threads. The BA-value of ALN coated Ti (MPA) was significantly higher than for the other implant types. Another pattern was observed for the BIC values with no significant differences between the differently prepared screws. In fact, MPA showed the lowest BIC value and MPR the highest. MPR showed an average

55% contact, with some samples as high as 84% contact. Finally, MPR resulted in good bone anchorage at the surface, while samples with immobilized ALN showed an increased bone density in the threads and at some distance (order of 100 μm) away from the surface (lower figure). Thus, two groups of osteoporosis drugs with different mechanisms of action, ALN and RLX, both significantly improved bone-anchorage around Ti implants leaving behind questions in terms of their mechanisms of action.

13.4 Study IV

BPs have strong affinity to bone apatite, which counts for their efficacy in inhibition of osteoclastogenesis. Traditionally, systemic delivery is prescribed for patients with compromised bone, yet only a fraction (order of 1 %) reaches bone apatite. In contrast to this, the local delivery to site of healing would theoretically concentrate all of the delivered compound to implant close bone. The hypothesis in this study was that BP (^{14}C-ALN) that is released from implants *in vivo* stays, due to its high affinity to hydroxyl apatite in the close vicinity of the surface. The combination of SEM, radiolabelled luminescence and liquid scintillation counting (LSC) confirmed the local efficacy of ALN. ^{14}C-labelled ALN was delivered into rat tibia from mesoporous Ti implants and the healing analysed after 1d, 3d, 7d, 1w, and 8w (n=4). Autoradiography revealed that the drug was released from all implant threads and distributed equally to into both the medullary space and cortex. Whereas vascular perfusion distributed the compound, the amounts delivered to cortical bone remained on site for up 8 weeks.

At 4 and 8 weeks, most ^{14}C-ALN remained within the closest few 100 μm around the implant surface, although a larger diffusion was seen in bone. In fact, at all instances the compound remained within 400 μm from implant surface. Intensity measurements indicated that more ALN was observed where the bone density was higher, which translated into a correlation between bone growth and drug release and moreover into a mechanism of action distant to implant surface. The LSC results demonstrated that the activity level remained relatively constant, ranging from 15-24.000 CPM (ca. 320.3 ng), until the final time point of 8 weeks, which is translated in to that ALN remains at the implant site for a long time and exerts likely its effects during this time.

13.5 Study V

For more than four decades BPs, and in particular N-BPs, have been known to induce suppression of osteoclast activity. Encouraged by the above findings of high local efficacy and bone affinity, we aimed in this study to compare local vs. systemic delivery of ALN either from

mesoporous Ti implants loaded with ALN or by intravenous injection of ALN in terms of bone anchorage (RTQ), BA (histomorphometry), and BIC (μCT) in a mature, ovariectomized rat model. In total 32 rats either received implants loaded with and without ALN (~300 ng) or non-loaded implants assisted by i.v. injection of 0.5 mL ALN (1 mg/kg) or saline. Bone healing was followed for 4 weeks. Rats were monitored before and after hysterectomy and prior to surgery as well as during healing in terms of effect of the surgically induced osteoporosis. Comparison of RTQ data proved a high efficacy of local delivery in comparison with to the single intravenous injection of ALN, with a significant 46%* (*$p<0.05$) difference in favour of local delivery. Once again implants with ALN promoted a 41%* (*$p<0.05$) higher RTQ than that of implants without the drug. Histomorphometry indicated a higher bone-area (BA) values for implants with immobilized ALN than that for implants without the drug, 77.1% and 73.4% (4 rats, 8 implants) respectively. Moreover, BIC analysis by μCT within the first 10 μm from implant surface indicated that implants with ALN promoted a higher implant anchorage than implants without ALN or ALN given systemically, an improvement by30%* (n=4, *$p<0.05$). The concentration of ALN injected i.v. was theoretically in the range of ca. 8 μg/g tibia. The implication is that when ALN is given systemically, the drug may be hindered in performing its action due to a limited distribution in traumatized tissue, hence the current RTQ, BA, and BIC results from systemical delivery proves inferior. So, histomorphometric and μCT data are complementary to this observation. We observed here evidence of a superior local delivery effect with enhanced bone-implant anchorage and bone quality around the implants. The results contribute to a further understanding of the action of bisphosphonates and route of delivery for implant patients with compromised bone quality.

14 DISCUSSION

For each of the sections, the headline is referring to one of the 5 studies written in Roman numbers in parenthesis.

14.1 Effect of UVO on Properties of TiO_2 (I)

The spontaneously formed native TiO_2 coating on metallic Ti is subject to changes when exposed to radical physicochemical environments[201]. Ozone/TiO_2/UV is known to form a very reactive catalytic combination, and hence we speculate that a stoichiometrically more ordered titanium dioxide (Ti(IV)O_2) with improved stoichiometry and crystallinity was formed in parallel with altered oxide hydroxylation from ambient water. Considering the high resolution XPS data, results of control and UVO- and heat-treated smooth TiO_2 are summarized in **Fig. 14.1**.

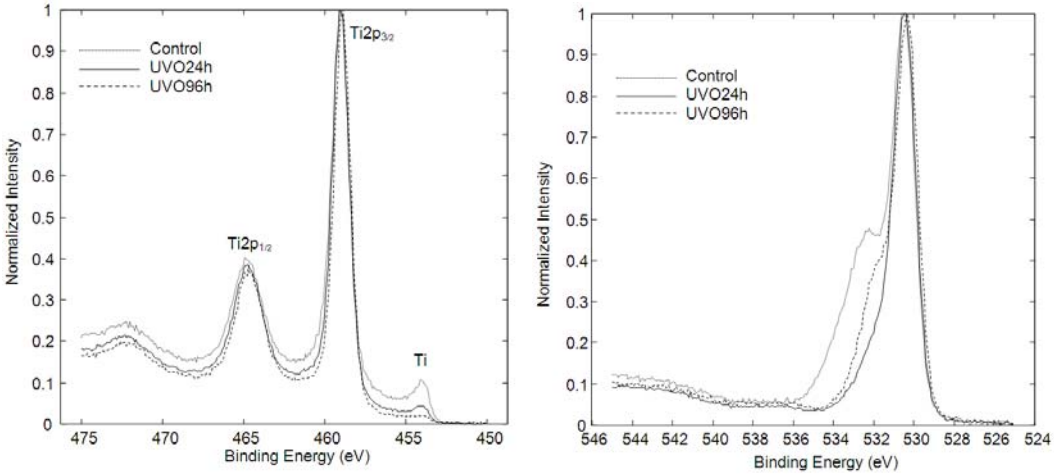

Fig. 14.1. (left) Normalized XPS Ti2p3/2 high resolution spectra of spontaneously oxidized Ti (control), and after surface UVO-treatment 24 hours and 96 hours. The Ti2p3/2 metal intensity at 454.1 eV decreased with time and was assigned to Ti- metal, i.e. the oxide thickness increased upon UVO-treatments. (right) Normalized XPS O1s high resolution spectra of spontaneously oxidized Ti (control), and after surface UVO-treatment 24 hours and 96 hours. The intensity at 532.5 eV decreased with time and was assigned to physisorbed water (H-O-H), and the increased intensity at 531.8 eV to increased Ti-oxide hydroxylation (OH groups).

The atomic % of Ti2p-, O1s-, and C1s-electrons indicate an irreversible chemical shift due to the UVO-treatment that could only partly be reversed by heat-treatment at ambient conditions. The decrease of C1s-electrons is a clear result of the cleaning-effect of the UVO-exposure. The increase of O1s-electrons and decrease of Ti2p electrons suggest oxide reorganisation, molecular or atomic oxygen (from degraded ozone) surface binding[202] and a minor thickening of oxide layer upon the illumination with simultaneously increased hydroxylation and splitting of humidity water. It was in fact reported that the O1s region in XPS analysis of Ti is usually comprised of XPS peaks caused by TiO_2 at 530.3 eV, TiOH at ca. 531.3 eV and water at ca. 532.5 eV[203].

AFM analyses of optically PVD-prepared titanium surfaces, prior to and after annealing at 300°C, showed neither significant increase in surface roughness nor a changed topography. The X-ray and AFM analyses, when taken together exclude a strong transition to crystalline TiO_2 or a large oxide thickening, since no significant changes were observed in 2θ-angles of native Ti granules on control- and annealed PVD-prepared Ti-surfaces (**Fig. 14.2**). We have reported an increased crystallinity upon annealing at 300-700°C, although without quantification of the crystallization. There is indication of a chemical reorganisation and increased crystallization of the outmost atomic layers of the oxide that we could not separate out or, alternatively, a

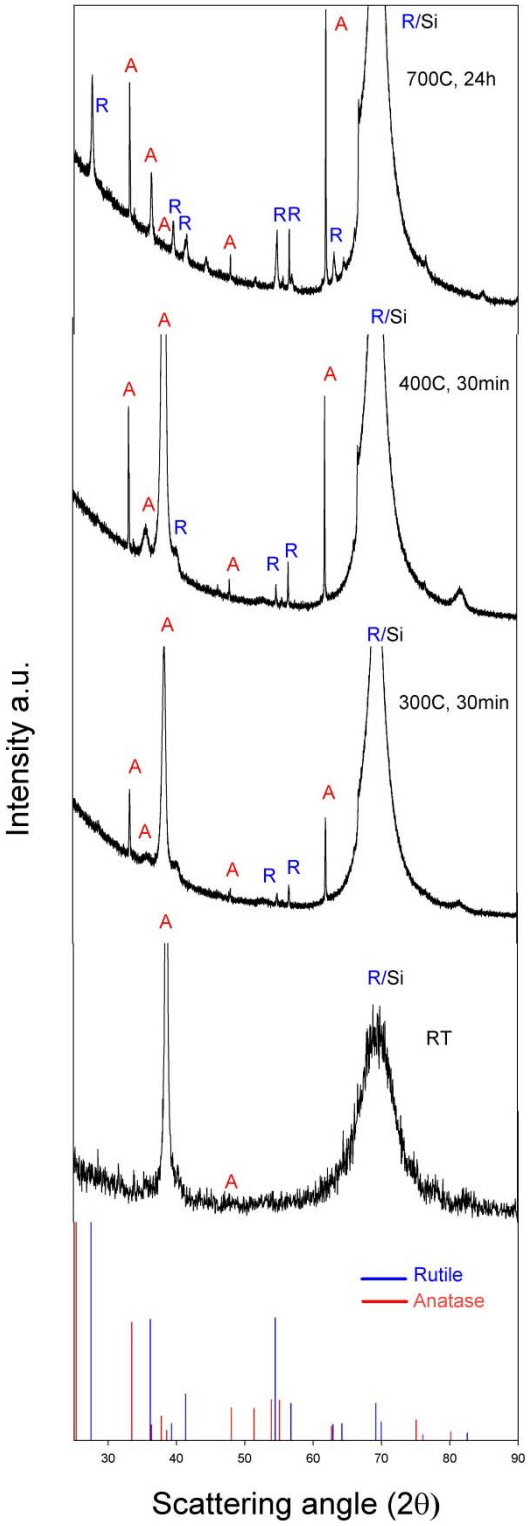

Fig. 14.2. X-Ray Diffraction intensity spectra of control (room temperature, RT) and annealed (300-700°C/24 h) optically smooth Ti-surfaces. Peaks around 2θ≈38° are observed with no significant crystallization effect as a result of mild annealing at 300°C.

decreased content of TiOH (Ti- hydroxide), Ti_2O_3, or other oxide stoichiometries that differ from $Ti(IV)O_2$.

In a previous work, the investigators studied the water/hydroxyl desorption behaviour of hydroxylated/hydrated rutile and TiO_2 particles as a function of temperature[26]. It was then reported, that hydroxides formed during dissociative water adsorption desorbed typically at the temperature of 370°C, whereas molecularly chemisorbed water (non-dissociatively coordinated to Ti cations) desorbed in the range of 250-320≈C depending on the initial water coverage. This interpretation is supported by the present findings. Other authors, however, have observed temperature-programmed desorption peaks at ca. 250°C and as low as 110°C and ascribed them to the desorption regime of hydroxide and molecularly adsorbed water, respectively[204, 205].

14.2 Complement Deposition after Mild Treatments (I)

Blood plasma deposition with concomitant anti-C3c binding versus the surface annealing temperature of PVD-titanium or UVO-illumination is shown in **Fig. 14.3**. The total plasma binding remained approximately constant on the differently treated surfaces, 20-30 Å. The anti-C3c binding on top of the blood plasma, on the other hand, displayed a clear decrease with increasing annealing temperature and disappeared totally at 300°C and above or when the surface was UVO-treated for 12 hours or more. Thus, it appears that the humoral part of the innate immune system reacts differently towards annealed or UVO-treated, and spontaneously formed titanium oxides.

The collected data suggest that the main reason for a changed immune complement deposition on Ti was a shift in oxide stoichiometry, which likely shifted towards a more crystalline $Ti(IV)O_2$ but with extensive surface hydroxylation. Also the surface charge may have shifted, although we managed not to measure this. Finally, the surfaces were much cleaner after the UVO and heat treatments than before.

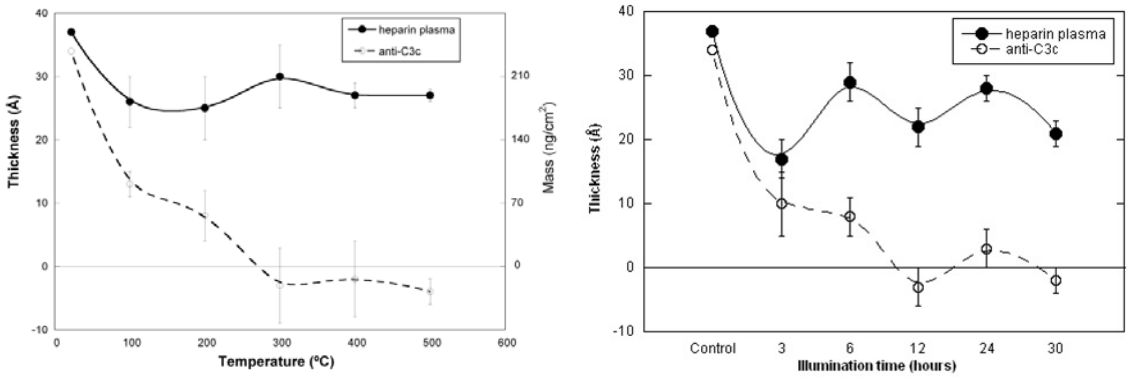

Fig. 14.3. Adsorption curves for complement factor C3 assessed by binding of anti-C3c *in situ* ellipsometry as a function of temperature (left) or time of UV-illumination (right). Surfaces deposited in heparin plasma for 60 min. first.

14.3 Gene Expression before and after UVO (I-II)

Activation of the intrinsic pathway of coagulation and the complement systems on Ti have been systemically investigated by Tengvall et al.[206]. The passive oxide layer on Ti corresponds to a point of zero charge (PZC) in the range of 4.7-6.2[38], and explains the negative charge at physiological conditions, like that in blood plasma. This in turn explains the activation and attachment of Hageman factor, (FXII) and High Molecular Weight Kininogen (HMWK), the initiators of the intrinsic pathway cascade. A negatively charged surface is also hydrophilic. Later it was found that also complement proteins bind to Ti surfaces while in contact with blood plasma. In experiments with competitive adsorption of plasma proteins, it was observed that C3c-binding overcame adsorption of albumin, IgG, fibrinogen and other plasma proteins on top of Ti surfaces after a prolonged immersion in heparin plasma[207].

Now, this property of Ti was modified in study I, and we found that upon incubation in blood plasma of UVO treated or heated Ti, the C3 binding was strongly attenuated. In study II we explored the *in vivo* response to Ti implants with differing complement activation properties, and analysed the ex vivo mRNA expression of selected inflammation markers, TNF-α and IL-1β. As a positive control, surfaces with complement activating immunoglobin G (IgG) were used, which during the early healing phase, i.e. 3–24 h of subcutaneous implantation is shown to recruit significantly more inflammatory cells to the implant interface than machined Ti reference without IgG[208]. In turn, Tumour Necrosis Factor alpha (TNF-α) and Interleukin-1beta (IL-1β) have been connected to increased inflammatory responses in relation to surfaces in context of bone[209, 210]. TNF-α is synthesized as a 26 kDa protein by immune cells and has important immunoregulatory effects, but is expressed also by other cell types and has important roles also for many other biological and pathological processes. It is thoroughly documented as a

proinflammatory molecule, well demonstrated by the successful therapy with TNF- blockers in inflammatory disorders like rheumatoid arthritis and inflammatory bowel disease[92]. IL-1 exist in two forms, IL-1α and IL-1β, and is the most studied cytokine due to its broad range of actions in immunity and inflammation and is extremely important for the normal bone healing[211]. The major sources of IL-1 are monocytes, macrophages and dendritic cells [212, 213], but many other cell types, such as osteoblast-like cells[214], epithelial cells, fibroblasts and endothelial cells also produce IL-1[215]. The 31 kDa IL-1β precursor is inactive and requires processing by the IL-1 converting enzyme, also known as caspase-1, to form the 17 kDa secreted active form[214] (see also Chapter 9.1).

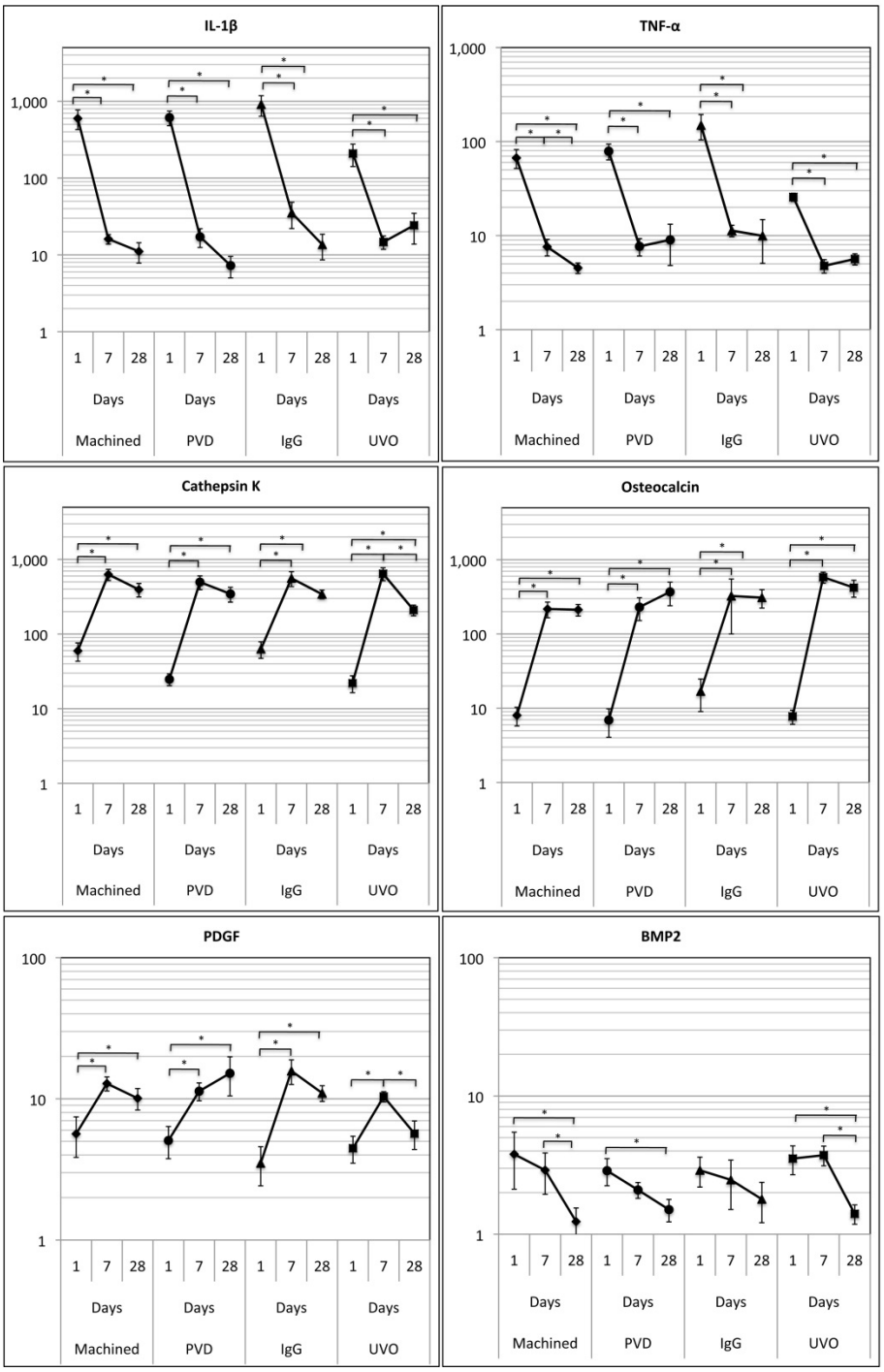

Fig. 14.4. Relative gene expression of IL-1β, TNF-α, CATK, OC, PDGF and BMP2 on implant surfaces through time points 1, 7 and 28 days post-surgery (*P < 0.05).

In study II, the relative gene expression levels of both TNF-α and IL-1β were clearly different between test and control surfaces ($p < 0.05$). The effect of UVO-treatment or IgG-coating was most evident at early time points after implantation, i.e. at 1 day and 7 days. Expressions of TNF-α and IL-1β were tenfold higher on pro-inflammatory, IgG-coated surfaces, while UVO-treated group showed a remarkably lower expression of inflammatory activity. This effect

remained for a week while the difference decreased thru 28 days. The inflammation around implants in rat tibia is expected to fade after ~2 weeks post-implantation[216], and hence the steady decrease in inflammation from day 1 to day 7 and day 28 was expected. Although a direct correlation would need further statistical comparison, the effect on inflammation was higher on surface-adherent cells (**Fig. 14.4**) than in peri-implant tissue (**Fig. 14.5**), which was harvested ~250 μm away from the surface. The latter observation probably reflects the fact that more inflammatory cells were recruited to the damaged bone surface implant interface than to less compromised tissue further away from surface[217].

In general, following the time course of 18S expression (data not shown), a millionfold increase in the absolute quantity of 18S per sample was observed at the surface from day 1 to day 7, and then the expression remained high throughout 4 weeks. The low quantity of 18S at day 1 of implantation indicates a low number of surface attached cells upon harvesting. For peri-implant samples, the 18S quantities remained relatively constant throughout the 4 weeks, indicating a high stability of 18S as reference gene. However, as we shall see in study III, stability of reference gene may be a subject to relativity.

The onset of inflammation was orchestrated by a cascade reaction not purely restricted to TNF-α and IL-1β. While we will leave the discussion around osteoimmunology to the next section, we will here comment on influence of other cytokines and intercellular mechanisms preceding inflammation. The local release of inflammatory mediators, such as the chemicals released from injured tissue (e.g. prostaglandins), products of coagulation and complement (e.g. C3a, C4a,b and C5a) and fibrinolytic peptides (FDPs), initiates the cascade that controls early inflammatory events. These events involve the production and release of primary acute phase cytokines, TNF-α, IL-1β along with IL-6. By activation of their target cells, these cytokines generate a second wave of cytokines, including members of the chemokine family. The latter are small inducible secondary cytokines with a characteristic cysteine residue motif. Chemokines are divided into four families depending on the spacing of their first two cysteine residues, namely CC, CXC, C and CX_3C[93]. In fact, it could have been of interest to assess the activity of anti-inflammatory cytokines, such as IL-10, which are produced by most cells in the immune system, including macrophages and certain set of regulatory T-cells[92]. We will return to this cytokine in study III.

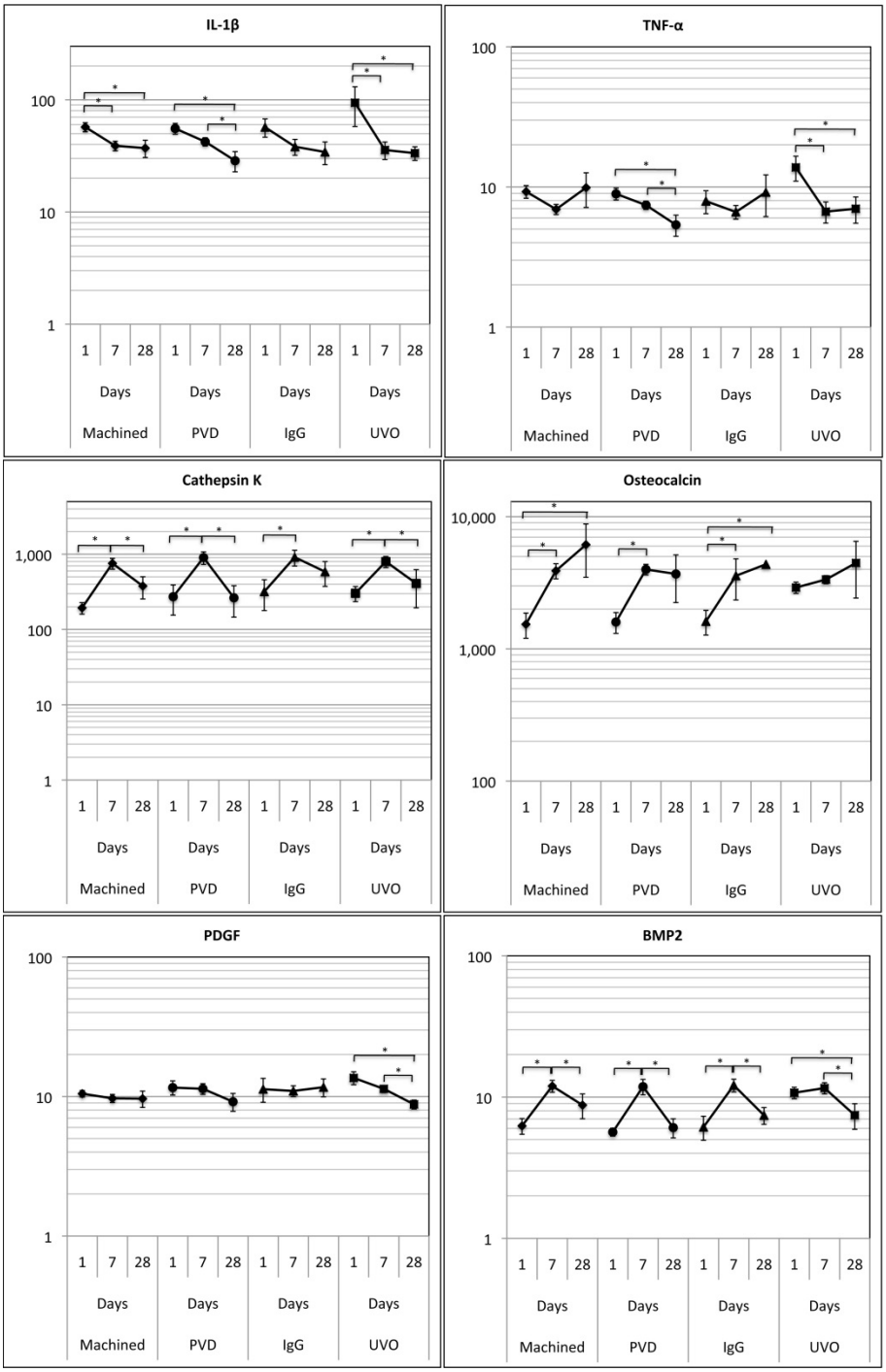

Fig. 14.5. Relative gene expression of IL-1b, TNF-a, CATK, OC, PDGF and BMP2 in peri-implant tissue through time-points 1, 7 and 28 days post-surgery (*P < 0.05).

14.4 Bone-growth and -anchorage after UVO (II)

Several molecules produced during the inflammatory phase, either by the infiltrating leukocytes or by the resident cells, have been found to be able to regulate bone resorption and bone formation *in vitro* as well as *in vivo*. The first evidence for a crosstalk between inflammatory cells

and bone was the finding by Horton et al. showing that human peripheral blood leukocytes stimulated by phytohemagglutinin, or by solubilized dental plaque, released an activity which could stimulate bone resorption in organ cultured fetal rat long bones[218]. While the details still remain unknown, this was the starting point in the field today recognized as osteoimmunology, i.e. the interplay between inflammation and osteogenesis. In our study with pro- and anti-inflammatory surfaces we emphasized on isolating the effect of early onset of inflammation on bone growth. As noted, CATK and OC are markers of bone resorption and bone formation, respectively. CATK is most often ascribed to collagenase activity by osteoclasts and OC to mature osteoblasts[82] and regulation of insulin[219]. Collectively, these markers signal bone growth and remodelling. Bone morphogenetic protein 2 (BMP-2) is shown to stimulate the production of bone[220], while PDGF is mitogenic for bone cells[221]. It also activates monocytes and promotes bone resorption[222]. First, an up-regulation of bone healing and remodelling markers of surface cells, i.e. OC and CATK, was observed after 7 and 28 days, with a maximum at 7 days, and was in fact a trend for all types of implants. At the earliest time point, day 1, the CATK and OC expressions were highest on IgG-coated Ti. No significant differences between the surfaces in PDGF and BMP-2 expressions were observed at day 1.

By comparing the relative mRNA expressions at different locations after 1 day of implantation, it was observed that the peri-implant cells indicated higher bone healing and remodelling activity than surface-located cells, observed as relative expressions of CATK and OC. Surprisingly, the CATK expression by implant-located cells was significantly lower at UVO-treated Ti and PVD-coated Ti and may be related to their lower activation of inflammation and the direct coupling between inflammation and osteoclastic activity[223].

After 1 week of implantation, significantly increased bone growth and remodelling activity and decreased inflammatory activity by surface-located cells was observed (**Fig. 14.4**). Cells from UVO-treated Ti now displayed higher CATK expression, significantly higher OC expression and a significantly lower TNF-α expression than IgG-coated Ti. The results in **Fig. 14.4** suggest that the main consequence of the UVO treatment was stronger bone growth and, consequently, OC expression was significantly higher when compared with all other surfaces.

While gene expression after 4 weeks of follow up indicated a somehow downregulated inflammatory and bone remodelling activity, the histomorphometric, histological and removal torque analysis proved a significant effect of UVO-treatment/mild heating. The total BA inside the threads was after 4 weeks of implantation ~60% for all implant types, lowest for IgG-coated surfaces (58%) and highest for the UVO-treated surfaces (65%), and interestingly a significantly

higher BIC-value for UVO-treated surfaces was found already after 7 days of implantation compared to machined ones, a trend which was maintained thru 4 weeks. And finally, RTQ analysis manifested the functional effect of UVO-treatment of surfaces. The value at breakpoint was significantly higher after 7 days for UVO-treated surfaces compared to the machined control (**Fig. 14.6**). This supports the finding of high bone contact from BIC analysis, because the observed RTQ value was 25% higher for UVO-treated surfaces compared with machined ones ($P < 0.05$). After 28 days, the machined and UVO-treated surfaces showed the highest RTQ (**Fig. 14.6**). However, no statistically significant differences were observed between the implants. The IgG-coated and PVD-coated Ti surfaces, both complement activators, displayed, however, the lowest values. One is intrigued to conclude that a trend was observed.

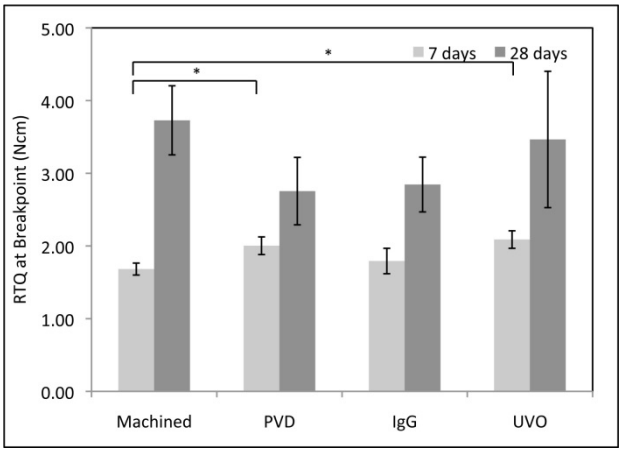

Fig. 14.6. RTQ at breakpoint of machined, PVD-coated, IgG-coated and UVO-treated Ti surfaces after 7 and 28 days, respectively. After 1 week, the UVO-treated surface showed the highest RTQ value, significantly higher than machined surfaces and in the same range as the PVD-coated surface (*$P < 0.05$).

14.5 Mesoporous TiO_2 Coating as a Drug Delivery System (III)

Our previous studies contributed significantly to our understanding of the functional interplay between inflammation and osteogenesis and possible control mechanisms that could be modulated by mild surface treatments. In Study I it was observed that sol-gel prepared and heated TiO_2 surfaces displayed a very low complement activation capability in blood plasma. Mesoporous (MP) coatings can be synthesized by the use of applied sol-gel chemistry and mild heating and offer another approach to influence bone remodelling mechanisms. Our partners at Chalmers have proved in this twinning project that MP coatings on Ti implant do not interfere negatively with bone growth[224]. Now, we have optimized the delivery system in terms of pore size and coating thickness and synchrotron Small Angle X-ray Scattering (SAXS) indicated a high range of order in the MP mesh with cubic structure. A single, high intensity peak in N_2 adsorption along with visual assessment in SEM and TEM confirmed this high order and narrow

pore size distribution. The latter is of importance in terms of controlling the reservoir capacity of the pores, i.e. how large or charged molecules that theoretically could be stored inside the pores.

Now, we aimed to increase the complexity of this approach by incorporation osteogenic drugs into the MP coating. Osteoporosis drugs, more precisely. This way, local delivery from mesoporous Ti implants could meet the challenges of prolonged drug bioavailability and efficiency, lowered systemic toxicity, controlled release rate over a longer period of time and presumably lower clinical costs[129, 133, 225, 226].

With our drugs in concern, the loading capacity was important to assess. This was determined in the present mesoporous oxides and was correlated to surface area and pore volume[126]. A long range structural order and a cubic TiO_2 structure was observed with 35 times larger surface area compared to non-porous TiO_2 controls prepared from same starting material, Ti-salts, but with exclusion of the pore forming detergent. The drug absorption/desorption were monitored by QCM-D and showed that ALN was successfully loaded into the hydrophilic mesoporous oxide with ~30 times higher concentrations compared to a hydrophilic non-porous surface. In this case, the drug uptake increased almost linearly with surface area. In contrast, the RLX uptake by the salinized and methylated (hydrophobic) mesoporous oxide was only three times larger than compared to its non-porous control. This was in part explained by the high affinity via hydrophobic interactions between the hydrophobic drug and a smooth hydrophobic surface, in combination with a higher steric repulsion for RLX compared to ALN. When the projected screw surface area, approximately 0.2 cm^2, was taken into account, 157 ng ALN and 268 ng RLX were stored into respective mesoporous implant film. If we then assume after a quick drug release out and a diffusion distance of 1 mm, the distribution volume is at the order of 0.1 cm^3. The resulting ALN and RLX concentrations become then 15–25x10^{-9} g/ml. For a comparison, commonly used cell culture concentrations of RLX are 10^{-6}–10^{-9}g/ml, i.e. in the same concentration range[153].

14.6 Osteogenic Response to Osteoporosis Drugs (III)

In our first study with implants with mesoporous TiO_2 films, evaluation of the effect of controlled release of ALN and RLX in the local site of implant healing proved a superior effect both in terms of gene expression, bone growth, and bone-implant anchorage. The distributed amounts of ALN in the present work, on the order of 100 ng/implant, is similar to previous works using the same animal model, where 100–300 ng/implant were released outside the metallic implants[122]. This brought about a stronger anchorage in-between bone and implant in terms of RTQ, as both ALN and RLX promoted a significantly higher osseointegration in

comparison with implants without drugs (**Fig. 14.7**). The actual osseointegration was also studied by elemental analysis across the interface area by EDS and in STEM. Interestingly, the gradual ingrowth of apatite elements, Ca, P, O, was counterbalanced by a gradual decrease in the presence of Ti in the interface (**Fig. 14.8**), demonstrating a mixing of oxide and Calcium Phosphate in the interfacial region.

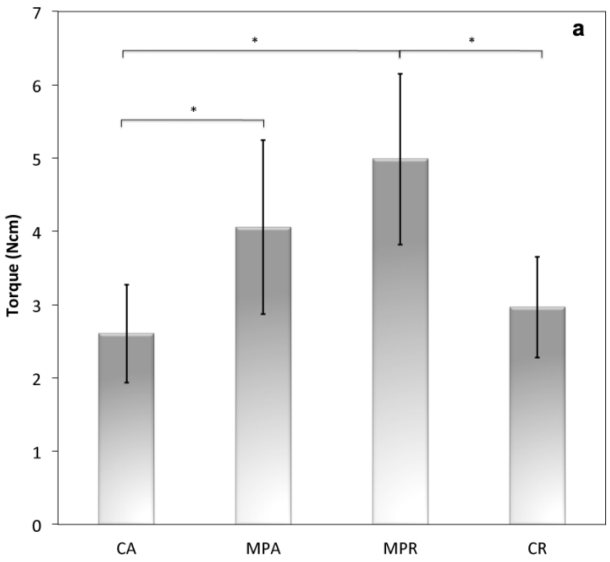

Fig. 14.7. RTQ 28 days post-surgery in rat tibia. The RLX releasing surface (MPR) showed strong bone anchorage, greater than that of the ALN releasing surface (MPA) or their respective controls, hydrophobic TiO2 (CA) and hydrophilic TiO2 (CR). *P < 0.05 (n = 8).

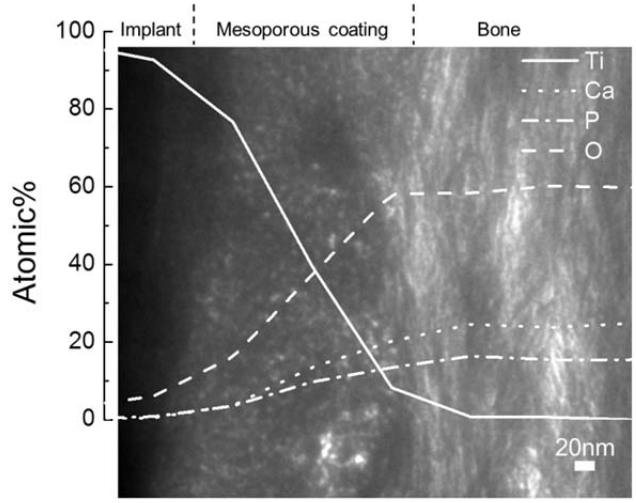

Fig. 14.8. A cross-sectional TEM image of the RLX-releasing surface after 28 days of implantation in rat tibia, The EDS line scan was performed across the metal implant, the mesoporous TiO2 coating and the surrounding bone, as indicated at the top of the image. At.% of Ti, Ca, P and O on the y-axis. Observe the presence of CaP within this mesoporous surface.

Gene expression data was partly complementary to functional evaluation. For implants releasing ALN, a down regulation of bone remodelling markers was observed at 28 days post-implantation, and especially of the osteoblast marker OC. N-BPs such as ALN are well known to suppress osteoclast metabolism via suppression of geranylgeranylation at the farnesyl diphosphate level[227]. ALN is suggested to regulate ephrinB1 gene expression of osteoclasts, which in turn interact with EphB1 or B3 receptors on osteoblasts and suppress osteoblast function. ALN may therefore, at this implantation time point, affect osteoclast precursors, which in turn act on osteoblast precursors of bone marrow cells through ephrinB1–EphB interactions[228]. Thus, ALN presumably affects the physiological bone metabolism mainly via the crosstalking between osteoclasts and osteoblasts. The net result is increased bone mass with decreased turnover kinetics, a phenomenon that can be used to improve prosthesis fixation by systemic[229] or local drug delivery[230].

The significantly higher CATK and OC expressions by RLX-exposed cells compared to ALN at 4 weeks of implantation suggests enhanced osteoblast and osteoclast activity in the close proximity of mesoporous Raloxifene loaded interfaces (MPR). The positive bone mass was building-up by RLX via oestrogen receptor modulation and stimulation of the release of osteoprotegerin (OPG) by osteoblasts, which in turn decrease the osteoclastic activity. RLX also suppresses resorptive paracrine factors such as TNF-a, IL-6 and IL-1b production by human trabecular osteoblasts. Such cytokines are associated with osteoclastogenesis[231, 232] and decrease RANKL release from osteoblasts in an OPG-independent manner[152]. Collectively, the above mechanisms contribute to suppression of osteoclastogenesis and result in enhanced bone mass by RLX.

14.7 Inflammatory Response to Local Drug Delivery (III)

We have touched upon the terminology of osteoimmunology and concluded in the first two studies that the early onset of inflammation could be attenuated by a mild heating or UVO-illumination of Ti implants. Although a confirmative effect of inflammation on osteogenesis was not reached, we know from the clinic that patients with rheumatoid arthritis have increased risk of osteoporosis[233]. Also, emerging evidence show that systemic bone loss and increased fracture risk can be seen in children with chronic inflammatory disease[234]. The need for further understanding and ideally controlling excessive inflammatory responses to bone implants remains to be addressed. In our approach with local drug delivery, we observed that local delivery of ALN or RLX, especially the latter, brings about the capability to affect the local inflammatory response. Surprisingly, the RLX results at 4 weeks also showed a significant up-

regulation of TNF-a, an indication that it is not as well understood as this inflammatory marker is, as mentioned previously, often linked to increased osteoclastic and reduced osteoblastic activity.

TNF-a-induced osteoclastogenesis is, however, RANKL dependent, and RLX is known to suppress this ligand. Both of the drug-loaded surfaces downregulated expression of IL-10 and IL-12β after 24 hours of healing (not published data) (**Fig. 14.9**), which indicates different healing kinetics or pathways for the differently prepared surfaces. Collection of gene expression data for IL-1β failed during the qPCR analysis by our provider, and we are therefore not able to discuss this marker.

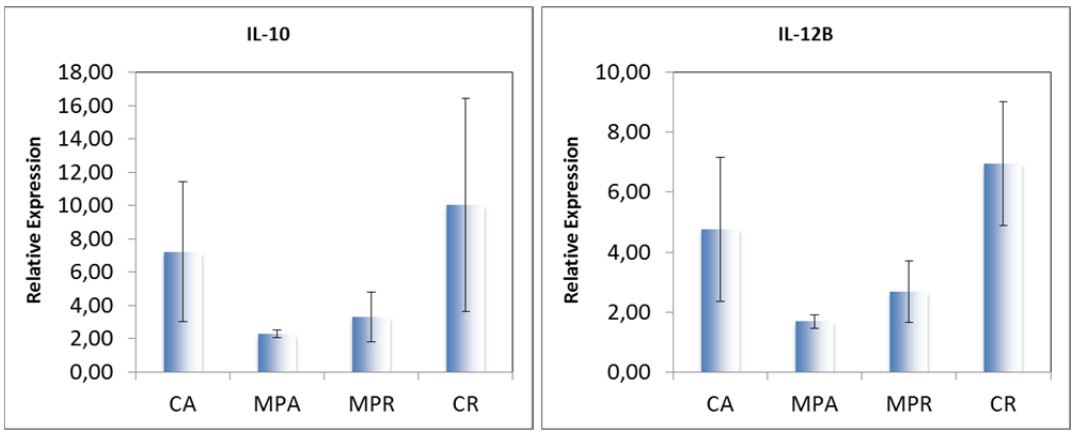

Fig. 14.9. Relative expression of IL-10 and IL-12β from implant-adherent cells after 24 hours of healing.

14.8 Pharmacokinetics of Alendronate (IV)

In this study, we immobilized ^{14}C-labelled ALN to mesoporous TiO_2 and visualized the pharmacodynamics of ALN in bone after 8 weeks of implantation. Next to some diffusion to blood marrow, the radiolabeled ALN mostly remained in the locality of the implant site. This could be displayed for all time points between 3 days and 8 weeks of healing, showing that the ALN diffusion was higher in bone marrow than in the denser cortical bone. Moreover, images corresponding to 4 and 8 weeks of implantation demonstrated a somewhat longer ALN transport in bone, although most ^{14}C-ALN remained within the closest few 100 µm around the implant surface (**Fig. 14.10**). The total intensity obtained from autoradiography corresponded to activity less than 10 nm in depth for the cross-section. Therefore LSC was used also to measure the entire activity in the bone around all the samples. The results of LSC measurements is given as activity (CPM) for the samples, and the amount of ^{14}C-ALN remained at the same level throughout the entire study of 8 weeks (320.3 ng (± 64.0 ng, n = 5). This is in accordance with

previous knowledge that BPs have high affinity to CaP and that the half life time of BPs in bone is at the order of years[139].

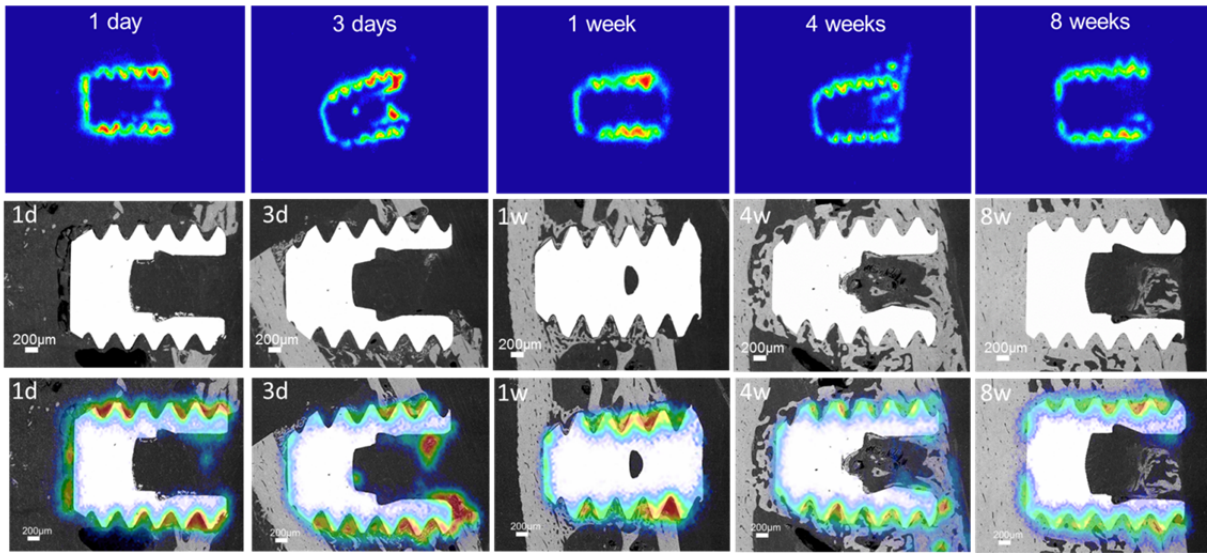

Fig. 14.10. (first row) The timeline of the autoradiography images, where all the different time points of healing *in vivo* is included. The intensity is coded from blue to red, where red corresponds to high radioactivity. (second row) SEM micrographs acquired in backscattering mode are presented for the corresponding samples as in the autoradiography images. (third row) the autoradiography and the SEM images are overlapped.

The efficacy of the local treatment was also demonstrated with backscattered SEM, by which the *de novo* bone formation could be visualized. At 4 and 8 weeks of healing, superior results of the bone formation around the test surface were observed at sites with local ^{14}C-ALN.

The advantageous effects of local delivery of BPs have been known for more than a decade. Aspenperg et al. showed that osseointegration of stainless steel screws was improved when BP was administered systemically or applied locally[235].

In other studies, BPs were bound to the implant, resulting in stronger fixation[120, 121]. The positive effect of BPs was also demonstrated clinically when ibandronate was applied directly on the exposed bone surface before insertion of knee prostheses. This led to improved prostheses stability and lowered migration after 1 year, as shown by X-ray analysis[236]. The rationale in success of BPs lies mainly in two of their key features: high affinity to bone and high drug efficacy.

Phosphate groups in the BP molecule have a strong affinity to calcium minerals, such as hydroxyapatite crystallites of bone. Any BP dissolved in body fluids will therefore tend to become immobilized to bone surfaces. When osteoclasts resorb bone, the BP will be internalized by the resorbing cell. In this way, the BPs become targeted by the osteoclasts and may be reused

at the locality as osteoclasts go into apoptosis, release their BP contents, which bind to surrounding bone and in turn to be internalized by new osteoclasts during the bone remodelling process. Nitrogen-containing BPs, such as pamidronate, alendronate, and ibandronate decrease bone resorption through the inhibition of the enzyme farnesyl diphosphate synthase in the mevalonate pathway. BPs without nitrogen form instead a toxic ATP-analogue in the osteoclasts[237]. In both cases the net result appears to be that osteoclasts either undergo apoptosis or at least lose their bone resorbing capacity[122].

14.9 Local vs. Systemic Delivery of Alendronate (V)

The high ALN efficacy in local applications originates likely from its long residence time in bone, i.e. the drug concentration remains for a long period of time within its therapeutic index – the ideal concentration between the minimum effective level and the toxic level. This differs from systemic delivery, in all its forms, where a drug reaches a certain maximum level in circulation, followed by a steady decay shortly thereafter, much depending on the properties of the drug. Specifically for BPs, it is worth mentioning that patients gain from BPs inherent high affinity to hydroxyapatite also when systemic delivery is applied, since more than 40% of delivered (i.v.) ALN dose becomes absorbed by bone, and then predominantly at bone growth zones. The terminal HA-bound half-life of alendronate is about 200 days in rat. Based on urinary excretion, the terminal half-life was estimated to be about 1000 days for the dog[139].

With these considerations in mind we evaluated the efficacy of ALN for a more rapid bone formation around the implants after a single injection in comparison to a local drug delivery system using a mesoporous Ti coating [238]. However, this time we implanted our model screws in a different rat model, the ovariectomized (OVX) rat, while the previous studies used normal male rats. The rationale behind this was two-fold. First, we wanted to evaluate the mesoporous Ti oxide system in a clinically more relevant osteoporotic model. Secondly, the OVX rat model is recommended by the FDA guidelines for the approval testing of new agents for osteoporosis treatment.

As we had hypothesized, the comparison of RTQ data showed that the local ALN release was superior to a single intravenous injection of ALN, with a significant difference of 46%* (*$p<0.05$) (**Fig. 14.11**). This confirms the efficacy of local delivery from mesoporous Ti implants as reported earlier[239].

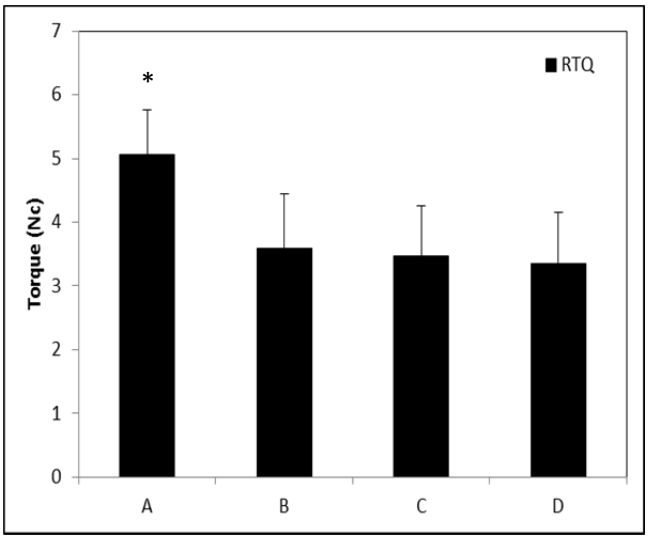

Fig. 14.11. Removal Torque (RTQ) analysis showing the effect of local vs. systemic delivery of ALN for bone-implant anchorage. The implant that was loaded with ALN showed a significantly higher RTQ than all other groups. (n=4, *p<0.05)

In study IV, we found that this coating system released approximately 0.3-0.5 μg of ALN to the site of bone healing around implants, more specifically within 400 μm from the implant surface. The current systemic delivery of 1 mg/kg ALN is expected to provide an average concentration of nearly 8 μg/g tibial bone, as based on studies by others[240]. However, the ALN binding to bone is considered to depend on its remodelling activity and localization of the compound. Having in mind that the ALN-bone binding is mediated by the HA phosphate groups, the accessibility of the apatite ALN is paramount for its intended function, antiosteolysis. It was previously found that systemically administered tritium labelled alendronate (^{3}H-ALN) in male rats was taken up at a lower degree on bone formation surfaces. This was expected to be due to lower accessibility to ALN of the hydroxyapatite behind the osteoid[141]. Similarly, in a recent study in dogs, McKenzie et al. reported that, the concentration of zoledronic acid when eluted from porous implants was largest on and within the implant, and with a rapid decrease at short distance away and with no uptake within the femoral cortex[241]. Bone adjacent to the site of implantation as well as in other anatomical locations was considered. It was also observed that BP remained within the metaphysis of long bones for a longer period of time than in diaphysis.

This above may explain the efficacy of direct delivery of ALN to HA-rich environments in peri-implant tibial diaphysis, due to the trauma and eroded tissue. This is despite the significant difference in the amount of locally or systemically delivered ALN, ca. 0.3-0.5 μg versus 8 μg/g, respectively. The implication is that when ALN is given systemically, the drug may be hindered in performing its action due to a limited distribution in traumatized tissue, hence the current

RTQ, BA, and BIC results from group C and D become comparable. Histomorphometric and μCT data are complementary to this observation. The μCT data indicate that local delivery of ALN from mesoporous Ti improved significantly the bone-implant contact (>30%) in comparison to the systemic delivery (**Fig. 14.12**).

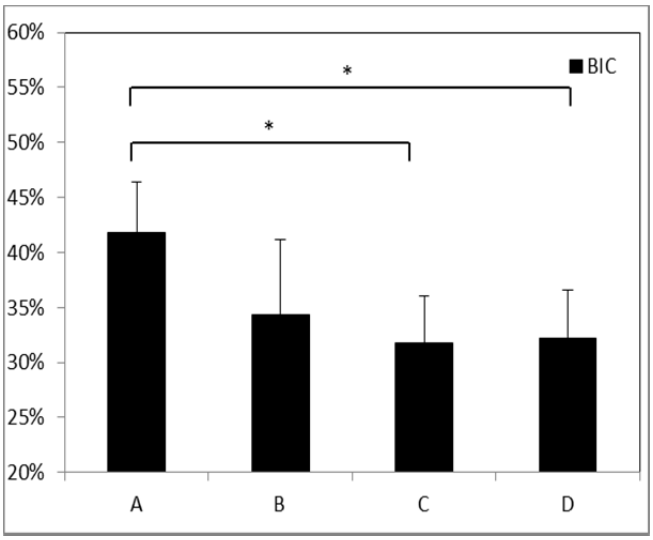

Fig. 14.12. MicroCT data of bone-implant-contact (BIC) within 10 μm of implant surface for all groups, showing a significant effect due to local delivery of ALN from mesoporous implants. (n=4, *p<0.05

In order for the systemic delivery to be able to overcome the local treatment, a much higher systemic dose is needed. This would in practice require repetitive doses. Indeed, it was found in a previous study that a cumulative dose of 35 mg/kg ALN resulted in a much higher concentration of the drug in the tibial joint and shaft, 32.9 μg/g and 10.1μg/g, respectively[240]. However, the possibility of side effects from higher and repetitive doses of BPs is a paramount consideration in clinics. The collected results indicate therefore that a local delivery of ALN from mesoporous Ti implants is superior to a single systemic bisphosphonate injection.

15 SUMMARY AND CONCLUSIONS

I study I, we addressed the innate complement activation property of TiO_2 and found that mild surface treatments could alter this property *in situ*. Model surfaces coated with Ti were heat-treated for up to 500°C or exposed to UVO-illumination for up to 96 hours and immersed in blood plasma prior to reaction with complement factor C3. Interestingly, we found that heat-treatments at 300°C or above or prolonged UVO-illumination attenuated adsorption of C3c. While we anticipated this as being a consequence of change in stoichiometry of the oxide, we believe that the behaviour of titanium dioxide in blood contact can be controlled through relatively simple means, such as mild heating and illumination in UV-light.

In study II, the abovementioned control of the biological behaviour of Ti was assessed in an animal model, where we measured the early and late immune and osteogenic response to complement activating and non-activating Ti implants. High immune activity was found around control implants in terms of mRNA expression of inflammatory markers and histological evaluation. On the other hand, UVO-treated implants showed a much lower activity of immune cells. As such, complement activating Ti implants elicited a stronger inflammatory response than UVO-treated Ti, with low complement activation during the first week of healing. In spite of this, the UVO-treated Ti induced only marginally more bone growth outside the implants.

In studies III-V, we developed and evaluated a mesoporous coating system for controlled drug delivery of osteoporosis drugs from Ti implants *in vivo*. Using the method of EISA, a highly ordered coating with a narrow pore size distribution was prepared just in an appropriate thickness to avoid interfering with surface properties otherwise, and with an accurate pore size in order to encapsulate two osteoporosis drugs, ALN and RLX.

Now, in study III we found that both ALN and RLX promoted an enhanced bone-implant anchorage when delivered locally from mesoporous Ti implants into rat tibia. A significantly improved RTQ, an increased expression of osteogenic markers, and higher BA and BIC following release of ALN and RLX after healing for 4 weeks, all confirmed the beneficial effect of this system. We found that RLX slightly outperformed ALN, which we expected to be a result of different mechanisms of action.

In study IV, we assessed the distribution kinetics of ALN for up to 8 weeks of healing *in vivo* and measured this by a combination of autoradiography with LSC. Radiolabelled ALN showed high affinity to bone mineral and remained intact in peri-implant tissue throughout the study time.

These results showed that when ALN is delivered locally, it stays in close vicinity of the implant and thereby literally eliminates the risks for systemic side-effects such as osteonecrosis of the jaw.

In study V, we aimed to compare the osteogenic capacity of systemic or local delivery of ALN in a clinically relevant, osteoporotic animal model. Otherwise healthy female rats were ovariectomized and onset of oestrogen deficiency was showed with hysterectomy. The osteogenic performance of mesoporous Ti implants loaded with ALN was compared with control implants and intravenous injection of ALN. We found that local delivery of ALN promoted a significantly stronger bone-anchorage in terms of RTQ, supported by higher BIC and BA, in comparison with a much higher dose given systemically yet without risks for side effects.

In conclusion, this thesis demonstrates that mild surface treatments can attenuate the complement activation property of TiO_2 both *in situ* and *in vivo* and that long term osseointegration is supposedly not altered by this property. Osteoporosis drugs can be delivered locally with the use of mesoporous TiO_2 coatings with benefits of higher bone-anchorage, drug efficacy, and with minimal risks of adverse reactions.

16 FUTURE PERSPECTIVES

The studies presented in this thesis offer a contribution to the highly active research on bone-anchored implants. The interplay between the early onset of complement activation and long term peri-implant bone healing has been of much debate due to an increasing number of patients suffering from implant loosening in relation to high inflammatory activity. Mild surface treatments and controlled delivery of specific drugs offer an optimal platform to address specific mediator mechanisms in healthy and pathological bone osteoimmunology and histogenesis. However, future scientific questioning must be invested in further understanding of intercellular mechanisms rather than targeting the single cell type.

For this reason, additional comparative studies are needed to fully determine the effect of nitrogen-containing BPs on the interplay between osteogenic cells, osteoblasts and osteocytes, and cells from the hematopoietic lineage. Osteoclasts share characteristics with other cells from this cyme, which inspires to perform broader genetic analysis of cellular and intercellular activity, such as the RANK/RANKL and the Wnt signalling systems. Although, the initial understanding of mechanism of action for BPs went thru osteoclastogenesis, it is now more convincing to include stem cells and osteoblasts in this mechanism. In fact, local drug delivery even offers an opportunity to isolate unhealthy side effects drugs. Such approaches require well-considered experimental designs, including clinical trials. Relevant questions are, whether if any amount of the locally given alendronate is distributed elsewhere in the body, and how much of systemically given alendronate is actually to be found in the peri-implant tissue? Or, how does the mechanism of action and pharmacokinetics of drugs and hormones such as insulin, thyroid stimulating hormone, immunosuppresive drugs, minerals or vitamins, strontium salts or peptides interplay with bone response when given locally?

Among mediator mechanisms that contribute to implant healing, those related to recruitment of stem cells are of particular future research interest. It is well-known that stem cells are recruited to sites of wound healing by mechanisms involving the SDF-1α/CXCR4 axis. This native ability of the body to withhold stem-cells in their niches of retention can be antagonized by delivering drugs locally to tissue adjacent to bone-implants. A system of optimal mesoporous coating and agents which target the abovementioned axis would theoretically offer an immense possibility to orchestrate native or in fact assist impaired bone-healing. In either case, we now know that an optimal experimental design is paramount when addressing such hypotheses.

17 ACKNOWLEDGEMENTS

"And, when you want something, all the universe conspires in helping you to achieve it."

Paulo Coelho, The Alchemist

It is with a blend of joy and excitement I am taking a firm step into the universe of science. The intriguing course of this journey was probably destined to bewilderment if not a long list of magnificent people helped me down the road.

Most of all, I would not have been able to finish this dissertation without the guidance, advice and support of my supervisor Professor Pentti Tengvall, to whom I express my deepest appreciation. From the very moment I arrived in Gothenburg, he has been there for me as a mentor and a friend, who so genially managed to mould my thoughts and curiosity into matter, which I hopefully one day can call that of a scientist. He is a true inspiration.

I gratefully thank my co-supervisor Associate Professor Anders Palmquist for his invaluable presence during the scientific discussions, which have paved the way for the being and actual writing of this thesis. Your door has always been open for me, which I generously have made use of.

Very special thanks to Professor Peter Thomsen and Associate Professor Jukka Lausmaa for their insightful advices, entrepreneurship and for giving me an invaluable opportunity to explore new thoughts.

I express a profound gratitude to the twin-team at Chalmers, my co-supervisor Associate Professor Martin Andersson, collaborator Professor Mats Halvarsson and twin PhD student Johan Karlsson. Johan, I will be looking forward to your dissertation at which I know you will be a rocking star and I look forward to continue working with you.

A major research project like this is never the work of one alone. I thank all my co-authors for an extremely collaborative piece of work, for their contributions and scientific knowledge to which I owe a debt of gratitude.

I show my deepest thankfulness to all ex and present colleagues and investigators at the Department of Biomaterials. Each and every one of you has been an invaluable member of the crew behind this thesis and I have felt blessed with you in my surroundings at times where it all felt like a puzzle. Special thanks to Petra, Birgitta, Anna, Maria, Lena, and Ann for motherly assistance during *in vitro* and *in vivo* studies, which often had an extra pitch of ambitions. Also

warm thanks to Maria and Magnus for their friendship and familiar handling of administrative work.

I thank all personnel at EBM for their assistance during my time there, exclusively veterinarian and my friend Haamid for the wise dialogues and warm friendship.

Special thanks to Dr. Hossein Agheli for his assistance with analytical tools at Chalmers and scientific discussions.

A sparkling thanks to all international visitors; Taka, Silvia, Kohei, Kazuyo, Shima who have visited our laboratory thru the years, for their friendship and companion. Special thanks to Kazuyo, who has so caringly devoted her time to teach me how to perform animal studies with *the precision of a surgeon*.

I gratefully thank all collaborators at Turku University, Linköping University and Leibniz Institute of Polymer Research Dresden for their hospitality and scientific discussions.

Last but not least, I warmly thank my friends Cemil, Adam, Kristian, Christopher, Kostas, Jesus, Agne, Josefin, and all comrades from FOKUS-A for your cheerful friendship and faith in me at all times and throughout many, many years. My friend Simon, I will always love you and cherish you in my heart.

Above all, I heartily thank my family for their unconditional support, both spiritually and emotionally throughout my dissertation, and for their infinite love and outstanding nature. In particular, the patience and understanding shown by my mother, father and sisters during the final year is greatly appreciated. A special thanks to my uncle Erdogan, who have made contributions to every single element of my conscious.

This thesis could not have been realized without the funding from the twinning project within Materials for Health which is an Area of Advance at Chalmers University of Technology, BIOMATCELL VINN Excellence Center of Biomaterials and Cell Therapy, Swedish Research Council (VR-project K2009-52X-21061-01-3), and Hjalmar Svensson Foundation. I sincerely acknowledge all financial support.

18 REFERENCES

1. Bothe, R.T., Beaton, K.E, Davenport, H.A. *Surg. Gynecol. Obstet.* **71** (1940).
2. Beder, O.E. & Eade, G. An investigation of tissue tolerance to titanium metal implants in dogs. *Surgery* **39**, 470-473 (1956).
3. Leventhal, G.S. Titanium, a metal for surgery. *J. Bone Joint Surg. Am.* **33-A**, 473-474 (1951).
4. Van Noort, R. Titanium - the Implant Material of Today. *J. Mater. Sci.* **22**, 3801-3811 (1987).
5. Dasse, K.A., Monzyk, B.F., Burckle, E.C., Busch, J.R. & Gilbert, R.J. Development of a photolytic artificial lung: Preliminary concept validation. *ASAIO J.* **49**, 556-563 (2003).
6. Li, J.W., Zhu, W., Liu, J.F., Liu, X. & Liu, H.Q. The hemocompatibility and the reabsorption function of TiO2 nanotubes biomembranes. *Chin. Sci. Bull.* **57**, 2022-2028 (2012).
7. Williams, D.F. in Titanium in Medicine. (eds. D.M. Brunette, P. Tengvall, M. Textor & P. Thomsen) pp14-25 (Springer-Verlag, New York; 2001).
8. Freese, H.L., Volas, M.G., Wood, J.R. in Titanium in Medicine. (eds. D.M. Brunette, P. Tengvall, M. Textor & P. Thomsen) pp26-49 (Springer-Verlag, New York; 2001).
9. Vörös, J., Wieland, M., Ruiz-Taylor, L., Textor, M. & Brunette, D.M. in Titanium in Medicine. (eds. D.M. Brunette, P. Tengvall, M. Textor & P. Thomsen) pp115-121 (Springer-Verlag Berling Heidelberg, Berlin, Germany; 2001).
10. Branemark, P.I. et al. Osseointegrated implants in the treatment of the edentulous jaw. Experience from a 10-year period. *Scand. J. Plast. Reconstr. Surg. Suppl.* **16**, 1-132 (1977).
11. Albrektsson, T., Branemark, P.I., Hansson, H.A. & Lindstrom, J. Osseointegrated titanium implants. Requirements for ensuring a long-lasting, direct bone-to-implant anchorage in man. *Acta Orthop. Scand.* **52**, 155-170 (1981).
12. Adell, R., Lekholm, U., Rockler, B. & Branemark, P.I. A 15-year study of osseointegrated implants in the treatment of the edentulous jaw. *Int. J. Oral Surg.* **10**, 387-416 (1981).
13. Adell, R., Lekholm, U., Rockler, B. & Branemark, P.I. A 15-Year Study of Osseointegrated Implants in the Treatment of the Edentulous Jaw. *Int. J. Oral Surg.* **10**, 387-416 (1981).
14. Steinemann, S.G. Metal implants and surface reactions. *Injury-International Journal of the Care of the Injured* **27**, 16-22 (1996).
15. Ratner, B.D. in Titanium in Medicine. (ed. D.M. Brunette) 2-10 (Springer-Verlag, New York; 2001).
16. Tengvall, P., Lundstrom, I., Sjoqvist, L., Elwing, H. & Bjursten, L.M. Titanium-hydrogen peroxide interaction: model studies of the influence of the inflammatory response on titanium implants. *Biomaterials* **10**, 166-175 (1989).
17. Mills, A., Hill, G., Bhopal, S., Parkin, I.P. & O'Neill, S.A. Thick titanium dioxide films for semiconductor photocatalysis. *Journal of Photochemistry and Photobiology a-Chemistry* **160**, 185-194 (2003).
18. Sittig, C., Textor, M., Spencer, N.D., Wieland, M. & Vallotton, P.H. Surface characterization of implant materials cp Ti, Ti-6Al-7Nb and Ti-6Al-4V with different pretreatments. *Journal of Materials Science-Materials in Medicine* **10**, 35-46 (1999).

19. Pouilleau, J., Devilliers, D., Garrido, F., Durand-Vidal, S. & Mahé, E. Structure and composition of passive titanium oxide films. *Materials Science and Engineering B-Solid State Materials for Advanced Technology* **47**, 235-243 (1997).

20. Ellingsen, J.E., Thomsen, P. & Lyngstadaas, S.P. Advances in dental implant materials and tissue regeneration. *Periodontol. 2000* **41**, 136-156 (2006).

21. Geocities, Vol. 2009 (

22. Fraker, A.C., Ruff, A.W., Sung, P., Van Orden, A.C., Speck, K.M. in Titanium Alloys in Surgical Implans, Vol. ASTM Special Technical Publication. (ed. H.A. Luckey, Kubli, F.) 206-219 (ASTM, Philadelphia; 1983).

23. Lide, D.R. CRC Handbook of Chemistry and Physics. (CRS Press, London; 1994).

24. Textor, M., Sittig, C., Frauchiger, V., Tosatti, S., Brunette, D.M. in Titanium in Medicine. (eds. J. Vörös, M. Wieland, L. Ruiz-Taylor, M. Textor & D.M. Brunette) pp172-221 (Springer-Verlag, New York; 2001).

25. Schenk, R. in Titanium in Medicine. (eds. D.M. Brunette, P. Tengvall, M. Textor & P. Thomsen) pp145-171 (Springer-Verlag Berling Heidelberg, Berlin, Germany; 2001).

26. Munuera, G. & Stone, F.S. Adsorption of water and organic vapors on hydroxylated rutile. *Discuss. Faraday Soc.*, 205-& (1971).

27. Horbett, T.A. & Brash, J.L. Proteins at Interfaces - Current Issues and Future-Prospects. *ACS Symp. Ser.* **343**, 1-33 (1987).

28. Puleo, D.A. & Nanci, A. Understanding and controlling the bone-implant interface. *Biomaterials* **20**, 2311-2321 (1999).

29. Tengvall, P. & Askendal, A. Ellipsometric in vitro studies on blood plasma and serum adsorption to zirconium. *J. Biomed. Mater. Res.* **57**, 285-290 (2001).

30. Horbett, T.A. in Biomaterials Science. (ed. B.D. Ratner, Hoffman, A.S., Schoen, F.J., Lemons, J.E.) 133-141 (Academic Press, San Diego; 1996).

31. Walivaara, B., Aronsson, B.O., Rodahl, M., Lausmaa, J. & Tengvall, P. Titanium with different oxides: in vitro studies of protein adsorption and contact activation. *Biomaterials* **15**, 827-834 (1994).

32. Nowak, T., Handford, A.G. in Pathophysiology: Concepts and Applications for Health Care Professionals 81-123 (McGraw-Hill, New York; 2004).

33. Wettero, J., Askendal, A., Bengtsson, T. & Tengvall, P. On the binding of complement to solid artificial surfaces in vitro. *Biomaterials* **23**, 981-991 (2002).

34. Johnson, R.J. in Biomaterials Science. (ed. B.D. Ratner, Hoffman, A.S., Schoen, F.J., Lemons, J.E.) 173-188 (Academic Press, San Diego; 1996).

35. Walivaara, B., Askendal, A., Krozer, A., Lundstrom, I. & Tengvall, P. Blood protein interactions with chromium surfaces. *Journal of Biomaterials Science-Polymer Edition* **8**, 49-62 (1996).

36. Walivaara, B., Askendal, A., Lundstrom, I. & Tengvall, P. Blood protein interactions with titanium surfaces. *Journal of Biomaterials Science-Polymer Edition* **8**, 41-48 (1996).

37. Arvidsson, S., Askendal, A. & Tengvall, P. Blood plasma contact activation on silicon, titanium and aluminium. *Biomaterials* **28**, 1346-1354 (2007).

38. Tengvall, P. in Titanium in Medicine. (eds. D.M. Brunette, P. Tengvall, M. Textor & P. Thomsen) pp457-485 (Springer-Verlag Berling Heidelberg, Berlin, Germany; 2001).

39. Chenoweth, D.E. Complement Activation Produced by Biomaterials. *Artif. Organs* **12**, 508-510 (1988).

40. Law, S.K.A. & Reid, K.B.M. Complement In Focus, Edn. 2. (Oxford University Press, New York, USA; 1995).

41. Hulander, M. et al. Gradients in surface nanotopography used to study platelet adhesion and activation. *Colloids and Surfaces B-Biointerfaces* **110**, 261-269 (2013).

42. Fujishima, A. & Honda, K. ELECTROCHEMICAL PHOTOLYSIS OF WATER AT A SEMICONDUCTOR ELECTRODE. *Nature* **238**, 37-+ (1972).

43. Fujishima, A. Discovery and applications of photocatalysis-Creating a comfortable future by making use of light energy. *Japan Nanonet Bulletin* (2003).

44. Wang, R. et al. Light-induced amphiphilic surfaces. *Nature* **388**, 431-432 (1997).

45. Sawase, T. et al. Photo-induced hydrophilicity enhances initial cell behavior and early bone apposition. *Clin. Oral Implants Res.* **19**, 491-496 (2008).

46. Sawase, T. et al. A novel characteristic of porous titanium oxide implants. *Clin. Oral Implants Res.* **18**, 680-685 (2007).

47. Aita, H. et al. The effect of ultraviolet functionalization of titanium on integration with bone. *Biomaterials* **30**, 1015-1025 (2009).

48. Rupp, F. et al. Enhancing surface free energy and hydrophilicity through chemical modification of microstructured titanium implant surfaces. *Journal of Biomedical Materials Research Part A* **76A**, 323-334 (2006).

49. Company, J.C.L. (2009).

50. Piskarev, I.M. et al. Ozone formation in a high-current streamer electric discharge in air containing water and hydrocarbon vapors. *High Energy Chem.* **38**, 129-130 (2004).

51. Vig, J.R. UV OZONE CLEANING OF SURFACES. *Journal of Vacuum Science & Technology a-Vacuum Surfaces and Films* **3**, 1027-1034 (1985).

52. Ye, M.M., Chen, Z.L., Liu, X.W., Ben, Y. & Shen, J.M. Ozone enhanced activity of aqueous titanium dioxide suspensions for photodegradation of 4-chloronitrobenzene. *J. Hazard. Mater.* **167**, 1021-1027 (2009).

53. Vig, J.R. in Handbook of semiconductor wafer cleaning technology. (ed. W. Kern) 233-273 (Noyes Publications, New Jersey; 1993).

54. Chao, S.C., Pitchai, R. & Lee, Y.H. ENHANCEMENT IN THERMAL-OXIDATION OF SILICON BY OZONE. *J. Electrochem. Soc.* **136**, 2751-2752 (1989).

55. Rho, J.Y., Kuhn-Spearing, L. & Zioupos, P. Mechanical properties and the hierarchical structure of bone. *Med. Eng. Phys.* **20**, 92-102 (1998).

56. Seeley, R.R., Stephens, T.D. & Tate, P. Anatomy & Physiology, Edn. 6ed. (McGraw-Hill, New York, NY 10020; 2000).

57. Fazzalari, N.L. et al. Trabecular Microfracture. *Calcif. Tissue Int.* **53**, S143-S147 (1993).

58. Frost, H.M. Wolff's Law and bone's structural adaptations to mechanical usage: an overview for clinicians. *Angle Orthod.* **64**, 175-188 (1994).

59. Katagiri, T. & Takahashi, N. Regulatory mechanisms of osteoblast and osteoclast differentiation. *Oral Dis.* **8**, 147-159 (2002).

60. Lelovas, P.P., Xanthos, T.T., Thoma, S.E., Lyritis, G.P. & Dontasi, I.A. The Laboratory Rat as an Animal Model for Osteoporosis Research. *Comp. Med.* **58**, 424-430 (2008).

61. Jowsey, J. Studies of Haversian Systems in Man and Some Animals. *J. Anat.* **100**, 857-& (1966).

62. Scotti, C. et al. Recapitulation of endochondral bone formation using human adult mesenchymal stem cells as a paradigm for developmental engineering. *Proc. Natl. Acad. Sci. U. S. A.* **107**, 7251-7256 (2010).

63. Yamamoto, H., Sawaki, Y., Ohkubo, H. & Ueda, M. Maxillary advancement by distraction osteogenesis using osseointegrated implants. *Journal of Cranio-Maxillofacial Surgery* **25**, 186-191 (1997).

64. Wang, X.D., Mabrey, J.D. & Agrawal, C.M. An interspecies comparison of bone fracture properties. *Bio-Med. Mater. Eng.* **8**, 1-9 (1998).

65. Egermann, M., Goldhahn, J. & Schneider, E. Animal models for fracture treatment in osteoporosis. *Osteoporos. Int.* **16**, S129-S138 (2005).

66. Pearce, A.I., Richards, R.G., Milz, S., Schneider, E. & Pearce, S.G. Animal models for implant biomaterial research in bone: A review. *Eur. Cells Mater.* **13**, 1-10 (2007).

67. Jingushi, S. & Bolander, M.E. in The Bone-Biomaterial Interface. (ed. J.E. Davies) 250-262 (University of Toronte Press, Toronto; 1990).

68. Ai-Aql, Z.S., Alagl, A.S., Graves, D.T., Gerstenfeld, L.C. & Einhorn, T.A. Molecular mechanisms controlling bone formation during fracture healing and distraction osteogenesis. *J. Dent. Res.* **87**, 107-118 (2008).

69. Wang, F.S. et al. Temporal and spatial expression of bone morphogenetic proteins in extracorporeal shock wave-promoted healing of segmental defect. *Bone* **32**, 387-396 (2003).

70. Chung, R., Cool, J.C., Scherer, M.A., Foster, B.K. & Xian, C.J. Roles of neutrophil-mediated inflammatory response in the bony repair of injured growth plate cartilage in young rats. *J. Leukoc. Biol.* **80**, 1272-1280 (2006).

71. Kuroda, S., Virdi, A.S., Dai, Y., Shott, S. & Sumner, D.R. Patterns and localization of gene expression during intramembranous bone regeneration in the rat femoral marrow ablation model. *Calcif. Tissue Int.* **77**, 212-225 (2005).

72. Frost, H.M. The Biology of Fracture-Healing - an Overview for Clinicians .1. *Clin. Orthop.*, 283-293 (1989).

73. Dahlin, C., Johansson, C.B. in Osteology Guidelines for Oral & Maxillofacial Reneration. (ed. W.V. Giannobile, Nevins, M.) 103-123 (Quintessence Publishing Co., Ltd, Surrey; 2011).

74. Uchida, S. et al. Vascular endothelial growth factor is expressed along with its receptors during the healing process of bone and bone marrow after drill-hole injury in rats. *Bone* **32**, 491-501 (2003).

75. Wolff, J. Das Gesetz der Transformation der knochen. (Hirschwald, Berlin; 1892).

76. Frost, H.M. The Biology of Fracture-Healing - an Overview for Clinicians .2. *Clin. Orthop.*, 294-309 (1989).

77. Misch, C.E., Qu, Z.M. & Bidez, M.W. Mechanical properties of trabecular bone in the human mandible: Implications for dental implant treatment planning and. Surgical placement. *J. Oral Maxillofac. Surg.* **57**, 700-706 (1999).

78. Axhausen, G. Die pathologisch-anatomischen Grundlagen der Lehre von der freien Knochentransplantation beim Menschen und beim Tier. *Med Klin (Suppl)* **2**, 23-58 (1908).

79. Frost, H.M. Some Abcs of Skeletal Patho-Physiology .1. Introduction to the Series. *Calcif. Tissue Int.* **45**, 1-3 (1989).

80. Bu, R.F. et al. Expression and function of TNF-family proteins and receptors in human osteoblasts. *Bone* **33**, 760-770 (2003).

81. Dimitriou, R., Tsiridis, E. & Giannoudis, P.V. Current concepts of molecular aspects of bone healing. *Injury-International Journal of the Care of the Injured* **36**, 1392-1404 (2005).

82. Omar, O. et al. Integrin and chemokine receptor gene expression in implant-adherent cells during early osseointegration. *Journal of Materials Science-Materials in Medicine* **21**, 969-980 (2010).

83. Cho, T.J., Gerstenfeld, L.C. & Einhorn, T.A. Differential temporal expression of members of the transforming growth factor beta superfamily during murine fracture healing. *J. Bone Miner. Res.* **17**, 513-520 (2002).

84. Kon, T. et al. Expression of osteoprotegerin, receptor activator of NF-kappa B ligand (osteoprotegerin ligand) and related proinflammatory cytokines during fracture healing. *J. Bone Miner. Res.* **16**, 1004-1014 (2001).

85. Landry, P., Sadasivan, K., Marino, A. & Albright, J. Apoptosis is coordinately regulated with osteoblast formation during bone healing. *Tissue Cell* **29**, 413-419 (1997).

86. Olmedo, M.L. et al. Regulation of osteoblast levels during bone healing. *J. Orthop. Trauma* **13**, 356-362 (1999).

87. Cabal-Hierro, L. & Lazo, P.S. Signal transduction by tumor necrosis factor receptors. *Cell. Signal.* **24**, 1297-1305 (2012).

88. Thomson, B.M., Mundy, G.R. & Chambers, T.J. Tumor Necrosis Factors-Alpha and Factors-Beta Induce Osteoblastic Cells to Stimulate Osteoclastic Bone-Resorption. *J. Immunol.* **138**, 775-779 (1987).

89. Zhou, F.H., Foster, B.K., Zhou, X.F., Cowin, A.J. & Xian, C.J. TNF-alpha mediates p38 MAP kinase activation and negatively regulates bone formation at the injured growth plate in rats. *J. Bone Miner. Res.* **21**, 1075-1088 (2006).

90. Hofbauer, L.C. et al. Interleukin-1 beta and tumor necrosis factor-alpha, but not interleukin-6, stimulate osteoprotegerin ligand gene expression in human osteoblastic cells. *Bone* **25**, 255-259 (1999).

91. Wei, S., Kitaura, H., Zhou, P., Ross, F.P. & Teitelbaum, S.L. IL-1 mediates TNF-induced osteoclastogenesis. *J. Clin. Invest.* **115**, 282-290 (2005).

92. Souza, P.P.C. & Lerner, U.H. The role of cytokines in inflammatory bone loss. *Immunol. Invest.* **42**, 555-622 (2013).

93. Graves, D.T. & Jiang, Y. Chemokines, a Family of Chemotactic Cytokines. *Crit. Rev. Oral Biol. Med.* **6**, 109-118 (1995).

94. Bendre, M.S. et al. Interleukin-8 stimulation of osteoclastogenesis and bone resorption is a mechanism for the increased osteolysis of metastatic bone disease. *Bone* **33**, 28-37 (2003).

95. Owens, J.M., Gallagher, A.C. & Chambers, T.J. IL-1O modulates formation of osteoclasts in murine hemopoietic cultures. *J. Immunol.* **157**, 936-940 (1996).

96. Toupadakis, C.A. et al. Long-term administration of AMD3100, an antagonist of SDF-1/CXCR4 signaling, alters fracture repair. *J. Orthop. Res.* **30**, 1853-1859 (2012).

97. Zwingenberger, S. et al. Stem cell attraction via SDF-1 expressing fat tissue grafts. *Journal of Biomedical Materials Research Part A* **101A**, 2067-2074 (2013).

98. Perez-Amodio, S., Beertsen, W. & Everts, V. (Pre-)Osteoclasts induce retraction of osteoblasts before their fusion to osteoclasts. *J. Bone Miner. Res.* **19**, 1722-1731 (2004).

99. Garnero, P. et al. The collagenolytic activity of cathepsin K is unique among mammalian proteinases. *J. Biol. Chem.* **273**, 32347-32352 (1998).

100. Albrektsson, T. et al. Is Marginal Bone Loss around Oral Implants the Result of a Provoked Foreign Body Reaction? *Clin. Implant Dent. Relat. Res.* (2013).

101. Branemark, P.I. et al. Osseo-Integrated Implants in Treatment of Edentulous Jaw - Experience from a 10-Year Period. *Scand. J. Plast. Reconstr. Surg. Hand Surg.*, 7-132 (1977).

102. Meyer, U. et al. Ultrastructural characterization of the implant/bone interface of immediately loaded dental implants. *Biomaterials* **25**, 1959-1967 (2004).

103. Holahan, C.M. et al. Effect of Osteoporotic Status on the Survival of Titanium Dental Implants. *Int. J. Oral Maxillofac. Implants* **23**, 905-910 (2008).

104. Klibanski, A. et al. Osteoporosis prevention, diagnosis, and therapy. *Jama-Journal of the American Medical Association* **285**, 785-795 (2001).

105. Cooper, C., Campion, G. & Melton, L.J. Hip-Fractures in the Elderly - a Worldwide Projection. *Osteoporos. Int.* **2**, 285-289 (1992).

106. Melton, L.J., Chrischilles, E.A., Cooper, C., Lane, A.W. & Riggs, B.L. How Many Women Have Osteoporosis. *J. Bone Miner. Res.* **7**, 1005-1010 (1992).

107. Randell, A. et al. Direct clinical and welfare costs of osteoporotic fractures in elderly men and women. *Osteoporos. Int.* **5**, 427-432 (1995).

108. Reginster, J.Y. & Burlet, N. Osteoporosis: A still increasing prevalence. *Bone* **38**, 4-9 (2006).

109. Goldhahn, J., Suhm, N., Goldhahn, S., Blauth, M. & Hanson, B. Influence of osteoporosis on fracture fixation - a systematic literature review. *Osteoporos. Int.* **19**, 761-772 (2008).

110. Marco, F., Milena, F., Gianluca, G. & Vittoria, O. Peri-implant osteogenesis in health and osteoporosis. *Micron* **36**, 630-644 (2005).

111. Hayashi, K., Uenoyama, K., Mashima, T. & Sugioka, Y. Remodeling of Bone around Hydroxyapatite and Titanium in Experimental Osteoporosis. *Biomaterials* **15**, 11-16 (1994).

112. Fini, M. et al. Biomaterials for orthopedic surgery in osteoporotic bone: A comparative study in osteopenic rats. *Int. J. Artif. Organs* **20**, 291-297 (1997).

113. Fini, M. et al. Biocompatibility and osseointegration in osteoporotic bone - A preliminary in vitro and in vivo study. *Journal of Bone and Joint Surgery-British Volume* **83B**, 139-143 (2001).

114. Rocca, M., Fini, M., Giavaresi, G., Aldini, N.N. & Giardino, R. Tibial implants: biomechanical and histomorphometric studies of hydroxyapatite-coated and uncoated stainless steel

and titanium screws in long-term ovariectomized sheep. *Int. J. Artif. Organs* **24**, 649-654 (2001).

115. Hu, Y., Cai, K.Y., Luo, Z. & Jandt, K.D. Layer-By-Layer Assembly of beta-Estradiol Loaded Mesoporous Silica Nanoparticles on Titanium Substrates and Its Implication for Bone Homeostasis. *Adv. Mater.* **22**, 4146-+ (2010).

116. Wei, G.X. et al. A Bioabsorbable Delivery System for Antibiotic-Treatment of Osteomyelitis - the Use of Lactic-Acid Oligomer as a Carrier. *Journal of Bone and Joint Surgery-British Volume* **73**, 246-252 (1991).

117. Thoma, K. & Alex, R. Biodegradable Gentamicin-Loaded Controlled Release Implants Made of Beta-Tricalcium Phosphate Ceramics .1. Studies on the Preparation and Characterization of Porous Ceramic Beta-Tricalcium Phosphate Matrices. *Pharmazie* **46**, 193-197 (1991).

118. Roos-Jansaker, A.M., Renvert, S. & Egelberg, J. Treatment of peri-implant infections: a literature review. *J. Clin. Periodontol.* **30**, 467-485 (2003).

119. Binderman, I., Adut, M. & Yaffe, A. Effectiveness of local delivery of alendronate in reducing alveolar bone loss following periodontal surgery in rats. *J. Periodontol.* **71**, 1236-1240 (2000).

120. Tengvall, P., Skoglund, B., Askendal, A. & Aspenberg, P. Surface immobilized bisphosphonate improves stainless-steel screw fixation in rats. *Biomaterials* **25**, 2133-2138 (2004).

121. Wermelin, K., Tengvall, P. & Aspenberg, P. Surface-bound bisphosphonates enhance screw fixation in rats--increasing effect up to 8 weeks after insertion. *Acta Orthop.* **78**, 385-392 (2007).

122. Wermelin, K., Suska, F., Tengvall, P., Thomsen, P. & Aspenberg, P. Stainless steel screws coated with bisphosphonates gave stronger fixation and more surrounding bone. Histomorphometry in rats. *Bone* **42**, 365-371 (2008).

123. Wermelin, K., Aspenberg, P., Linderback, P. & Tengvall, P. Bisphosphonate coating on titanium screws increases mechanical fixation in rat tibia after two weeks. *J. Biomed. Mater. Res. A* **86**, 220-227 (2008).

124. Abtahi, J., Tengvall, P. & Aspenberg, P. A bisphosphonate-coating improves the fixation of metal implants in human bone. A randomized trial of dental implants. *Bone* **50**, 1148-1151 (2012).

125. Abtahi, J., Agholme, F., Sandberg, O. & Aspenberg, P. Effect of Local vs. Systemic Bisphosphonate Delivery on Dental Implant Fixation in a Model of Osteonecrosis of the Jaw. *J. Dent. Res.* **92**, 279-283 (2013).

126. Vallet-Regi, M., Balas, F. & Arcos, D. Mesoporous materials for drug delivery. *Angewandte Chemie-International Edition* **46**, 7548-7558 (2007).

127. Kresge, C.T., Leonowicz, M.E., Roth, W.J., Vartuli, J.C. & Beck, J.S. Ordered Mesoporous Molecular-Sieves Synthesized by a Liquid-Crystal Template Mechanism. *Nature* **359**, 710-712 (1992).

128. Zhao, D.Y. et al. Triblock copolymer syntheses of mesoporous silica with periodic 50 to 300 angstrom pores. *Science* **279**, 548-552 (1998).

129. Rosler, A., Vandermeulen, G.W.M. & Klok, H.A. Advanced drug delivery devices via self-assembly of amphiphilic block copolymers. *Adv. Drug Delivery Rev.* **53**, 95-108 (2001).

130. Andersson, M. et al. Ag/AgCl-loaded ordered mesoporous anatase for photocatalysis. *Chem. Mater.* **17**, 1409-1415 (2005).

131. Antonelli, D.M. & Ying, J.Y. SYNTHESIS OF HEXAGONALLY PACKED MESOPOROUS TIO2 BY A MODIFIED SOL-GEL METHOD. *Angewandte Chemie-International Edition in English* **34**, 2014-2017 (1995).

132. Zhang, Y. et al. Osteogenic properties of hydrophilic and hydrophobic titanium surfaces evaluated with osteoblast-like cells (MG63) in coculture with human umbilical vein endothelial cells (HUVEC). *Dent. Mater.* **26**, 1043-1051 (2010).

133. Vivero-Escoto, J.L., Slowing, I.I., Wu, C.-W. & Lin, V.S.Y. Photoinduced Intracellular Controlled Release Drug Delivery in Human Cells by Gold-Capped Mesoporous Silica Nanosphere. *J. Am. Chem. Soc.* **131**, 3462-+ (2009).

134. Wei, D.Q., Zhou, Y. & Yang, C.H. Characteristic, cell response and apatite-induction ability of microarc oxidized TiO2-based coating containing P on Ti6Al4V before and after chemical-treatment and dehydration. *Ceram. Int.* **35**, 2545-2554 (2009).

135. Izquierdo-Barba, I., Colilla, M. & Vallet-Regi, M. Nanostructured Mesoporous Silicas for Bone Tissue Regeneration. *J. Nanomater* (2008).

136. Menschutkin, M. Ueber die Einwirkung des Chloracetyls auf phosphorige Säure. *Ann Chem Pharm* **133**, 317-320 (1865).

137. Fleisch, H., Russell, R.G.G., Bisaz, S., Casey, P.A. & Muhlbaue.Rc Influence of Pyrophosphate Analogues (Diphosphonates) on Precipitation and Dissolution of Calium Phosphate in Vitro and in Vivo. *Calcif. Tissue Res.* **S 2**, 10-& (1968).

138. Giuliani, N. et al. Bisphosphonates stimulate formation of osteoblast precursors and mineralized nodules in murine and human bone marrow cultures in vitro and promote early osteoblastogenesis in young and aged mice in vivo. *Bone* **22**, 455-461 (1998).

139. Lin, J.H., Duggan, D.E., Chen, I.W. & Ellsworth, R.L. Physiological Disposition of Alendronate, a Potent Anti-Osteolytic Bisphosphonate, in Laboratory-Animals. *Drug Metab. Dispos.* **19**, 926-932 (1991).

140. Hoggarth, C.R., Bennett, R. & Daleyyates, P.T. The Pharmacokinetics and Distribution of Pamidronate for a Range of Doses in the Mouse. *Calcif. Tissue Int.* **49**, 416-420 (1991).

141. Sato, M. et al. Bisphosphonate Action - Alendronate Localization in Rat Bone and Effects on Osteoclast Ultrastructure. *J. Clin. Invest.* **88**, 2095-2105 (1991).

142. Roelofs, A.J., Thompson, K., Ebetino, F.H., Rogers, M.J. & Coxon, F.P. Bisphosphonates: Molecular Mechanisms of Action and Effects on Bone Cells, Monocytes and Macrophages. *Curr. Pharm. Des.* **16**, 2950-2960 (2010).

143. Reszka, A.A. & Rodan, G.A. Bisphosphonate mechanism of action. *Curr. Rheumatol. Rep.* **5**, 65-74 (2003).

144. Rodan, G.A. & Fleisch, H.A. Bisphosphonates: mechanisms of action. *The Journal of clinical investigation* **97**, 2692-2696 (1996).

145. Wikipedia, t.f.e. ((2012).

146. Shaw, N.J. & Bishop, N.J. Bisphosphonate treatment of bone disease. *Arch. Dis. Child.* **90**, 494-499 (2005).

147. Giuliani, N., Pedrazzoni, M., Passeri, G. & Girasole, G. Bisphosphonates inhibit IL-6 production by human osteoblast-like cells. *Scand. J. Rheumatol.* **27**, 38-41 (1998).

148. Borromeo, G.L. et al. Is bisphosphonate therapy for benign bone disease associated with impaired dental healing? A case-controlled study. *Bmc Musculoskeletal Disorders* **12** (2011).

149. Ruggiero, S.L., et al. (ed. A.A.o.O.a.M. Surgeons) (AAOMS, 2009).

150. Rodan, G.A. Mechanisms of action of bisphosphonates. *Annu. Rev. Pharmacol. Toxicol.* **38**, 375-388 (1998).

151. Taranta, A. et al. The selective estrogen receptor modulator raloxifene regulates osteoclast and osteoblast activity in vitro. *Bone* **30**, 368-376 (2002).

152. Yan, M.Z. et al. Raloxifene inhibits bone loss and improves bone strength through an Opg-independent mechanism. *Endocrine* **37**, 55-61 (2010).

153. Bambini, F. et al. Raloxifene covalently bonded to titanium implants by interfacing with (3-aminopropyl)-Triethoxysilane affects osteoblast-like cell gene expression. *Int. J. Immunopathol. Pharmacol.* **19**, 905-914 (2006).

154. Albrektsson, T. & Johansson, C. Osteoinduction, osteoconduction and osseointegration. *Eur. Spine J.* **10**, S96-S101 (2001).

155. Koster, J.C., Hackeng, W.H.L. & Mulder, H. Diminished effect of etidronate in vitamin D deficient osteopenic postmenopausal women. *Eur. J. Clin. Pharmacol.* **51**, 145-147 (1996).

156. Marie, P.J., Ammann, P., Boivin, G. & Rey, C. Mechanisms of action and therapeutic potential of strontium in bone. *Calcif. Tissue Int.* **69**, 121-129 (2001).

157. Marie, P.J. Strontium ranelate: a novel mode of action optimizing bone formation and resorption. *Osteoporos. Int.* **16**, S7-S10 (2005).

158. Bassett, J.H.D. & Williams, G.R. Critical role of the hypothalamic-pituitary-thyroid axis in bone. *Bone* **43**, 418-426 (2008).

159. Abe, E. et al. TSH is a negative regulator of skeletal remodeling. *Cell* **115**, 151-162 (2003).

160. Sun, L. et al. Intermittent recombinant TSH injections prevent ovariectomy-induced bone loss. *Proc. Natl. Acad. Sci. U. S. A.* **105**, 4289-4294 (2008).

161. Slavin, J. The role of cytokines in wound healing. *J. Pathol.* **178**, 5-10 (1996).

162. Kirkpatrick, C.J. et al. Tissue response and biomaterial integration: the efficacy of in vitro methods. *Biomol. Eng.* **19**, 211-217 (2002).

163. Rogers, S.D., Howie, D.W., Graves, S.E., Pearcy, M.J. & Haynes, D.R. In vitro human monocyte response to wear particles of titanium alloy containing vanadium or niobium. *Journal of Bone and Joint Surgery-British Volume* **79B**, 311-315 (1997).

164. Haynes, D.R., Rogers, S.D., Hay, S., Pearcy, M.J. & Howie, D.W. The Differences in Toxicity and Release of Bone-Resorbing Mediators Induced by Titanium and Cobalt-Chromium-Alloy Wear Particles. *Journal of Bone and Joint Surgery-American Volume* **75A**, 825-834 (1993).

165. van Beek, E., Pieterman, E., Cohen, L., Lowik, C. & Papapoulos, S. Farnesyl pyrophosphate synthase is the molecular target of nitrogen-containing bisphosphonates. *Biochem. Biophys. Res. Commun.* **264**, 108-111 (1999).

166. Bergstrom, J.D., Bostedor, R.G., Masarachia, P.J., Reszka, A.A. & Rodan, G. Alendronate is a specific, nanomolar inhibitor of farnesyl diphosphate synthase. *Arch. Biochem. Biophys.* **373**, 231-241 (2000).

167. Davies, C.M. et al. Mechanically loaded ex vivo bone culture system 'Zetos': Systems and culture preparation. *Eur. Cells Mater.* **11**, 57-75 (2006).

168. Russell, W.M.S., Burch, R.L. & Hume, C.W. The principles of humane experimental technique. (1959).

169. FDA. (ed. F.a.D. Administration) (FDA Division of Metabolism and Endocrine Drug Products, Washington DC; 1994).

170. FDA, Vol. 2013 (FDA, 2013).

171. Hazzard, D.G., Bronson, R.T., Mcclearn, G.E. & Strong, R. Selection of an Appropriate Animal-Model to Study Aging Processes with Special Emphasis on the Use of Rat Strains. *Journals of Gerontology* **47**, B63-B64 (1992).

172. Ravaglioli, A. et al. Mineral evolution of bone. *Biomaterials* **17**, 617-622 (1996).

173. Roshan-Ghias, A., Arnoldi, J., Procter, P. & Pioletti, D.P. In vivo assessment of local effects after application of bone screws delivering bisphosphonates into a compromised cancellous bone site. *Clin. Biomech.* **26**, 1039-1043 (2011).

174. Frost, H.M. & Jee, W.S.S. On the Rat Model of Human Osteopenias and Osteoporosis. *Bone Miner.* **18**, 227-236 (1992).

175. Sterck, J.G.H., Klein-Nulend, J., Lips, P. & Burger, E.H. Response of normal and osteoporotic human bone cells to mechanical stress in vitro. *American Journal of Physiology-Endocrinology and Metabolism* **274**, E1113-E1120 (1998).

176. Spencer, G.R. Animal-Model of Human-Disease - Pregnancy and Lactational Osteoporosis. *Am. J. Pathol.* **95**, 277-280 (1979).

177. Lill, C.A., Fluegel, A.K. & Schneider, E. Effect of ovariectomy, malnutrition and glucocorticoid application on bone properties in sheep: A pilot study. *Osteoporos. Int.* **13**, 480-486 (2002).

178. Palle, S., Vico, L., Bourrin, S. & Alexandre, C. Bone tissue response to four-month antiorthostatic bedrest: a bone histomorphometric study. *Calcif. Tissue Int.* **51**, 189-194 (1992).

179. Jilka, R.L., Weinstein, R.S., Takahashi, K., Parfitt, A.M. & Manolagas, S.C. Linkage of decreased bone mass with impaired osteoblastogenesis in a murine model of accelerated senescence. *J. Clin. Invest.* **97**, 1732-1740 (1996).

180. Wronski, T.J., Dann, L.M., Scott, K.S. & Cintron, M. Long-Term Effects of Ovariectomy and Aging on the Rat Skeleton. *Calcif. Tissue Int.* **45**, 360-366 (1989).

181. Thompson, D.D., Simmons, H.A., Pirie, C.M. & Ke, H.Z. Fda Guidelines and Animal-Models for Osteoporosis. *Bone* **17**, S125-S133 (1995).

182. Benesch, J., Askendal, A. & Tengvall, P. Quantification of adsorbed human serum albumin at solid interfaces: a comparison between radioimmunoassay (RIA) and simple null ellipsometry. *Colloids and Surfaces B-Biointerfaces* **18**, 71-81 (2000).

183. McCrackin, F.L. A Fortran program for analysis of ellipsometer measurements. (NIST Research Library, Washington, DC.; 1969).

184. Grosso, D. et al. Fundamentals of mesostructuring through evaporation-induced self-assembly. *Adv. Funct. Mater.* **14**, 309-322 (2004).

185. Alberius, P.C.A. et al. General predictive syntheses of cubic, hexagonal, and lamellar silica and titania mesostructured thin films. *Chem. Mater.* **14**, 3284-3294 (2002).

186. Jarmar, T. et al. Technique for preparation and characterization in cross-section of oral titanium implant surfaces using focused ion beam and transmission electron microscopy. *J. Biomed. Mater. Res. A* **87A**, 1003-1009 (2008).

187. Hook, F. et al. A comparative study of protein adsorption on titanium oxide surfaces using in situ ellipsometry, optical waveguide lightmode spectroscopy, and quartz crystal microbalance/dissipation. *Colloids Surf., B* **24**, 155-170 (2002).

188. Sauerbrey, G. Verwendung von Schwingquarzen zur Wägung dünner Schichten und zur Mikrowägung. *Z. Phys. A: Hadron Nucl.* **155**, 206-222 (1959).

189. Hausmann, E., Raisz, L.G. & Miller, W.A. Endotoxin - Stimulation of Bone Resorption in Tissue Culture. *Science* **168**, 862-& (1970).

190. French, D.L., Muir, J.M. & Webber, C.E. The ovariectomized, mature rat model of postmenopausal osteoporosis: an assessment of the bone sparing effects of curcumin. *Phytomedicine* **15**, 1069-1078 (2008).

191. Diehl, K.H. et al. A good practice guide to the administration of substances and removal of blood, including routes and volumes. *J. Appl. Toxicol.* **21**, 15-23 (2001).

192. Branemark, R., Ohrnell, L.O., Nilsson, P. & Thomsen, P. Biomechanical characterization of osseointegration during healing: An experimental in vivo study in the rat. *Biomaterials* **18**, 969-978 (1997).

193. Branemark, R. & Skalak, R. An in-vivo method for biomechanical characterization of bone-anchored implants. *Med. Eng. Phys.* **20**, 216-219 (1998).

194. Pfaffl, M.W. A new mathematical model for relative quantification in real-time RT-PCR. *Nucleic Acids Res.* **29** (2001).

195. Rozen, S. & Skaletsky, H. Primer3 on the WWW for general users and for biologist programmers. *Methods Mol. Biol.* **132**, 365-386 (2000).

196. Donath, K. & Breuner, G. A Method for the Study of Undecalcified Bones and Teeth with Attached Soft-Tissues - the Sage-Schliff (Sawing and Grinding) Technique. *J. Oral Pathol. Med.* **11**, 318-326 (1982).

197. Johansson, C.B. & Morberg, P. Importance of Ground Section Thickness for Reliable Histomorphometrical Results. *Biomaterials* **16**, 91-95 (1995).

198. Coutu, D.L. et al. Periostin, a member of a novel family of vitamin K-dependent proteins, is expressed by mesenchymal stromal cells. *J. Biol. Chem.* **283**, 17991-18001 (2008).

199. Wennerberg, A., Jimbo, R., Allard, S., Skarnemark, G. & Andersson, M. In Vivo Stability of Hydroxyapatite Nanoparticles Coated on Titanium Implant Surfaces. *Int. J. Oral Maxillofac. Implants* **26**, 1161-1166 (2011).

200. Barrett, E.P., Joyner, L.G. & Halenda, P.P. The determination of pore volume and area distributions in porous substances .1. Computations from nitrogen isotherms. *J. Am. Chem. Soc.* **73**, 373-380 (1951).

201. Tengvall, P. & Lundstrom, I. Physico-chemical considerations of titanium as a biomaterial. *Clin. Mater.* **9**, 115-134 (1992).

202. Simmons, G.W. & Beard, B.C. Characterization of acid-base properties of the hydrated oxides on iroan and titanium metal-surfaces. *J. Phys. Chem.* **91**, 1143-1148 (1987).

203. McCafferty, E. & Wightman, J.P. An X-ray photoelectron spectroscopy sputter profile study of the native air-formed oxide film on titanium. *Appl. Surf. Sci.* **143**, 92-100 (1999).

204. Jobin, M., Taborelli, M., Emch, R., Zenhausern, F. & Descouts, P. Hydroxylation and crystallization of electropolished titanium surface. *Ultramicroscopy* **42**, 637-643 (1992).

205. Lo, W.J., Chung, Y.W. & Somorjai, G.A. Electron-spectroscopy studies of chemisorption of O2, H2 and H2O on TiO2(100) surfaces with varied stoichiometry - evidence for photogeneration of Ti+3 and for its importance in chemisorption. *Surf. Sci.* **71**, 199-219 (1978).

206. Walivaara, B., Aronsson, B.O., Rodahl, M., Lausmaa, J. & Tengvall, P. Titanium with Different Oxides - in-Vitro Studies of Protein Adsorption and Contact Activation. *Biomaterials* **15**, 827-834 (1994).

207. Arvidsson, S., Askendal, A. & Tengvall, P. Blood plasma contact activation on silicon, titanium and aluminium. *Biomaterials* **28**, 1346-1354 (2007).

208. Kalltorp, M., Askendal, A., Thomsen, P. & Tengvall, P. Inflammatory cell recruitment, distribution, and chemiluminescence response at IgG precoated- and thiol functionalized gold surfaces. *J. Biomed. Mater. Res.* **47**, 251-259 (1999).

209. Omar, O. et al. In vivo gene expression in response to anodically oxidized versus machined titanium implants. *Journal of Biomedical Materials Research Part A* **92A**, 1552-1566 (2010).

210. Suska, F. et al. IL-1alpha, IL-1beta and TNF-alpha secretion during in vivo/ex vivo cellular interactions with titanium and copper. *Biomaterials* **24**, 461-468 (2003).

211. Bonar, S.L. et al. Constitutively Activated NLRP3 Inflammasome Causes Inflammation and Abnormal Skeletal Development in Mice. *PLoS ONE* **7** (2012).

212. Dinarello, C.A. The Interleukin-1 Family - 10 Years of Discovery. *FASEB J.* **8**, 1314-1325 (1994).

213. Netea, M.G. et al. Differential requirement for the activation of the inflammasome for processing and release of IL-1 beta in monocytes and macrophages. *Blood* **113**, 2324-2335 (2009).

214. Miura, M., Zhu, H., Rotello, R., Hartwieg, E.A. & Yuan, J.Y. Induction of Apoptosis in Fibroblasts by Il-1-Beta-Converting Enzyme, a Mammalian Homolog of the C-Elegans Cell-Death Gene Ced-3. *Cell* **75**, 653-660 (1993).

215. Arend, W.P., Palmer, G. & Gabay, C. IL-1, IL-18, and IL-33 families of cytokines. *Immunol. Rev.* **223**, 20-38 (2008).

216. Anderson, J.M., Rodriguez, A. & Chang, D.T. Foreign body reaction to biomaterials. *Semin. Immunol.* **20**, 86-100 (2008).

217. Rammelt, S., Corbeil, D., Manthey, S., Zwipp, H. & Hanisch, U. Immunohistochemical in situ characterization of orthopedic implants on polymethyl metacrylate embedded cutting and grinding sections. *J. Biomed. Mater. Res. A* **83**, 313-322 (2007).

218. Horton, J.E., Mergenha.Se, Simmons, H.A., Raisz, L.G. & Oppenhei.Jj Bone Resorbing Activity in Supernatant Fluid from Cultured Human Peripheral-Blood Leukocytes. *Science* **177**, 793-& (1972).

219. Fernandez-Real, J.M. & Ricart, W. Osteocalcin: a new link between bone and energy metabolism. Some evolutionary clues. *Curr. Opin. Clin. Nutr. Metab. Care* **14**, 360-366 (2011).

220. Urist, M.R. Bone - Formation by Autoinduction. *Science* **150**, 893-& (1965).

221. Lynch, S.E., Wisner-Lynch, L., Nevins, M. & Nevins, M.L. A new era in periodontal and periimplant regeneration: use of growth-factor enhanced matrices incorporating rhPDGF. *Compend. Contin. Educ. Dent.* **27**, 672-678; quiz 679-680 (2006).

222. Key, L.L., Jr., Carnes, D.L., Jr., Weichselbaum, R. & Anast, C.S. Platelet-derived growth factor stimulates bone resorption by monocyte monolayers. *Endocrinology* **112**, 761-762 (1983).

223. Dewhirst, F.E., Stashenko, P.P., Mole, J.E. & Tsurumachi, T. Purification and Partial Sequence of Human Osteoclast-Activating Factor - Identity with Interleukin-1-Beta. *J. Immunol.* **135**, 2562-2568 (1985).

224. Karlsson, J. et al. In vivo biomechanical stability of osseointegrating mesoporous TiO2 implants. *Acta Biomater.* **8**, 4438-4446 (2012).

225. Zhang, C. et al. Self-activated luminescent and mesoporous strontium hydroxyapatite nanorods for drug delivery. *Biomaterials* **31**, 3374-3383 (2010).

226. Wei, W. et al. Preparation of Hierarchical Hollow CaCO(3) Particles and the Application as Anticancer Drug Carrier. *J. Am. Chem. Soc.* **130**, 15808-+ (2008).

227. Licata, A.A. Discovery, clinical development, and therapeutic uses of bisphosphonates. *Ann. Pharmacother.* **39**, 668-677 (2005).

228. Shimizu, E., Tamasi, J. & Partridge, N.C. Alendronate Affects Osteoblast Functions by Crosstalk through EphrinB1-EphB. *J. Dent. Res.* **91**, 268-274 (2012).

229. Meraw, S.J., Reeve, C.M. & Wollan, P.C. Use of alendronate in peri-implant defect regeneration. *J. Periodontol.* **70**, 151-158 (1999).

230. Yoshinari, M., Oda, Y., Inoue, T., Matsuzaka, K. & Shimono, M. Bone response to calcium phosphate-coated and bisphosphonate-immobilized titanium implants. *Biomaterials* **23**, 2879-2885 (2002).

231. Viereck, V. et al. Raloxifene concurrently stimulates osteoprotegerin and inhibits interleukin-6 production by human trabecular osteoblasts. *J. Clin. Endocrinol. Metab.* **88**, 4206-4213 (2003).

232. Harkonen, P.L. & Vaananen, H.K. Monocyte-macrophage system as a target for estrogen and selective estrogen receptor modulators. *Ann Ny Acad Sci* **1089**, 218-227 (2006).

233. Braun, T. & Schett, G. Pathways for bone loss in inflammatory disease. *Curr. Osteoporos. Rep.* **10**, 101-108 (2012).

234. Burnham, J.M. Inflammatory diseases and bone health in children. *Curr. Opin. Rheumatol.* **24**, 548-553 (2012).

235. Skoglund, B., Holmertz, J. & Aspenberg, P. Systemic and local ibandronate enhance screw fixation. *J. Orthop. Res.* **22**, 1108-1113 (2004).

236. Hilding, M. & Aspenberg, P. Local peroperative treatment with a bisphosphonate improves the fixation of total knee prostheses: a randomized, double-blind radiostereometric study of 50 patients. *Acta Orthop.* **78**, 795-799 (2007).

237. Paspaliaris, V. & Leaver, D.D. Clodronate Inhibits Contraction and Prevents the Action of L-Type Calcium-Channel Antagonists in Vascular Smooth-Muscle. *J. Bone Miner. Res.* **6**, 835-841 (1991).

238. Harmankaya, N. et al. Bone remodelling following systemic or local delivery of Alendronate in ovariectomized rats. *Unpublished data* (2013).

239. Harmankaya, N. et al. Raloxifene and alendronate containing thin mesoporous titanium oxide films improve implant fixation to bone. *Acta Biomater.* **9**, 7064-7073 (2013).

240. Lin, J.H., Chen, I.W. & Duggan, D.E. Effects of Dose, Sex, and Age on the Disposition of Alendronate, a Potent Antiosteolytic Bisphosphonate, in Rats. *Drug Metab. Dispos.* **20**, 473-478 (1992).

241. McKenzie, K., Bobyn, J.D., Roberts, J., Karabasz, D. & Tanzer, M. Bisphosphonate Remains Highly Localized After Elution From Porous Implants. *Clin. Orthop.* **469**, 514-522 (2011).